

Inside-out cross-covariance for spatial multivariate data

Michele Peruzzi*

Abstract

As the spatial features of multivariate data are increasingly central in researchers' applied problems, there is a growing demand for novel spatially aware methods that are flexible, easily interpretable, and scalable to large data. We develop inside-out cross-covariance (IOX) models for multivariate spatial likelihood-based inference. IOX leads to valid cross-covariance matrix functions which we interpret as inducing spatial dependence on independent replicates of a correlated random vector. The resulting sample cross-covariance matrices are “inside-out” relative to the ubiquitous linear model of coregionalization (LMC). However, unlike LMCs, our methods offer direct marginal inference, easy prior elicitation of covariance parameters, the ability to model outcomes with unequal smoothness, and flexible dimension reduction. As a covariance model for a q -variate Gaussian process, IOX leads to scalable models for noisy vector data as well as flexible latent models. For large n cases, IOX complements Vecchia approximations and related process-based methods relying on sparse graphical models. We demonstrate competitive performance of IOX on synthetic datasets as well as on colorectal cancer proteomics data. An R package implementing the proposed methods is available at github.com/mkln/spiox.

Keywords: Gaussian process, cokriging, dimension reduction, coregionalization, Bayesian hierarchical models.

1 Introduction

Multivariate data with spatial dependence are increasingly common in fields such as ecology, environmental science, remote sensing, epidemiology, with growing interest in applying spatially aware methods to ‘omics’ data, such as proteomics and genomics. Researchers aim to understand how the joint dependence across multiple variables changes as a function of

*Department of Biostatistics, University of Michigan–Ann Arbor.

space. For example, in community ecology, joint species distribution models assume that species interactions are influenced by both their spatial context and the co-location with other species. Similarly, cancer development impacts the spatial arrangement of cells of different types within the tumor microenvironment. In these contexts, we expect multivariate spatial models to uncover deeper insights than univariate or non-spatial multivariate models, but their increased computational cost often limits their practical utility. In fact, any method for multivariate spatial data must balance flexibility and interpretability with scalability and parsimony. Achieving this balance is particularly difficult when we have a large number of spatially resolved variables (e.g., $q > 10$) observed at many spatial sites (n in the thousands). In such cases, fully flexible methods struggle to scale, whereas dimension reduction techniques can lead to interpretability or performance issues relative to univariate or non-spatial models.

These challenges can be addressed in principle by modeling spatial dependence across multiple variables via a q -variate Gaussian process (GP). The GP is a flexible probabilistic framework for modeling spatial dependence of vector-valued outcomes. It can also act as a prior process in a Bayesian hierarchical regression for inferring spatial and cross-variable dependence, estimation of non-linear exposure effects, and predictions at unobserved locations. A GP is fully specified by its mean and cross-covariance matrix functions. The mean can typically be assumed to be zero or modeled as a separate component of the Bayesian hierarchy, if necessary. Cross-covariance matrix functions vary in terms of parsimony, interpretability, modeling flexibility, parameter identifiability, and computational feasibility. The choice of cross-covariance matrix function thus reflects the challenges we mentioned above. Let $\mathbf{M}_{q \times q}$ be the set of $q \times q$ real-valued matrices and $\mathcal{D} \subset \mathfrak{R}^d$ the spatial domain of dimension d , then a cross-covariance matrix function is $\mathbf{C} : \mathcal{D} \times \mathcal{D} \rightarrow \mathbf{M}_{q \times q}$

such that $\mathbf{C}(\boldsymbol{\ell}, \boldsymbol{\ell}') = \mathbf{C}(\boldsymbol{\ell}', \boldsymbol{\ell})^\top$ and $\sum_{i=1}^n \sum_{j=1}^n \mathbf{x}_i^\top \mathbf{C}(\boldsymbol{\ell}_i, \boldsymbol{\ell}_j) \mathbf{x}_j > 0$ for any integer n , any finite set $\{\boldsymbol{\ell}_1, \boldsymbol{\ell}_2, \dots, \boldsymbol{\ell}_n\}$, and for all $\mathbf{x}_i, \mathbf{x}_j \in \mathbb{R}^q \setminus \{\mathbf{0}\}$. Then, if $\{\mathbf{y}(\boldsymbol{\ell}), \boldsymbol{\ell} \in \mathcal{D}\}$ is a q -variate GP with cross-covariance matrix function $\mathbf{C}(\cdot, \cdot)$, the (i, j) th entry of $\mathbf{C}(\boldsymbol{\ell}, \boldsymbol{\ell}')$ evaluates to $C_{ij}(\boldsymbol{\ell}, \boldsymbol{\ell}') = \text{cov}(y_i(\boldsymbol{\ell}), y_j(\boldsymbol{\ell}'))$. Following Genton & Kleiber (2015), we call $C_{ii}(\cdot, \cdot)$ the marginal covariance and $C_{ij}(\cdot, \cdot), i \neq j$ as the cross-covariance functions. Building a cross-covariance matrix function boils down to specifying q^2 distinct covariance and cross-covariance functions and establishing the validity of the overall model; both tasks are increasingly difficult as q grows.

The linear model of coregionalization (LMC, Matheron 1982, Wackernagel 2003, Schmidt & Gelfand 2003, see also Alie et al. 2024) writes $C_{ij}(\cdot, \cdot)$ as a linear combination of $k \leq q \ll q^2$ univariate correlation functions, i.e., $C_{ij}(\boldsymbol{\ell}, \boldsymbol{\ell}') = \sum_{r=1}^k a_{ir} a_{rj} \rho_r(\boldsymbol{\ell}, \boldsymbol{\ell}')$. If $k < q$, we refer to the LMC as a spatial factor model. The LMC is the most popular cross-covariance model for multivariate data due to its computational tractability: it can be extended to model nonstationarity (Gelfand et al. 2004), spatially-varying regression coefficients (Gelfand et al. 2003 and Reich et al. 2010, both assuming separability), space-time data (Berrocal et al. 2010, De Iaco et al. 2019); it can be included as a latent process in Bayesian hierarchies for non-Gaussian data (Peruzzi & Dunson 2024), used as a dimension reduction tool in the large n , large q setting by letting $k \ll q$ (Taylor-Rodriguez et al. 2019, Zhang & Banerjee 2022). LMCs and methods based on linear combinations of independent GPs are very popular in many fields (see, e.g., Teh et al. 2005, Finley et al. 2008, Fricker et al. 2013, Álvarez & Lawrence 2011, Moreno-Muñoz et al. 2018, Liu et al. 2022, Townes & Engelhardt 2023). Statistical software packages for multivariate spatial data typically implement LMCs (Pebesma 2004, Finley et al. 2015, Tikhonov et al. 2020, Finazzi & Fassò 2014, Krainski et al. 2019).

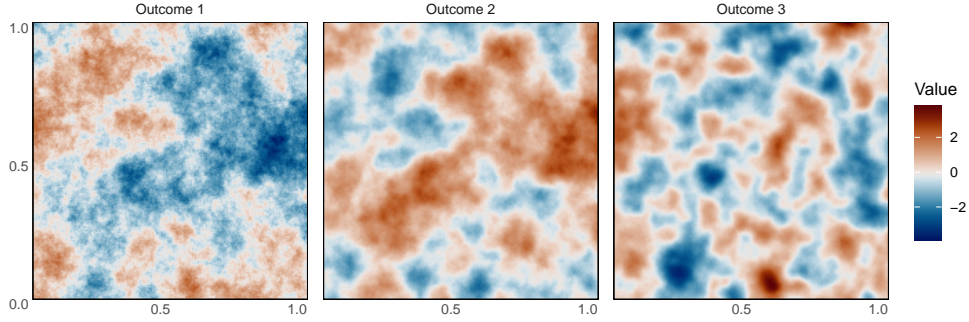


Figure 1: Three spatially correlated outcomes generated via GP-IOX at $n = 40,000$ gridded locations. We let $\sigma_{ii} = 1$ for $i \in \{1, 2, 3\}$ and $\sigma_{12} = -0.9, \sigma_{13} = 0.7, \sigma_{23} = -0.5$ and choose $\rho_i(\cdot, \cdot)$ as Matérn (Vecchia-approximated with $m = 50$ neighbors) with range $1/5, 1/15, 1/30$ and smoothness $0.5, 1.2, 1.9$, respectively.

The LMC has several major limitations: it is inadequate in modeling outcomes with different smoothness (Genton & Kleiber 2015); some of its parameters lead to difficult interpretations and prior elicitation, e.g., the spatial range of outcome j is a non-linear function of all the k spatial range parameters (Schmidt & Gelfand 2003, Section 3.4); LMCs do not facilitate the inclusion of independent measurement error in response models. Finally, the infill asymptotics of LMCs are poorly understood (Zhang 2007, see also Velandia et al. 2017). These issues limit the flexibility of LMCs and reduce their inferential usefulness. Alternative methods that solve some of the limitations of the LMC include the multivariate Matérn model (Gneiting et al. 2010, see also Apanasovich et al. 2012, Emery et al. 2022, Yarger et al. 2024), approaches based on latent dimensions (Apanasovich & Genton 2010), and convolution methods (Gaspari & Cohn 1999, Majumdar & Gelfand 2007). However, these methods are only suitable to very small q as they do not lead to exploitable structure in the sample covariance or facilitate dimension reduction, or require numerical integration for computing $C_{ij}(\cdot, \cdot)$. The Supplement provides more details on the limitations of LMCs and includes a more detailed discussion on the multivariate Matérn model.

In this article, we introduce the Inside-Out Cross-covariance (IOX) model for multi-

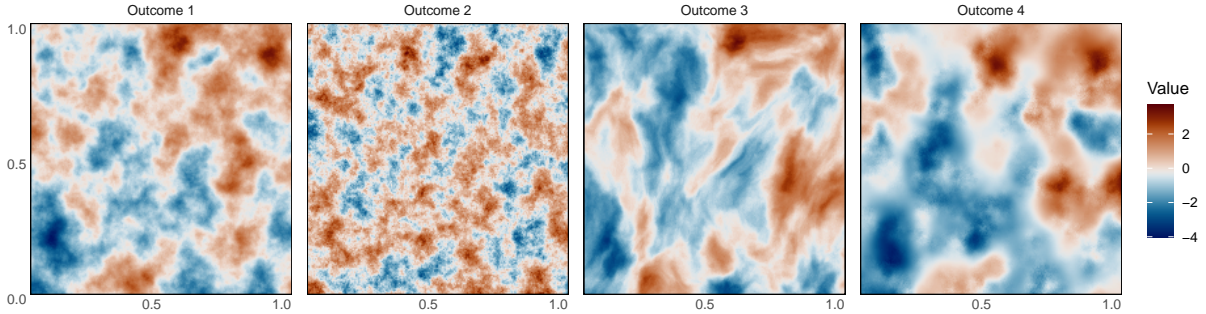


Figure 2: Four spatially correlated outcomes generated via GP-IOX at $n = 40,000$ gridded locations. Outcomes 1 and 2 have stationary marginal covariances, whereas 3 and 4 are nonstationary.

variate spatial data. IOX leads to parsimonious cross-covariance matrix functions defined on the basis of q univariate correlation functions and a covariance matrix Σ . Constructively, IOX induces multivariate spatial dependence by applying outcome-specific spatial Cholesky transforms to n i.i.d. q -vectors, thereby introducing within-outcome spatial correlation while preserving cross-outcome dependence. IOX offers novel avenues for dimension reduction via clustering or low-rank assumptions. Our model resolves several major flaws of LMCs: in IOX, there is a one-to-one link between the marginal covariance of the j th variable and the j th univariate correlation function used to define it, facilitating prior elicitation and interpretable process-based inference. Furthermore, IOX is flexible in allowing different smoothness, nugget effects, or nonstationarity of one or more outcomes. Figure 1 shows a realization of a noise-free GP-IOX where three Matérn outcomes have different smoothness. In Figure 2, we generate four spatially correlated outcomes via IOX; one of them is nonstationary via deformation of the spatial domain as in Sampson & Guttorp (1992), another has a spatially-varying sill. More details about Figure 2 are in the Supplement. Relative to multivariate Matérn models, IOX is more flexible in allowing the marginal covariances to be defined freely (e.g., not Matérn), and more scalable because it results in sample covariance matrices whose structure we may exploit for likelihood-based inference

in large scale settings. When building IOX using q stationary Matérn covariances, IOX is more flexible than a parsimonious multivariate Matérn (Gneiting et al. 2010) because it allows the marginal ranges to be defined freely, and more parsimonious than a general multivariate Matérn because IOX does not directly parametrize the cross-covariances.

Because IOX leads to structured covariance matrices, we envision it as a novel tool for developing flexible and interpretable models for high-dimensional multivariate spatial data. In large q settings, scalable methods have been developed for multivariate areal or count-valued data (Bradley et al. 2015, 2018). Recently, Krock et al. (2023) modeled multivariate spatial data using linear combinations of fixed basis functions. Their low-rank approach achieves scalability by assuming sparsity in an underlying graphical model of the basis function weights but remains limited in its ability to flexibly characterize cross-covariance structures. Dey et al. (2022) introduce Graphical Gaussian Processes (GGPs), which model multivariate spatial data under sparse network dependency assumptions. Constructing a GGP requires users to pre-specify a cross-covariance matrix function, whose properties and validity conditions are inherited by the resulting GGP. For instance, a LMC-based GGP cannot accommodate outcomes with unequal smoothness, and a multivariate Matérn GGP must satisfy validity conditions as in Emery et al. (2022). In introducing IOX as a novel cross-covariance model, we offer new ways for future developments of flexible GGPs.

Our definition of IOX requires the specification of a fixed set of *reference* locations \mathcal{S} . As a consequence, our model is nonstationary even when built using q stationary correlation functions. However, this has minimal practical impact, as IOX is no more complex than other cross-covariance models when n is large. In these settings, GPs scale poorly and they must be replaced with scalable alternatives. Vecchia approximations (Vecchia 1988) and related methods based on sparse directed acyclic graphs (DAGs; see, e.g., Datta et al.

2016, Shirota et al. 2019, Quiroz et al. 2023, Peruzzi et al. 2022) have desirable theoretical properties and excellent practical performance (Zhu et al. 2024, Schäfer et al. 2024, Heaton et al. 2019). Several other scalable GPs can be cast as “sparse DAG” methods (Banerjee et al. 2008, 2010, Katzfuss 2017, Katzfuss & Gong 2019, Peruzzi & Dunson 2022). The main advantage of sparse DAG methods is that they enable process-based inference and can thus be seamlessly embedded into Bayesian hierarchies for added flexibility. Process-based inference using sparse DAGs *always* leads to nonstationary GPs, as one must specify a set \mathcal{S} when implementing any sparse DAG GP. IOX can simply use the same \mathcal{S} . As is standard practice in implementing Vecchia-related methods, we choose \mathcal{S} as the set of observed locations in all our applications.

We outline IOX in Section 2 and prove its validity. We develop the GP-IOX in Section 3 and the related posterior sampling algorithms in Section 4. Section 5 applies IOX on simulated and colorectal cancer data. Proofs, as well as additional details, comparisons, and algorithms, are available in the Supplement. Software for fitting Bayesian spatial regression models using IOX is available at github.com/mkln/spiox.

2 Inside-out cross-covariance

Let the spatial domain $\mathcal{D} \subset \mathfrak{R}^d$ be of dimension d , typically $d = 2$ for longitude and latitude or x,y coordinates on an image. Introduce q univariate correlation functions $\rho_j(\cdot, \cdot) : \mathcal{D} \times \mathcal{D} \rightarrow \mathfrak{R}$. For example, we may let $\rho_j(\boldsymbol{\ell}, \boldsymbol{\ell}') = \exp\{-\phi_j \|\boldsymbol{\ell} - \boldsymbol{\ell}'\|\}$ or a more complex Matérn correlation parametrized by vector $\boldsymbol{\theta}_j$. Letting $\boldsymbol{\theta}_j = (\phi_j, \nu_j)$, the Matérn correlation function is $\mathcal{M}_{\nu_j}(\boldsymbol{\ell}, \boldsymbol{\ell}'; \phi_j) = \frac{2^{1-\nu_j}}{\Gamma(\nu_j)} \phi_j^{\nu_j} \|\boldsymbol{\ell} - \boldsymbol{\ell}'\|^{\nu_j} K_{\nu_j}(\phi_j \|\boldsymbol{\ell} - \boldsymbol{\ell}'\|)$ where K_{ν_j} is the modified Bessel function of the second kind of order ν_j . The inclusion of nugget effects is possible, as we discuss later. Suppose $\mathcal{A} = \{\mathbf{a}_1, \dots, \mathbf{a}_{n_A}\} \subset \mathcal{D}$ and $\mathcal{B} = \{\mathbf{b}_1, \dots, \mathbf{b}_{n_B}\} \subset \mathcal{D}$, then we

denote as $\rho_h(\mathcal{A}, \mathcal{B})$ the $n_A \times n_B$ matrix whose (i, j) element is $\rho_h(\mathbf{a}_i, \mathbf{b}_j)$, and let $\rho_h(\mathcal{A}) := \rho_h(\mathcal{A}, \mathcal{A})$ and $\rho_h(\boldsymbol{\ell}, \mathcal{A}) := \rho_h(\{\boldsymbol{\ell}\}, \mathcal{A})$. Choose a set of *reference* locations $\mathcal{S} = \{\boldsymbol{\ell}_1, \dots, \boldsymbol{\ell}_n\} \subset \mathcal{D}$. In applications, we choose \mathcal{S} as the sample locations. The set of non-reference locations $\mathcal{S}^c = \mathcal{D} \setminus \mathcal{S}$ may be thought of as a superset of the prediction locations. We do not make any distributional assumption in this section. After defining our cross-covariance model, we study its properties and prove the validity of the resulting cross-covariance matrix function. All proofs and derivations are in the Supplement.

Definition 2.1 (Inside-out cross-covariance). Let $\boldsymbol{\Sigma} = (\sigma_{ij})_{i,j=1}^q$ be a positive semidefinite matrix, $\rho_i(\cdot, \cdot)$ for $i = 1, \dots, q$ and \mathcal{S} as above. We define the IOX cross-covariance as:

$$C_{ij}(\boldsymbol{\ell}, \boldsymbol{\ell}') = \sigma_{ij} [\mathbf{h}_i(\boldsymbol{\ell}) \mathbf{L}_i \mathbf{L}_j^\top \mathbf{h}_j(\boldsymbol{\ell}')^\top + \xi_{ij}(\boldsymbol{\ell}, \boldsymbol{\ell}')], \quad (1)$$

where $\mathbf{h}_i(\boldsymbol{\ell}) = \rho_i(\boldsymbol{\ell}, \mathcal{S}) \rho_i(\mathcal{S})^{-1}$, \mathbf{L}_i is the lower Cholesky factor of $\rho_i(\mathcal{S})$, i.e. it is lower triangular and such that $\mathbf{L}_i \mathbf{L}_i^\top = \rho_i(\mathcal{S})$, $\xi_{ij}(\boldsymbol{\ell}, \boldsymbol{\ell}') = \mathbb{1}_{\{\boldsymbol{\ell}=\boldsymbol{\ell}'\}} \sqrt{r_i(\boldsymbol{\ell}) r_j(\boldsymbol{\ell}')}$, and $r_i(\boldsymbol{\ell}) = \rho_i(\boldsymbol{\ell}, \boldsymbol{\ell}) - \mathbf{h}_i(\boldsymbol{\ell}) \rho_i(\mathcal{S}, \boldsymbol{\ell})$. We let $\mathbb{1}_{\{c\}} = 1$ if c is true, 0 otherwise.

A constructive sampling scheme highlights why IOX is “inside-out” relative to the LMC. Suppose we sample at \mathcal{S} . We begin by computing $\mathbf{L}_j = \text{chol}(\rho_j(\mathcal{S}))$ for $j = 1, \dots, q$. Sample $U_r, r = 1, \dots, nq$ as uncorrelated white noise with unit variance and build the $n \times q$ matrix \mathbf{U} ; denote its j th column as \mathbf{u}_j . Set $\mathbf{V} = \mathbf{U} \boldsymbol{\Lambda}^T$ where $\boldsymbol{\Lambda} \boldsymbol{\Lambda}^T = \boldsymbol{\Sigma}$. Let \mathbf{Y} be the $n \times q$ matrix whose j th column is $\mathbf{y}_j = \mathbf{L}_j \mathbf{v}_j$. Then, $\text{cov}\{\mathbf{Y}[r, i], \mathbf{Y}[c, j]\} = C_{ij}(\boldsymbol{\ell}_r, \boldsymbol{\ell}_c)$ as in (1). We have first introduced cross-variable dependence on \mathbf{U} , then injected spatial dependence on the columns of \mathbf{V} . The LMC performs operations in reverse: it starts by injecting spatial dependence via $\mathbf{v}_j = \mathbf{L}_j \mathbf{u}_j$, then couples the outcomes by setting $\mathbf{Y} = \mathbf{V} \boldsymbol{\Lambda}^T$. Refer to Section C in the Supplement for additional details. Next, we show that IOX leads to easily interpretable inference and prior elicitation of marginal covariance parameters.

Proposition 2.1 (Marginal covariance).

$$C_{ii}(\boldsymbol{\ell}, \boldsymbol{\ell}') = \begin{cases} \sigma_{ii}\rho_i(\boldsymbol{\ell}, \boldsymbol{\ell}') & \text{if } \boldsymbol{\ell} \in \mathcal{S} \text{ or } \boldsymbol{\ell}' \in \mathcal{S} \text{ or } \boldsymbol{\ell} = \boldsymbol{\ell}', \\ \sigma_{ii}\rho_i(\boldsymbol{\ell}, \mathcal{S})\rho_i(\mathcal{S})^{-1}\rho_i(\mathcal{S}, \boldsymbol{\ell}') & \text{if } \boldsymbol{\ell}, \boldsymbol{\ell}' \in \mathcal{S}^c \text{ and } \boldsymbol{\ell} \neq \boldsymbol{\ell}'. \end{cases}$$

The first case ($\boldsymbol{\ell} \in \mathcal{S}$ or $\boldsymbol{\ell}' \in \mathcal{S}$ or $\boldsymbol{\ell} = \boldsymbol{\ell}'$) is the most relevant in practice and motivates our choice of \mathcal{S} as the observed locations in Section 3. In fact, by letting \mathcal{S} correspond to the observed locations, the tasks of parameter estimation and prediction at new locations will both solely depend on the cross-covariance model when at least one of $\boldsymbol{\ell}$ or $\boldsymbol{\ell}'$ are in \mathcal{S} . In this key scenario, Proposition 2.1 shows that IOX retains $\rho_i(\boldsymbol{\ell}, \boldsymbol{\ell}')$ as the marginal covariance for outcome i . More in general, for all $\boldsymbol{\ell}, \boldsymbol{\ell}' \in \mathcal{D}$, $C_{ii}(\cdot, \cdot)$ is still a function of $\rho_i(\cdot, \cdot)$ only, leading to direct interpretation of its parameters. $C_{ii}(\boldsymbol{\ell}, \boldsymbol{\ell}')$ is equivalent to the modified predictive process covariance (Finley et al. 2009) on knots \mathcal{S} , which is known to approximate $\rho_i(\cdot, \cdot)$ increasingly well as the size of \mathcal{S} increases, and reduces to the predictive process covariance (Banerjee et al. 2008) only in the residual case $\boldsymbol{\ell}, \boldsymbol{\ell}' \in \mathcal{S}^c$. From a Bayesian perspective, Proposition 2.1 simplifies prior elicitation, as one can take advantage of exploratory tools like variograms to build informative priors.

Next, we study the role of σ_{ij} for $i \neq j$ and show that two variables have a cross-covariance of σ_{ij} at zero distance if their marginal correlations functions are the same. Otherwise, σ_{ij} bounds the cross-covariance $C_{ij}(\boldsymbol{\ell}, \boldsymbol{\ell}')$ from above—this behavior also occurs in the multivariate Matérn model due to the necessary validity conditions (refer to the Supplement for more details).

Proposition 2.2 (Cross-covariance and σ_{ij}). For all $\boldsymbol{\ell}, \boldsymbol{\ell}' \in \mathcal{D}$ and all $i, j = 1, \dots, q$, the cross-covariance is $C_{ij}(\boldsymbol{\ell}, \boldsymbol{\ell}') \leq \sigma_{ij}$. If $\rho_i(\cdot, \cdot) = \rho_j(\cdot, \cdot)$, then $C_{ij}(\boldsymbol{\ell}, \boldsymbol{\ell}) = \sigma_{ij}$.

$C_{ij}(\cdot, \cdot)$ is nonstationary even when each of the $\rho_i(\cdot, \cdot)$ are stationary and isotropic due to its dependence on \mathcal{S} . We showed in Proposition 2.1 that we can rely on $\rho_i(\cdot, \cdot)$ and its

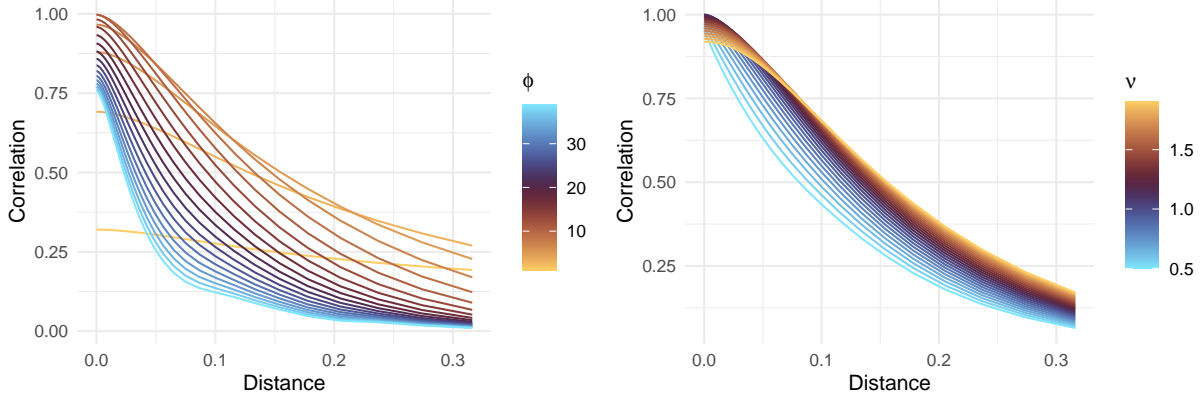


Figure 3: We plot $C_{ij}(\boldsymbol{\ell}, \boldsymbol{\ell} + \mathbf{h})/\sigma_{ij} = \mathbf{h}_i(\boldsymbol{\ell})\mathbf{L}_i\mathbf{L}_j^\top\mathbf{h}_j(\boldsymbol{\ell} + \mathbf{h})^\top$ at varying distances $\|\mathbf{h}\|$ and taking $\rho_i(\cdot, \cdot)$ as a Matérn correlation with $\nu_i = 1$, $\phi_i = 10$ and $\rho_j(\cdot, \cdot)$ as a Matérn with $\nu_j = 1$ and varying the values of ϕ_j (left), or with $\phi_j = 10$ and varying the values of ν_j (right), averaged over locations of a gridded set \mathcal{S} of size 400.

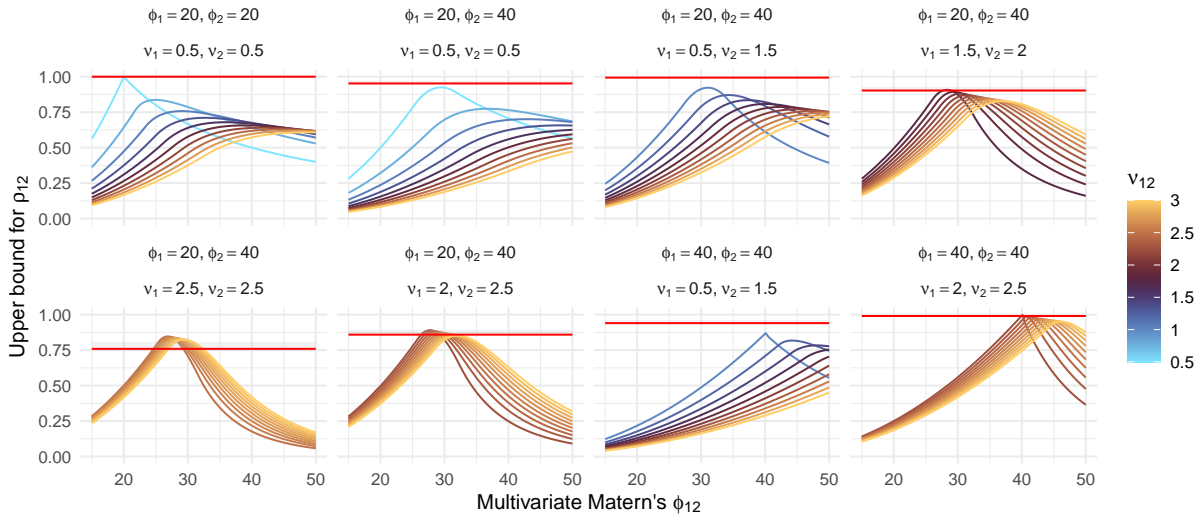


Figure 4: Maximum allowable cross-correlation at zero distance of a bivariate IOX on two Matérn margins (red horizontal lines), compared to a bivariate Matérn model, at different values of $\phi_1, \nu_1, \phi_2, \nu_2$ (subplots), ϕ_{12} (x-axes), and ν_{12} (by line color). IOX cross-correlations are averaged over locations of a gridded set \mathcal{S} of size 400.

parameters to interpret $C_{ii}(\cdot, \cdot)$. For $i \neq j$, we can easily draw interpretable covariance curves by averaging the values of $C_{ij}(\cdot, \cdot)$ across locations. In Figure 3, we compute and visualize the scaling factor, i.e., $C_{ij}(\cdot, \cdot)/\sigma_{ij}$, when $\rho_i(\cdot, \cdot)$ and $\rho_j(\cdot, \cdot)$ are Matérn. Each curve is monotonically decreasing and corresponds to a different value of ϕ_j (left) or ν_j (right). For example, in the left subfigure, different lines correspond to different values of ϕ_j , keeping $\phi_i = 10$ and $\nu_i = 1$; the highest correlation is achieved at $\|\mathbf{h}\| = 0$ by setting $\phi_j = \phi_i = 10$, in which case $C_{ij}(\boldsymbol{\ell}, \boldsymbol{\ell})/\sigma_{ij} = 1$. In other words, cross-correlation between the two margins is highest at $\|\mathbf{h}\| = 0$ when the two marginal correlation functions coincide. It then decreases when we pick $\phi_j \neq \phi_i$. Figure 4 compares IOX with the bivariate Matérn model on the maximum allowable cross-correlation at zero distance. For IOX, the colocated correlation coefficient can be computed by averaging values of $C_{ij}(\boldsymbol{\ell}, \boldsymbol{\ell})/\sigma_{ij}$ across the spatial domain. For the bivariate Matérn, we compute the upper bound given by equation (13) of Gneiting et al. (2010) at several combinations of $\phi_1, \phi_2, \nu_1, \nu_2, \phi_{12}, \nu_{12}$. While some combinations of the bivariate Matérn parameters achieve higher correlations, IOX is competitive in all cases. We give more details and analyze the role of \mathcal{S} in shaping $C_{ij}(\boldsymbol{\ell}, \boldsymbol{\ell}')$ in the Supplement.

We now outline two equivalent definitions of the cross-covariance matrix function of IOX. The first does not involve $nq \times nq$ matrices, whereas the second facilitates likelihood inference. We prove the validity of this cross-covariance matrix function in Proposition 2.4.

Proposition 2.3 (IOX cross-covariance matrix function). Let $\boldsymbol{\ell}, \boldsymbol{\ell}' \in \mathcal{S}$.

$$\begin{aligned} \mathbf{C}(\boldsymbol{\ell}, \boldsymbol{\ell}') &= \boldsymbol{\Sigma} \odot [\mathbf{K}(\boldsymbol{\ell}, \boldsymbol{\ell}') + \mathbf{d}(\boldsymbol{\ell}, \boldsymbol{\ell}')\mathbf{d}(\boldsymbol{\ell}, \boldsymbol{\ell}')^\top] \\ &= \{\oplus \mathbf{h}_i(\boldsymbol{\ell})\mathbf{L}_i\}(\boldsymbol{\Sigma} \otimes \mathbf{I}_n)\{\oplus \mathbf{L}_i^\top \mathbf{h}_i(\boldsymbol{\ell}')^\top\} + \mathbf{D}(\boldsymbol{\ell}, \boldsymbol{\ell}')\boldsymbol{\Sigma}\mathbf{D}(\boldsymbol{\ell}, \boldsymbol{\ell}'), \end{aligned} \tag{2}$$

where $\mathbf{K}(\boldsymbol{\ell}, \boldsymbol{\ell}')$ is the $q \times q$ matrix whose i, j element is $\mathbf{h}_i(\boldsymbol{\ell})\mathbf{L}_i\mathbf{L}_j^\top\mathbf{h}_j(\boldsymbol{\ell}')^\top$, $\mathbf{d}(\boldsymbol{\ell}, \boldsymbol{\ell}')$ is a vector of dimension q whose i th element is $\mathbb{1}_{\{\boldsymbol{\ell}=\boldsymbol{\ell}'\}}\sqrt{r_i(\boldsymbol{\ell})}$, $\mathbf{D}(\boldsymbol{\ell}, \boldsymbol{\ell}') = \text{diag}\{\mathbf{d}(\boldsymbol{\ell}, \boldsymbol{\ell}')\}$, “ \oplus ” is the direct sum operator and we denote with $\{\oplus \mathbf{h}_i(\boldsymbol{\ell})\mathbf{L}_i\}$ the $q \times nq$ block-diagonal matrix

with $\mathbf{h}_i(\boldsymbol{\ell})\mathbf{L}_i$ as its i th block, while “ \odot ” is the Hadamard element-by-element product.

The following corollary specifies the structure of IOX at locations in \mathcal{S} .

Corollary 2.1. If $\boldsymbol{\ell} \in \mathcal{S}$ then $\mathbf{h}_i(\boldsymbol{\ell})\mathbf{L}_i = \mathbf{L}_i[\boldsymbol{\ell}, :]$, the row of \mathbf{L}_i corresponding to $\boldsymbol{\ell}$. Then,

$$\mathbf{C}(\mathcal{S}) = (\boldsymbol{\Sigma} \otimes \mathbf{1}_{n,n}) \odot \mathbf{K} = \{\oplus \mathbf{L}_i\}(\boldsymbol{\Sigma} \otimes \mathbf{I}_n)\{\oplus \mathbf{L}_i^\top\}, \quad (3)$$

where \mathbf{K} is the $nq \times nq$ matrix whose (i, j) th block is $\mathbf{L}_i\mathbf{L}_j^\top$; $\mathbf{1}_{n,n}$ is the $n \times n$ matrix of 1s.

In (3), cross-variable dependence appears *inside*, spatial dependence is *outside*. In the LMC, where $\mathbf{C}(\mathcal{S}) = (\boldsymbol{\Lambda} \otimes \mathbf{I}_n)\{\oplus \rho_i(\mathcal{S})\}(\boldsymbol{\Lambda}^\top \otimes \mathbf{I}_n)$, where $\boldsymbol{\Lambda}\boldsymbol{\Lambda}^\top = \boldsymbol{\Sigma}$, cross-variable dependence appears *outside*, spatial dependence is *inside*.

Proposition 2.4. $\mathbf{C}(\boldsymbol{\ell}, \boldsymbol{\ell}')$ is a valid cross-covariance matrix function.

The main take-away of Proposition 2.4 is that IOX can be built upon any off-the-shelf univariate correlation functions without additional conditions or constraints. This yields flexibility in modeling outcome-specific features such as nonstationarities (as in Figure 2) or covariate dependence. The lack of additional restrictions distinguishes IOX from multivariate Matérns. We provide a more detailed comparison in the Supplement.

We establish a connection between IOX and LMCs in the separable or intrinsic specification, i.e. $\rho_i(\cdot, \cdot) = \rho(\cdot, \cdot)$ for all i . Separability is restrictive in forcing all outcomes to be modeled via the same spatial covariance (with the same range and smoothness).

Proposition 2.5. In the separable specification, i.e., $\rho_i(\cdot, \cdot) = \rho(\cdot, \cdot)$ for all i , IOX and LMC coincide at \mathcal{S} .

Finally, define $\mathcal{T} = \mathcal{S} \cup \{\boldsymbol{\ell}, \boldsymbol{\ell}'\}$ with $\boldsymbol{\ell} \neq \boldsymbol{\ell}'$. The following proposition shows that the Schur complement of $\mathbf{C}(\mathcal{S})$ in $\mathbf{C}(\mathcal{T})$ is the zero matrix. If we assume a joint Gaussian distribution for all variables in \mathcal{T} , then this proposition implies that the observation vectors at $\boldsymbol{\ell}$ and $\boldsymbol{\ell}'$ are conditionally independent given their values at \mathcal{S} .

Proposition 2.6. Suppose $\boldsymbol{\ell}, \boldsymbol{\ell}' \in \mathcal{S}^c$, $\boldsymbol{\ell} \neq \boldsymbol{\ell}'$. Then, $\mathbf{C}(\boldsymbol{\ell}, \boldsymbol{\ell}') - \mathbf{C}(\boldsymbol{\ell}, \mathcal{S})\mathbf{C}(\mathcal{S})^{-1}\mathbf{C}(\mathcal{S}, \boldsymbol{\ell}') = \mathbf{0}$.

Finally, IOX allows outcome-specific nugget effects without impacting the validity of the resulting cross-covariance matrix function. Because the measurement error process may be unrelated to the underlying multivariate spatial process, we seek flexibility in modeling nugget effects independently from other model components. Suppose for each $j = 1, \dots, q$ we let $\rho_j(\boldsymbol{\ell}, \boldsymbol{\ell}') = (1 - \alpha)\rho_j^*(\boldsymbol{\ell}, \boldsymbol{\ell}') + \alpha\mathbb{1}_{\{\boldsymbol{\ell}=\boldsymbol{\ell}'\}}$, where $\alpha \in (0, 1)$. This parametrization leads to a decomposition of $C_{jj}(\boldsymbol{\ell}, \boldsymbol{\ell}) = \sigma_{ii}$ into purely spatial variance $\sigma_{ii}(1 - \alpha)$ and nugget effect $\sigma_{ii}\alpha$. It is possible to parametrize each $\rho_j(\boldsymbol{\ell}, \boldsymbol{\ell}')$ more freely; in the Supplement, we show that IOX can be defined on the basis of q univariate covariance functions without compromising the validity of the approach.

Because IOX allows outcome-specific nugget effects, it is more flexible than a LMC. Refer to the Supplement for a more in-depth discussion of nugget effects and LMCs. We have shown that IOX is a valid cross-covariance matrix function. We can define a GP based on it, which we call the GP-IOX. The next section details properties and develops models based on GP-IOX.

3 IOX Gaussian process models

Let $\mathbf{C}(\cdot, \cdot)$ be the IOX cross-covariance matrix function (2), denote $\mathbf{Q} = \boldsymbol{\Sigma}^{-1}$, and let $\mathcal{S} = \{\boldsymbol{\ell}_1, \dots, \boldsymbol{\ell}_n\}$ be the set of observed locations. To simplify exposition, we assume we observe all outcomes at all locations. Let \mathbf{Y} as the $n \times q$ matrix whose (i, j) entry is $y_j(\boldsymbol{\ell}_i)$. Finally, $\mathbf{y} = \text{vec}(\mathbf{Y}) = (\mathbf{y}_1^\top, \dots, \mathbf{y}_q^\top)^\top$ and $\mathbf{y}(\boldsymbol{\ell}_i) = (y_1(\boldsymbol{\ell}_i), \dots, y_q(\boldsymbol{\ell}_i))^\top$. Define \mathbf{W} , \mathbf{w}_j , and $\mathbf{w}(\boldsymbol{\ell}_i)$ similarly. We begin this section by studying the joint density induced by GP-IOX on \mathcal{S} as well the density of one process component conditional on all others. We then move to defining response and latent models using GP-IOX.

Proposition 3.1. Let $\mathbf{w}(\cdot) \sim GP(\mathbf{0}, \mathbf{C}(\cdot, \cdot))$. The GP-IOX log-density is

$$\log p(\mathbf{w} \mid \boldsymbol{\theta}, \mathbf{Q}) = \text{const} + \frac{n}{2} \log \det(\mathbf{Q}) + \sum_{ij} \log \mathbf{L}_j^{-1}[i, i] - \frac{1}{2} \text{Tr}(\mathbf{V} \mathbf{Q} \mathbf{V}^\top), \quad (4)$$

where $\mathbf{L}_j^{-1}[i, i]$ is the i th diagonal element of \mathbf{L}_j^{-1} , and \mathbf{V} is the $n \times q$ matrix whose j th row is $\mathbf{v}_j = \mathbf{L}_j^{-1} \mathbf{w}_j$.

A consequence of Proposition 3.1 is that, for a given \mathbf{V} and without additional assumptions on \mathbf{Q} , evaluating (4) scales as $O(nq^2)$. Therefore, the scalability of IOX to large n depends on the complexity of computing \mathbf{V} , which is the matrix we obtain by spatial “whitening” each column of \mathbf{W} . Section 4.3 details how to scalably compute \mathbf{V} . IOX also leads to easy-to-evaluate conditional densities $p(\mathbf{w}_j \mid \mathbf{w}_{j^c}, \boldsymbol{\theta}, \mathbf{Q})$, where $j^c = \{1, \dots, q\} \setminus \{j\}$. We use the following result to develop posterior sampling algorithms in Sections 4.1 and 4.2.

Proposition 3.2 (Conditional density). $p(\mathbf{w}_j \mid \mathbf{w}_{j^c}, \boldsymbol{\theta}, \mathbf{Q}) = N(\mathbf{w}_j; \mathbf{m}_j, \mathbf{M}_j)$, where $\mathbf{m}_j = -\mathbf{L}_j \sum_{r \in j^c} \frac{Q_{jr}}{Q_{jj}} \mathbf{v}_r$ and $\mathbf{M}_j^{-1} = Q_{jj} \rho_j(\mathcal{S})^{-1}$. Then, we evaluate $\log N(\mathbf{w}_j; \mathbf{m}_j, \mathbf{M}_j)$ as:

$$\begin{aligned} \log N(\mathbf{w}_j; \mathbf{m}_j, \mathbf{M}_j) &\propto -\frac{1}{2} \log |\mathbf{M}_j| - \frac{1}{2} (\mathbf{w}_j - \mathbf{m}_j)^\top \mathbf{M}_j^{-1} (\mathbf{w}_j - \mathbf{m}_j) \\ &= \frac{n}{2} \log Q_{jj} + \sum_{i=1}^n \log \mathbf{L}_j^{-1}[i, i] - \frac{1}{2Q_{jj}} \mathbf{Q}_j \cdot \mathbf{V}^\top \mathbf{V} \mathbf{Q}_j^\top, \end{aligned} \quad (5)$$

where Q_{jr} is the (j, r) th element and $\mathbf{Q}_j \cdot$ is the j th row of \mathbf{Q} .

3.1 Multivariate response model

We model the observed process directly as a GP-IOX. We assume all outcomes share a common set of p predictors; generalizations to outcome-specific sets of predictors are straightforward. Specifically, we let $\mathbf{y}(\cdot) \sim GP(\mathbf{B}^\top \mathbf{x}(\cdot), \mathbf{C}(\cdot, \cdot))$, where $\mathbf{x}(\boldsymbol{\ell})$ is the $p \times 1$ vector of predictors at any $\boldsymbol{\ell} \in \mathcal{D}$, and \mathbf{B} is a $p \times q$ matrix whose j th column, $\boldsymbol{\beta}_j$, represents the linear covariate effects on the j th outcome. Denote $\boldsymbol{\beta} = \text{vec}(\mathbf{B})$ and \mathbf{X} the $n \times p$ matrix

storing the covariates at \mathcal{S} . Propositions 3.1 and 3.2 apply to the centered process $\tilde{\mathbf{y}}(\cdot) = \mathbf{y}(\cdot) - \mathbf{B}^T \mathbf{x}(\cdot)$. For simplicity, we let $\rho_i(\cdot, \cdot) = \rho(\cdot, \cdot; \boldsymbol{\theta}_i)$, $i = 1, \dots, q$, and $\boldsymbol{\theta} = (\boldsymbol{\theta}_1^\top, \dots, \boldsymbol{\theta}_q^\top)^\top$.

We obtain

$$\mathbf{y} \sim N(\mathbf{X}_q \boldsymbol{\beta}, \mathbf{C}), \quad \mathbf{C} = \{\oplus \mathbf{L}_i\}(\boldsymbol{\Sigma} \otimes \mathbf{I}_n)\{\oplus \mathbf{L}_i^\top\}, \quad (6)$$

where $\mathbf{X}_q = \mathbf{I}_q \otimes \mathbf{X}$. We assign the priors $\boldsymbol{\Sigma} \sim \mathcal{W}^{-1}(\nu_\Sigma, \boldsymbol{\Psi}^{-1})$ (the inverse Wishart distribution with scale matrix $\boldsymbol{\Psi}^{-1}$ and ν_Σ degrees of freedom), $\boldsymbol{\beta} \sim N(\mathbf{m}_\beta, \mathbf{M}_\beta)$, and $\boldsymbol{\theta} \sim p(\boldsymbol{\theta})$, yielding conditionally conjugate updates for $\boldsymbol{\beta}$ and $\boldsymbol{\Sigma}$ (see Section 4.1).

3.2 Latent model

We specify the latent model as $\mathbf{y}(\cdot) = \mathbf{B}^T \mathbf{x}(\cdot) + \mathbf{w}(\cdot) + \boldsymbol{\varepsilon}(\cdot)$, where $\mathbf{w}(\cdot) \sim GP(\mathbf{0}, \mathbf{C}(\cdot, \cdot))$, $\boldsymbol{\varepsilon}(\boldsymbol{\ell}) \stackrel{iid}{\sim} N(\mathbf{0}, \boldsymbol{\Delta})$, and $\boldsymbol{\Delta}$ is a $q \times q$ covariance matrix. This yields:

$$\begin{aligned} \mathbf{y} &= \mathbf{X}_q \boldsymbol{\beta} + \mathbf{w} + \boldsymbol{\varepsilon}, & \boldsymbol{\varepsilon} &\sim N(\mathbf{0}, \boldsymbol{\Delta} \otimes \mathbf{I}_n), \\ \mathbf{w} &\sim N(\mathbf{0}, \mathbf{C}), & \mathbf{C} &= \{\oplus \mathbf{L}_i\}(\boldsymbol{\Sigma} \otimes \mathbf{I}_n)\{\oplus \mathbf{L}_i^\top\}, \end{aligned} \quad (7)$$

where all parameters that appear in both (6) and (7) can be assigned the same prior distributions. Although $\boldsymbol{\Delta}$ can be dense, we assume it is diagonal for simplicity, and assign the priors $\delta_{ii} \stackrel{iid}{\sim} Inv.G(a_d, b_d)$ for $i = 1, \dots, q$; therefore, \mathbf{w} captures all cross-outcome dependence as a q -variate noise-free GP-IOX. The latent model can be extended further: in the Supplement, we propose a latent factor model which assumes $\boldsymbol{\Sigma}$ is low-rank.

Although (7) has a Gaussian first stage, we can straightforwardly generalize to binomial and negative-binomial data via data augmentation schemes (Albert & Chib 1993, Polson et al. 2013). Our hierarchical setup remains useful in more general settings: efficient Hamiltonian Monte Carlo methods that use second order information about the target density have connections with Gibbs sampling of Gaussian models (see Girolami & Calderhead 2011, or Peruzzi & Dunson 2024 for the multivariate spatial setting).

3.3 Predictions at new locations

Having chosen \mathcal{S} as the set of observed locations, denote $\mathcal{T} = \{\mathbf{t}_1, \dots, \mathbf{t}_N\}$ as the test set. For any zero-mean multivariate GP $\mathbf{w}(\cdot)$ with cross-covariance matrix function $\mathbf{K}(\cdot, \cdot)$, the distribution of the Nq -dimensional vector $\mathbf{w}(\mathcal{T})$ conditional on $\mathbf{w} = \mathbf{w}(\mathcal{S})$ is Gaussian, with mean $\mathbf{K}(\mathcal{T}, \mathcal{S})\mathbf{K}(\mathcal{S})^{-1}\mathbf{w}$ and covariance $\mathbf{K}(\mathcal{T}) - \mathbf{K}(\mathcal{T}, \mathcal{S})\mathbf{K}(\mathcal{S})^{-1}\mathbf{K}(\mathcal{S}, \mathcal{T})$. In GP-IOX, Proposition 2.6 implies that $\text{cov}(\mathbf{w}(\mathbf{t}_r), \mathbf{w}(\mathbf{t}_s) \mid \mathbf{w}) = 0$ if $\mathbf{t}_r \neq \mathbf{t}_s$, i.e., $\mathbf{w}(\mathbf{t}_r)$ and $\mathbf{w}(\mathbf{t}_s)$ are conditionally independent given the data; therefore, we can focus on marginal predictions of the outcome vector at individual locations.

For a new location $\mathbf{t} \notin \mathcal{S}$, let $\mathbf{H}(\mathbf{t}) = \mathbf{C}(\mathbf{t}, \mathcal{S})\mathbf{C}(\mathcal{S})^{-1}$ and $\mathbf{R}(\mathbf{t}) = \mathbf{C}(\mathbf{t}) - \mathbf{H}(\mathbf{t})\mathbf{C}(\mathcal{S}, \mathbf{t})$. Then, in the response model, for every posterior sample of Σ, β, θ we draw from $p(\mathbf{y}(\mathbf{t}) \mid \mathbf{y}, \beta, \Sigma, \theta) = N(\mathbf{m}_y(\mathbf{t}), \mathbf{R}(\mathbf{t}))$ for each $\mathbf{t} \in \mathcal{T}$, where $\mathbf{m}_y(\mathbf{t}) = \mathbf{B}^T \mathbf{x}(\mathbf{t}) + \mathbf{H}(\mathbf{t})(\mathbf{y} - \mathbf{X}_q \beta)$. In the latent model, for every posterior sample of $\beta, \mathbf{w}, \Sigma, \theta, \Delta$ we sample $\mathbf{w}(\mathbf{t})$ from $p(\mathbf{w}(\mathbf{t}) \mid \mathbf{w}, \Sigma) = N(\mathbf{m}_w(\mathbf{t}), \mathbf{R}(\mathbf{t}))$, where $\mathbf{m}_w(\mathbf{t}) = \mathbf{H}(\mathbf{t})\mathbf{w}$, then let $\mathbf{y}(\mathbf{t}) = \mathbf{B}^T \mathbf{x}(\mathbf{t}) + \mathbf{w}(\mathbf{t}) + \Delta^{\frac{1}{2}}\mathbf{u}$ where $\mathbf{u} \sim N(\mathbf{0}, \mathbf{I}_q)$. The following proposition clarifies that IOX maintains for predictions the same marginal structure we outlined in Proposition 2.1; spatial cross-variable dependence in predictions is induced by the off-diagonal elements of $\mathbf{R}(\mathbf{t})$.

Proposition 3.3. $\mathbf{H}(\mathbf{t}) = \{\oplus \mathbf{h}_i(\mathbf{t})\}$ and $\mathbf{R}(\mathbf{t}) = \mathbf{D}(\mathbf{t}, \mathbf{t})\Sigma\mathbf{D}(\mathbf{t}, \mathbf{t})$. For $\mathbf{t} \notin \mathcal{S}$, $p(w_i(\mathbf{t}) \mid \mathbf{w}, \theta, \Sigma)$ only depends on $\rho_i(\cdot, \cdot)$ at \mathcal{S} , σ_{ii} and \mathbf{w}_i .

For predictions on $w_i(\mathbf{t})$ to depend on the entire \mathbf{W} , we can extend \mathcal{S} to include \mathbf{t} , then condition on data at $\mathcal{S} \setminus \{\mathbf{t}\}$. We demonstrate this via Proposition 3.4 for the case $q = 2$ and $\mathcal{S} = \{\ell_1, \ell_2\}$ without loss of generality.

Proposition 3.4. Suppose $q = 2$ and $\mathcal{S} = \{\ell_1, \ell_2\}$. Then $p(w_i(\ell_r) \mid \mathbf{w}(\ell_s))$ depends on both $w_i(\ell_s)$ and $w_j(\ell_s)$, for each choice of $i, j, r, s \in \{1, 2\}$, $i \neq j$ and $r \neq s$.

Proposition 3.4 clarifies how in the latent model (i.e., noisy observation of a smooth process), IOX borrows information across all observed data \mathbf{y} to recover the underlying signal \mathbf{w} . Although the set \mathcal{S} can be augmented with unobserved locations to allow marginal predictions to depend on all data, computational cost scales with the size of \mathcal{S} (see Supplement), exposing a trade-off between flexibility in predictions and computational efficiency. Finally, we study $p(\mathbf{w}_m(\mathbf{t}) \mid \mathbf{w}_o(\mathbf{t}), \mathbf{w})$, where $o \subset \{1, \dots, q\}$ (for *observed*) and $m = \{1, \dots, q\} \setminus o$ (for *missing*) its complement. Intuitively, we want to predict $\mathbf{w}_m(\mathbf{t})$ based not only on \mathbf{w} but also on $\mathbf{w}_o(\mathbf{t})$.

Proposition 3.5. $p(\mathbf{w}_m(\mathbf{t}) \mid \mathbf{w}_o(\mathbf{t}), \mathbf{w}) = N(\mathbf{w}_m(\mathbf{t}); \mathbf{h}_{m|o}, \mathbf{R}_{m|o}(\mathbf{t}))$, where $\mathbf{h}_{m|o} = \mathbf{H}_m(\mathbf{t})\mathbf{w} + \mathbf{H}_{m|o}(\mathbf{t})(\mathbf{w}_o(\mathbf{t}) - \mathbf{H}_o(\mathbf{t})\mathbf{w})$, $\mathbf{H}_o(\mathbf{t})$ is the submatrix of $\mathbf{H}(\mathbf{t})$ where we take the rows corresponding to o (similarly $\mathbf{H}_m(\mathbf{t})$ with rows m), and

$$\begin{aligned} \mathbf{H}_{m|o}(\mathbf{t}) &= \mathbf{D}_m(\mathbf{t}, \mathbf{t})\boldsymbol{\Sigma}_{m,o}\boldsymbol{\Sigma}_o^{-1}\mathbf{D}_o^{-1}(\mathbf{t}, \mathbf{t}) = -\mathbf{D}_m(\mathbf{t}, \mathbf{t})\mathbf{Q}_m^{-1}\mathbf{Q}_{m,o}\mathbf{D}_o^{-1}(\mathbf{t}, \mathbf{t}) \\ \mathbf{R}_{m|o}(\mathbf{t}) &= \mathbf{D}_m(\mathbf{t}, \mathbf{t})(\boldsymbol{\Sigma}_m - \boldsymbol{\Sigma}_{m,o}\boldsymbol{\Sigma}_o^{-1}\boldsymbol{\Sigma}_{o,m})\mathbf{D}_m(\mathbf{t}, \mathbf{t}) = \mathbf{D}_m(\mathbf{t}, \mathbf{t})\mathbf{Q}_m^{-1}\mathbf{D}_m(\mathbf{t}, \mathbf{t}), \end{aligned}$$

where $\boldsymbol{\Sigma}_{m,o}$ subsets $\boldsymbol{\Sigma}$ to its m rows and o columns, and similarly for \mathbf{Q} .

In particular, if $m = \{j\}$, $\mathbf{R}_{m|o}(\mathbf{t}) = \frac{r_j(\mathbf{t})}{Q_{jj}}$. In other terms, the predictive variance at an unobserved location when conditioning on all outcomes except j decreases if \mathbf{t} is close to \mathcal{S} based on $\rho_j(\cdot, \cdot)$, or when the other variables “explain” the j th variable (large Q_{jj}).

4 Computations with GP-IOX models

We outline the key details of posterior sampling for GP-IOX. Additional details, as well as methods for prior sampling of GP-IOX, are in the Supplement.

4.1 Posterior sampling of the multivariate response model

We target the posterior distribution $p(\boldsymbol{\Sigma}, \boldsymbol{\beta}, \boldsymbol{\theta} \mid \mathbf{y}) \propto p(\mathbf{y} \mid \boldsymbol{\Sigma}, \boldsymbol{\beta}, \boldsymbol{\theta})p(\boldsymbol{\Sigma})p(\boldsymbol{\theta})p(\boldsymbol{\beta})$. The sampling algorithm detailed in the Supplement is straightforward: $p(\boldsymbol{\beta} \mid \mathbf{y}, \boldsymbol{\Sigma}, \boldsymbol{\theta})$ is Gaussian; $p(\boldsymbol{\Sigma} \mid \mathbf{y}, \boldsymbol{\beta}, \boldsymbol{\theta})$ is inverse Wishart; $\boldsymbol{\theta}$ is updated via Metropolis-Hastings. There is a computational bottleneck in updating $\boldsymbol{\theta}$. A joint update targets $p(\boldsymbol{\theta} \mid \mathbf{y}, \boldsymbol{\beta}, \boldsymbol{\Sigma}) \propto p(\mathbf{y} \mid \boldsymbol{\theta}, \boldsymbol{\beta}, \boldsymbol{\Sigma})p(\boldsymbol{\theta})$, which we can evaluate using Proposition 3.1. A block update of $\boldsymbol{\theta}_j$ —the marginal correlation parameters for outcome j —targets $p(\boldsymbol{\theta}_j \mid \boldsymbol{\theta}_{j^c}, \mathbf{y})$. We assume independent prior $p(\boldsymbol{\theta}) = \prod_j p(\boldsymbol{\theta}_j)$, then (omitting other model parameters for simplicity) we find

$$p(\boldsymbol{\theta}_j \mid \boldsymbol{\theta}_{j^c}, \mathbf{y}) \propto p(\mathbf{y} \mid \boldsymbol{\theta}_j, \boldsymbol{\theta}_{j^c})p(\boldsymbol{\theta}_j \mid \boldsymbol{\theta}_{j^c}) = p(\mathbf{y}_j \mid \mathbf{y}_{j^c}, \boldsymbol{\theta})p(\mathbf{y}_{j^c} \mid \boldsymbol{\theta})p(\boldsymbol{\theta}_j) \propto p(\mathbf{y}_j \mid \mathbf{y}_{j^c}, \boldsymbol{\theta})p(\boldsymbol{\theta}_j),$$

where we evaluate $p(\mathbf{y}_j \mid \mathbf{y}_{j^c}, \boldsymbol{\theta})$ via Proposition 3.2. We use joint updates of $\boldsymbol{\theta}$ when q is small (e.g., Section 5.1), and block updates in all other settings.

4.2 Posterior sampling of the latent model

We sample from the joint posterior $p(\mathbf{w}, \boldsymbol{\beta}, \boldsymbol{\Sigma}, \boldsymbol{\Delta}, \boldsymbol{\theta} \mid \mathbf{y})$ by iterating through all full conditional distributions. In particular, the full conditional posterior distribution of \mathbf{w} is $p(\mathbf{w} \mid \mathbf{y}, \boldsymbol{\beta}, \boldsymbol{\Sigma}, \boldsymbol{\Delta}, \boldsymbol{\theta}) = N(\mathbf{m}_{\mathbf{w}|\mathbf{y}}, \mathbf{M}_{\mathbf{w}|\mathbf{y}})$, where

$$\mathbf{M}_{\mathbf{w}|\mathbf{y}}^{-1} = \mathbf{C}^{-1} + (\boldsymbol{\Delta}^{-1} \otimes \mathbf{I}_n) \quad \text{and} \quad \mathbf{M}_{\mathbf{w}|\mathbf{y}}^{-1} \mathbf{m}_{\mathbf{w}|\mathbf{y}} = (\boldsymbol{\Delta}^{-1} \otimes \mathbf{I}_n)(\mathbf{y} - \mathbf{X}_q \boldsymbol{\beta}),$$

which requires to solve a linear system on $\mathbf{M}_{\mathbf{w}|\mathbf{y}}^{-1}$ to compute $\mathbf{m}_{\mathbf{w}|\mathbf{y}}$; this operation is costly since $\mathbf{M}_{\mathbf{w}|\mathbf{y}}^{-1}$ has dimension $nq \times nq$. Alternatively, we can update \mathbf{w}_j given \mathbf{w}_{j^c} and the data for a sequential single-outcome sampler: we write the hierarchical model as

$$\mathbf{w}_j \mid \mathbf{w}_{j^c} \sim N(\mathbf{m}_j, \mathbf{M}_j), \quad \mathbf{y}_j = \mathbf{X} \boldsymbol{\beta}_j + \mathbf{w}_j + \boldsymbol{\varepsilon}_j, \quad \boldsymbol{\varepsilon}_j \sim N(\mathbf{0}, \delta_{jj} \mathbf{I}_n),$$

where \mathbf{M}_j and \mathbf{m}_j are the same as in Proposition 3.2, except we replace \mathbf{y} with \mathbf{w} . Then, we update \mathbf{w}_j via its conditional posterior $N(\mathbf{w}_j; \mathbf{m}_{\mathbf{w}_j|\mathbf{y}_j}, \mathbf{M}_{\mathbf{w}_j|\mathbf{y}_j})$, where $\mathbf{M}_{\mathbf{w}_j|\mathbf{y}_j} = (\mathbf{M}_j^{-1} +$

$\frac{1}{\delta_{jj}}\mathbf{I}_n)^{-1}$ and $\mathbf{M}_{w_j|y_j}^{-1}\mathbf{m}_{w_j|y_j} = \mathbf{M}_j^{-1}\mathbf{m}_j + \frac{1}{\delta_{jj}}(\mathbf{y}_j - \mathbf{X}\boldsymbol{\beta}_j)$. We compute $\mathbf{M}_j^{-1}\mathbf{m}_j$ directly as

$$\mathbf{M}_j^{-1}\mathbf{m}_j = \mathbf{Q}_{jj}\mathbf{L}_j^{-\top}\widetilde{\mathbf{W}}_{j^c}\boldsymbol{\Sigma}_{j^c}^{-1}\boldsymbol{\Sigma}_{j^c,j} = -\mathbf{L}_j^{-\top}\widetilde{\mathbf{W}}_{j^c}\mathbf{Q}_{j^c,j},$$

where $\widetilde{\mathbf{W}}_{j^c}$ is the $n \times q - 1$ matrix such that $\text{vec}(\widetilde{\mathbf{W}}_{j^c}) = \{\oplus_{j^c}\mathbf{L}_r^{-1}\}\mathbf{w}_{j^c}$. The bottleneck here is computing the conditional covariances $\mathbf{M}_{w_j|y_j}$ (i.e., solving the linear system $\mathbf{M}_{w_j|y_j}^{-1}\mathbf{x} = \mathbf{b}$), but each of them can be computed efficiently in parallel – for large n , we use the methods of Section 4.3. The sequential portion of the algorithm is the computation of $\mathbf{M}_j^{-1}\mathbf{m}_j$ and subsequent sampling of \mathbf{w}_j . The remainder of our posterior sampling algorithm requires to sample $\boldsymbol{\beta}$ from its Gaussian full conditional posterior distribution, whereas $\boldsymbol{\Sigma}$ is conditionally sampled from an inverse Wishart distribution and the diagonal elements of $\boldsymbol{\Delta}$ from an inverse Gamma distribution. Updating $\boldsymbol{\theta}$ proceeds like in the response model after replacing \mathbf{y} with \mathbf{w} . Additional details are in the Supplement, which also includes the single-site sampler for updating $\mathbf{w}(\ell_i)$ given $\mathbf{w}(\mathcal{S} \setminus \{\ell_i\})$.

4.3 Scaling IOX to high dimensional data

If n is large, computing \mathbf{L}_i or \mathbf{L}_i^{-1} for each $i = 1, \dots, q$ from $\rho_i(\mathcal{S})$ is prohibitively costly. We can easily construct GP-IOX based on Vecchia approximations and sparse DAGs, resulting in fast likelihood-based inference. Suppose $p(\mathbf{z})$ is the joint density of a $n \times 1$ vector \mathbf{z} at locations $\mathcal{S} = \{\ell_1, \dots, \ell_n\}$. Vecchia (1988) proposed the approximation $p(\mathbf{z}) \approx \prod_i p(z_i | \mathbf{z}_{N_m(i)})$, where $\mathbf{z}_{N_m(i)}$ is the subset of \mathbf{z} at the m locations closest to ℓ_i within the set $\{\ell_1, \dots, \ell_{i-1}\}$. This approximation yields a valid standalone stochastic process (Datta et al. 2016), and can be generalized to any underlying DAG across \mathcal{S} locations, see, e.g., Katzfuss & Guinness (2021), Peruzzi et al. (2022), Zhu et al. (2024). We can understand a DAG-based GP such as a nearest-neighbor GP (Datta et al. 2016) or any similarly constructed GP in two manners. First, they are approximations of a parent GP with correlation function

$\rho(\cdot, \cdot)$. Equivalently, they are exact GPs with (valid) correlation function $\tilde{\rho}(\cdot, \cdot)$, constructed from $\rho(\cdot, \cdot)$. We can thus build IOX and the corresponding GP-IOX directly using a set of $\tilde{\rho}_i(\cdot, \cdot)$, $i = 1 \dots, q$. By Proposition 2.4, the resulting IOX cross-covariance matrix function inherits its validity from the validity of each $\tilde{\rho}_i(\cdot, \cdot)$. Working with $\tilde{\rho}(\cdot, \cdot)$, we have $\tilde{\rho}(\mathcal{S}) = \tilde{\mathbf{L}}\tilde{\mathbf{L}}^\top = (\mathbf{I}_n - \mathbf{H})^{-1}\mathbf{R}^{\frac{1}{2}}\mathbf{R}^{\frac{1}{2}}(\mathbf{I}_n - \mathbf{H})^{-\top}$, where \mathbf{H} is a lower triangular $n \times n$ matrix with zero diagonal whose (i, j) entry is nonzero if and only if $j \rightarrow i$ in the DAG. Letting $[i]$ be the set of indices of the non-zero columns of \mathbf{H} at row i , the nonzeros at row i are $\mathbf{h}_i = \rho(\boldsymbol{\ell}_i, \boldsymbol{\ell}_{[i]})\rho(\boldsymbol{\ell}_{[i]})^{-1}$, i.e., the value of \mathbf{H} at $(i, [i]_r)$ is the r th element of \mathbf{h}_i . Building \mathbf{H} and $\tilde{\mathbf{L}}^{-1} = \mathbf{R}^{-\frac{1}{2}}(\mathbf{I}_n - \mathbf{H})$ requires $O(nm^3)$ flops. The posterior sampling algorithms we outlined in Sections 3.1 and 3.2 only involve \mathbf{L}_i^{-1} for $i = 1, \dots, q$, therefore they scale to large n when using $\tilde{\mathbf{L}}_i^{-1}$. Both response and latent models benefit from these methods in evaluating the likelihood for updating $\boldsymbol{\theta}$ (either the joint of (4) or the conditional of (5)). The sparse DAG yields efficient, single-site sampling of \mathbf{w} , as we detail in the Supplement.

Finally, if some outcomes require conditioning sets that include locations farther in space (Stein et al. 2004), one just needs to choose the appropriate outcome-specific DAG and build $\tilde{\mathbf{L}}_i^{-1}$ accordingly for each $i = 1, \dots, q$. Doing so in LMCs is not as straightforward because a factor-specific DAG does not translate to the same DAG for any of the outcomes.

If q is large, computing and storing \mathbf{L}_i for each $i = 1, \dots, q$ and each MCMC iteration becomes computationally intensive, even with methods based on sparse DAG as outlined above. We suggest two possible ways to reduce the computational overhead in large q settings. First, we can assume that not all outcome have distinct marginal correlation parameters. If outcomes can be grouped into G groups, then the number of distinct \mathbf{L}_i that need to be computed at each MCMC iteration is G or less. Second, we may assign $\boldsymbol{\theta}$ a categorical distribution and precompute all corresponding \mathbf{L}_i 's once. Even if the number

of options is large, these matrices are never updated during MCMC, leading to massive computational savings. Choosing the correlation hyperparameters from a fixed grid is common in cross-validatory approaches, see, e.g., Shirota et al. (2019), Zhang et al. (2021), Zhang & Banerjee (2022). We refer to this method as *IOX Grid* in Section 5.

5 Applications

We test GP-IOX in three settings: first, we consider simulated datasets with $q = 3$ outcomes to compare IOX to state-of-the-art methods for fitting multivariate Matérn models. Then, we increase the number of outcomes to $q = 24$ in order to showcase the performance of IOX and related dimension reduction methods in higher dimensional settings. Finally, we analyze a spatial proteomics dataset collected as part of a colorectal cancer study.

5.1 Toy examples on trivariate data

We analyze two scenarios. First, we sample from GP-IOX with Matérn margins, whereas in the second, we sample from a GP with multivariate Matérn cross-covariance. When we build IOX with univariate Matérn margins, the marginal covariance parameters of both IOX and multivariate Matérn models have the same interpretations. Therefore, we can cross-test the performance of IOX in estimating marginal parameters of multivariate Matérns, and, vice versa, the performance of a multivariate Matérn model in estimating marginal parameters of an IOX with Matérn margins. We include a LMC for completeness.

We repeat the same analysis on 60 datasets for each scenario, for a total of 120 datasets. Each dataset measures three outcomes at a different set of 2,500 spatial locations which are sampled uniformly on $[0, 1]^2$. Refer to the Supplement for additional setup details. We evaluate the performance in estimating the marginal parameters as well as the cross-

IOX data	ρ_{21}	ρ_{31}	ρ_{32}	ν_1	ν_2	ν_3	ϕ_1	ϕ_2	ϕ_3	τ_1^2	τ_2^2	τ_3^2	Time
IOX Response	0.0045	0.0208	0.0188	0.1100	0.0335	0.0474	2.89	2.01	2.28	0.0089	0.0007	0.0005	12
IOX Latent Sequential single-site	0.0065	0.0198	0.0187	0.0803	0.0293	0.0836	3.25	2.11	3.90	0.0013	0.0004	0.0005	22
IOX Latent Sequential single-outcome	0.0058	0.0197	0.0184	0.0763	0.0285	0.0842	3.36	2.13	3.87	0.0006	0.0005	0.0005	41
Mult. Matérn	0.0098	0.0246	0.0226	0.1170	0.0620	0.0616	7.53	3.31	2.32	0.0209	0.0026	0.0006	3
LMC	0.0936	0.3510	0.4020							0.0252	0.0025	0.0020	13

Mult. Matérn data	ρ_{21}	ρ_{31}	ρ_{32}	ν_1	ν_2	ν_3	ϕ_1	ϕ_2	ϕ_3	τ_1^2	τ_2^2	τ_3^2	Time
IOX Response	0.0228	0.0533	0.0506	0.1030	0.0465	0.0539	2.84	2.23	2.21	0.0219	0.0016	0.0009	11
IOX Latent Sequential single-site	0.0100	0.0431	0.0440	0.0351	0.0462	0.0998	3.92	2.34	3.45	0.0056	0.0002	0.0004	21
IOX Latent Sequential single-outcome	0.0129	0.0452	0.0454	0.0258	0.0551	0.1050	4.29	2.53	3.43	0.0037	0.0001	0.0004	40
Mult. Matérn	0.0074	0.0180	0.0234	0.0527	0.0436	0.0473	4.03	2.92	2.10	0.0109	0.0013	0.0004	7
LMC	0.0643	0.3450	0.3920							0.0269	0.0032	0.0024	12

Table 1: Average RMSE and time in minutes for estimating model parameters across 60 IOX-generated datasets (top) and 60 multivariate Matérn-generated datasets (bottom). Lowest RMSEs in bold. Full box plots are available in the Supplement.

correlations at zero distance ρ_{ij} .

We fit an IOX response model with joint updates of θ (Section 4.1) and test both the single-outcome sampler (Section 4.2) and single-site sampler (Supplement) for the latent model in Section 3.2. All IOX models use a Vecchia approximation with $m = 15$ neighbors for scalability. A Vecchia-approximated ($m = 15$) multivariate Matérn model, as in Emery et al. (2022), is fit via maximum likelihood using GpGpm v0.4.0 (Fahmy & Guinness 2022), available on GitHub. Posterior sampling for the LMC is performed with the meshed R package, version 0.3, available at <https://github.com/mkln/meshed>. Table 1 reports the root mean squared error (RMSE) for parameter estimation (averaged across datasets) and average wall clock time for model fitting. The Supplement includes summary box plots providing additional details. Timing refers to maximum likelihood for the Matérn model

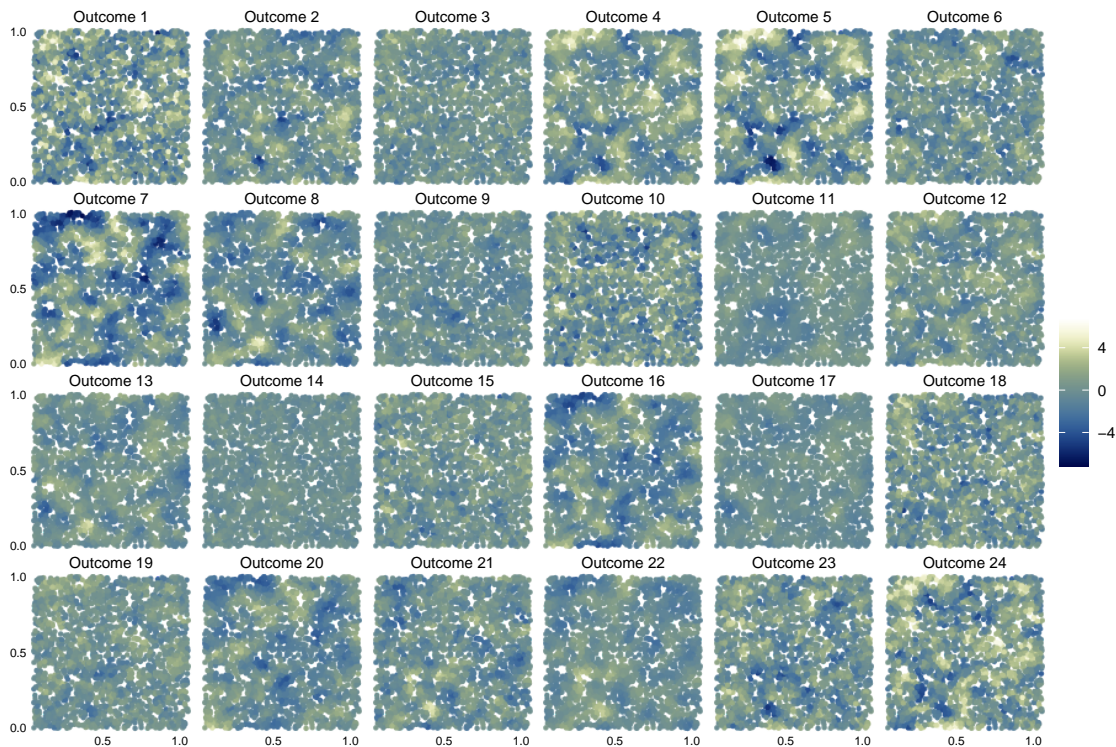


Figure 5: The first of 20 datasets sampled from GP-IOX for the comparison of Section 5.2.

and a 10,000-iteration MCMC chain for all others. The LMC model does not estimate outcome-specific spatial decay or smoothness, leaving those table cells blank.

Models based on GP-IOX outperform others in the estimation of all parameters in the IOX data scenario and are competitive in the multivariate Matérn scenario, achieving very similar when not better performance than the correctly specified multivariate Matérn model. The LMC lacks the flexibility in modeling these data, resulting in inferior performance in estimating the cross-correlation at zero.

5.2 Comparisons on spatial data with 24 outcomes

We move to the much more challenging problem of fitting multivariate models on data with $q = 24$ spatially correlated outcomes. We simulate 40 datasets, each of which includes synthetic data at a different set of $n = 2,500$ spatial locations distributed uniformly on

Method	IOX data					LMC data			
	ρ_{ij}	ν_j	Predictions (full)	Predictions (partial)	Time	ρ_{ij}	Predictions (full)	Predictions (partial)	Time
IOX Full	0.0167	0.0692	0.482	0.123	40	0.162	1.22	1.15	66
IOX Grid	0.0250	0.169	0.490	0.140	4.1	0.234	1.45	1.46	11
LMC	0.270		0.685	0.631	15	0.312	1.15	1.08	34
NNGP Indep. univariate	0.106	0.124	0.483		76	0.123	1.21		55
Non-spatial model	0.0610			0.386	3	0.0921		1.27	3

Table 2: RMSE in estimating $\rho_{ij}, i < j$, RMSPE in predicting $\mathbf{y}(\cdot)$ at 400 new locations (full vector or a random set of 4 variables, given the others), and wall clock time (in minutes) in two data scenarios, averaged across outcomes and 20 datasets for each of the two scenarios. Lowest RMSE or RMSPE in bold. Full box plots are available in the Supplement.

$[0, 1]^2$. The effective dimension of each dataset is $nq = 60,000$. Of the 40 datasets, we generate 20 by sampling from a GP-IOX, 20 from a LMC built on $k = 8$ latent processes. Refer to the Supplement for additional setup details.

In both scenarios, we target the estimation of the cross-correlation between the 24 outcomes at zero spatial distance, as well as predictions at a test set of 400 locations located on a 20×20 grid (the same across all 40 datasets). We compare models based on RMSE in estimating the zero-distance correlations $\rho_{ij}, i < j$, averaged across datasets, as well as the marginal smoothness in the IOX-generated data. We split the prediction task into two subtasks. In the first (labeled “full”), we perform predictions of the entire vector of 24 outcomes. In the second (“partial”), we make predictions for 4 outcomes (randomly selected at each location in the test set) using data about the other 20. In both subtasks, none of the data in the test set is used to train any of the models; we compare models via root mean square prediction error (RMSPE), averaged across datasets and variables.

We test estimation and prediction performance of several variants of the GP-IOX re-

sponse model: *IOX Full* estimates ϕ_j, ν_j, τ_j^2 in the IOX-generated data, whereas fixes $\nu_j = 1$ in the LMC-generated data, using Metropolis-within-Gibbs updates of $\boldsymbol{\theta}$ as described in Section 4.1; *IOX Grid* fixes $\phi_j = 30, \tau^2 = 10^{-3}$ for all j in the IOX-generated data scenario, and assumes a uniform prior on ν_j on a sequence of 30 equally-spaced numbers starting at 0.5 and ending at 2. We fit a scalable LMC with R package `meshed` (v0.3), fixing $k = 6$ in the IOX-generated data and $k = 8$ for LMC-generated data. Finally, we compare with spatial univariate methods and non-spatial multivariate methods. For the former, we fit 24 independent univariate NNGP models to each of the 40 datasets using R package `spNNGP` (Finley et al. 2022): in IOX-generated datasets, we fix $\phi_j = 30$ for all j and estimate smoothness, nugget effect, and variance. In LMC-generated datasets, we fix $\nu_j = 1$ for all j and estimate decay, nugget effect, and variance. We compute ρ_{ij} for the NNGP models as the correlation between samples from the posterior predictive distributions. The nonspatial multivariate method simply assumes $\mathbf{y}(\boldsymbol{\ell}) \stackrel{iid}{\sim} N(\mathbf{0}, \boldsymbol{\Sigma})$. Timing for all methods is calculated as model fitting plus prediction time. Model fitting for all methods involves MCMC for 10,000 iterations, discarding the first half as burn-in.

Table 2 summarises the result of this comparison; box plots are available in the Supplement. In the IOX data scenario, *IOX Full* outperforms all other methods and the LMC offers inferior performance to both spatial univariate and nonspatial multivariate methods. This result confirms the theoretical finding that LMCs are a poor fit for variables with different smoothness. In the LMC scenario, IOX-based models outperform the LMC in estimating zero-distance correlations; however, the non-spatial model is associated with the smallest average RMSE. In the prediction tasks, *IOX Full* exhibits similar performance to the LMC, demonstrating the flexibility of our proposed approach in diverse scenarios. In terms of compute time, the *IOX Full* model is comparable to a set of independent uni-

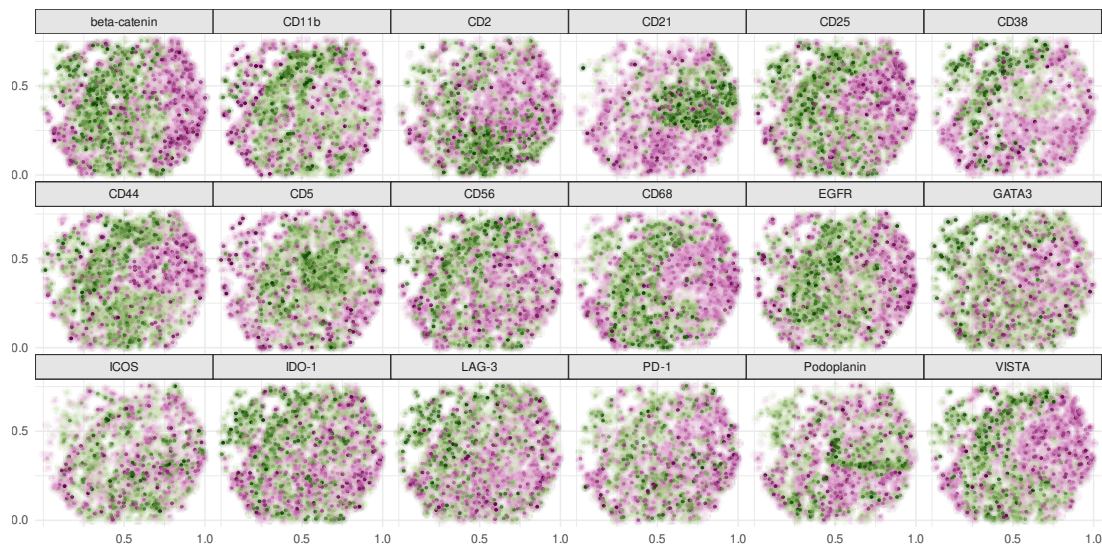


Figure 6: CRC CODEX data on 18 protein markers of a CRC patient. Green color corresponds to higher log-intensity of the marker.

variate models, demonstrating that IOX scales to large data settings in practice. The *IOX Grid* is computationally inexpensive but exhibits inferior overall performance relative to *Full*; therefore, it could be used as an exploratory tool in practice.

5.3 Cancer proteomics CODEX data

The tumor microenvironment (TME) is a heterogeneous ecosystem of cancer, stromal, and immune cells within extracellular matrix. The TME profoundly shapes oncogenesis, metastasis, and therapy response (Hanahan & Weinberg 2011, de Visser & Joyce 2023). Patient-derived tissues analyzed by advanced multiplexed imaging yield spatially resolved single-cell data linking protein markers, cellular phenotypes, and clinical variables. Within the TME, disease-specific co-localization patterns inform immune dynamics and prognosis (Yuan 2016, Giraldo et al. 2019, Tsujikawa et al. 2020).

We consider a colorectal cancer dataset previously analyzed in Schürch et al. (2020). This dataset was generated using co-detection by indexing (CODEX) technology optimized

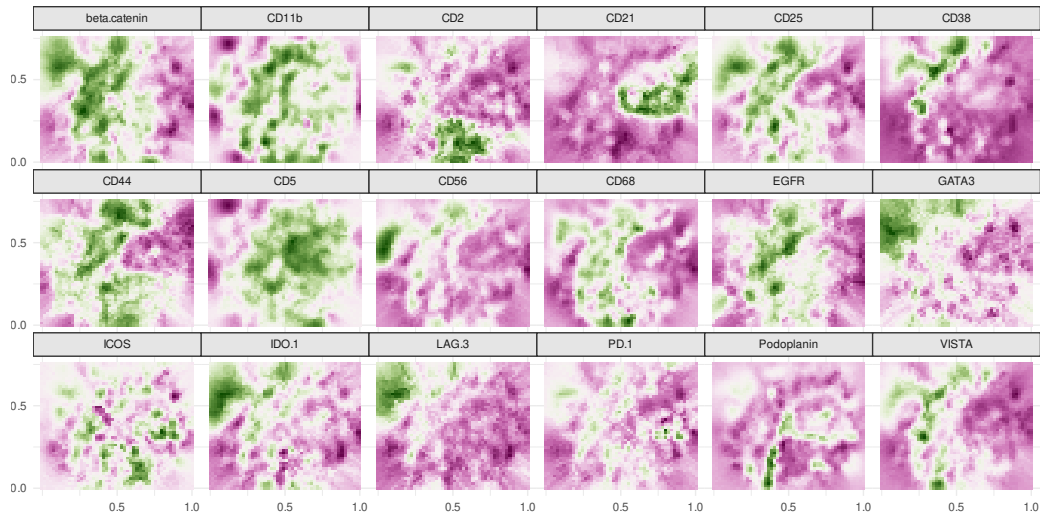


Figure 7: Intensity maps of the 18 protein markers from CRC CODEX data obtained via IOX (*Full* variant) by predicting the entire vector of variables at 2500 equally-spaced locations.

Method	APE (s.e.)	CRPS (s.e.)	Time (min)
IOX	0.063 (0.0065)	0.1823 (0.0085)	59
LMC $k = 6$	0.0699 (0.0076)	0.1962 (0.0089)	37
LMC $k = 8$	0.0675 (0.0074)	0.1922 (0.0090)	52
Non-spatial model	0.0686 (0.0066)	0.1978 (0.0089)	1

Table 3: Average percentage error, continuous rank probability score, and runtime in minutes of two IOXmodels, two LMCs, and a non-spatial model, on the CODEX CRC data analysis.

for formalin-fixed, paraffin-embedded tissue and tissue microarrays, leading to immunofluorescence imaging of the immune TME on 140 tissue regions of 35 advanced-stage colorectal cancer (CRC) patients. We restrict our analysis to a single tissue image (spot *55A*) from patient 28, and consider the 18 most common protein markers in this tissue. At each spatial location, the data include the intensity of expression of each of the 18 protein markers. After log-transforming the data, we obtain an aligned dataset of 18 continuous variables at 2,873 spatial locations, for a total dimension of 51,714. Figure 6 visualizes the dataset.

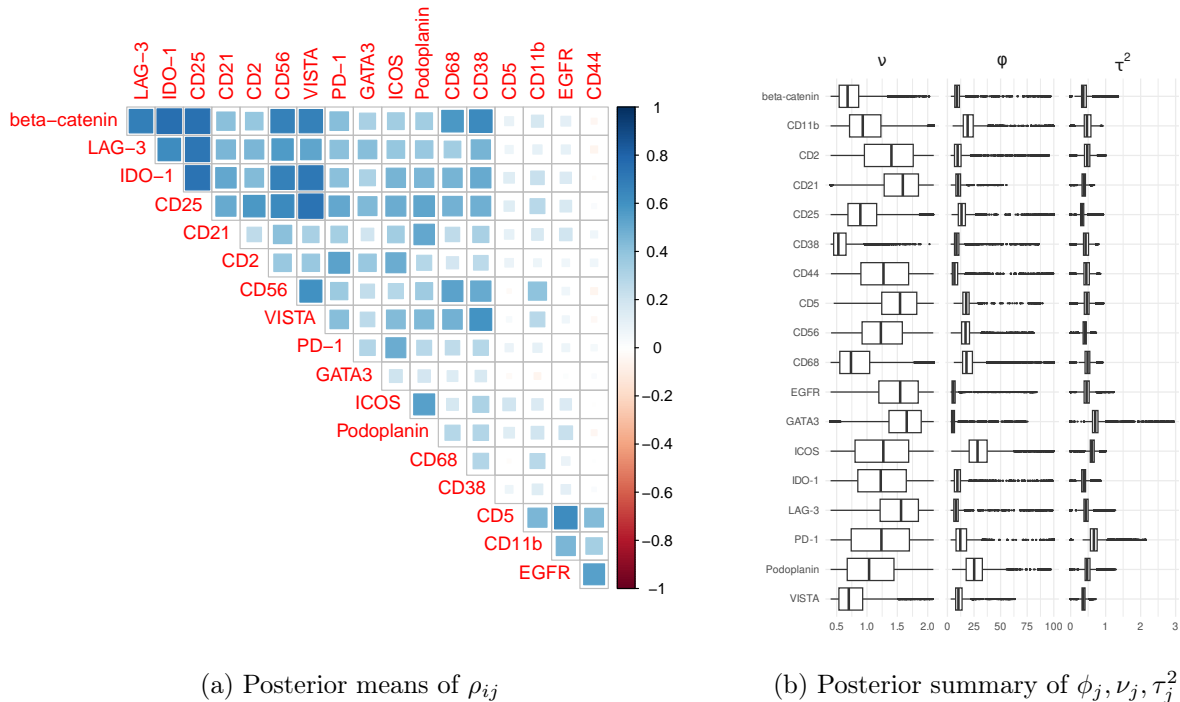


Figure 8: Posterior summaries for IOX parameters in the CODEX CRC analysis.

We estimate ϕ_j, ν_j, τ_j^2 for all j by fitting IOX using Metropolis-within-Gibbs updates of θ as described in Section 4.1. In fitting a multivariate spatial model to these data, we seek to understand how the TME organizes spatially, rather than making predictions within the imaged tissue. However, a model should demonstrate predictive value exceeding a non-spatial baseline to justify any conclusions about spatial dependence; otherwise, the inferred spatial structure may be attributed to overfitting. Therefore, we validate our approaches by comparing their predictive performance to LMCs (with 6 or 8 factors) and a nonspatial multivariate model. We use a test set $\mathcal{L}_{\text{test}}$ of 400 locations which we built by removing 2 randomly selected outcomes from the data at each of the locations in $\mathcal{L}_{\text{test}}$. Therefore, we predict the unobserved part of $\mathbf{y}(\ell)$ at each $\ell \in \mathcal{L}_{\text{test}}$. Table 3 summarizes our findings: IOX outperformed other methods in out-of-sample predictions. Dimension reduction using LMCs resulted in a deterioration of predictive performance that led to worse predictive

performance relative to a non-spatial model. Our analysis evidences tight co-localization of several protein markers, suggesting this patient’s immune system is present and stimulated but locally restrained. This TME appears to exhibit micro-regions with both activation and restraint, pointing to spatially heterogeneous immune pressure within the tumor.

6 Discussion

We have introduced IOX as a novel flexible class of cross-covariance functions for modeling multivariate spatial data. IOX leads to direct marginal inference and provides multiple avenues for flexible likelihood-based modeling and dimension reduction. In prioritizing inference of marginal covariances as well as overall parsimony, our method restricts $C_{ij}(\cdot, \cdot)$ through a product of the marginal Cholesky factors. Similar restrictions are common; see, e.g., Emery et al. (2022) for the multivariate Matérn. Extending IOX to more flexible parametrizations of $C_{ij}(\cdot, \cdot)$ is possible, as we show in the Supplement. There are multiple avenues for dimension reduction within the IOX framework. First, if some outcomes exhibit similar spatial dependence, we can group them and fit a single correlation model per cluster. This reduces computational cost by limiting the number of distinct \mathbf{L}_i factors. A second avenue for dimension reduction follows from a low-rank assumption on Σ . Refer to the Supplement for implications of this assumption.

Nonstationarities and covariate-dependence can be introduced into IOX by choosing appropriate univariate correlations functions. Alternatively, one can directly take advantage of the structure of IOX. For example, if $\mathbf{w}(\cdot)$ is a q -variate GP, \mathbf{w}_i the vector of values of the i th margin of $\mathbf{w}(\cdot)$, and $\mathbf{D}_{w_i} = \text{diag}(\mathbf{w}_i)$, then we can model q outcomes via $C_{ij}(\boldsymbol{\ell}, \boldsymbol{\ell}') = \sigma_{ij} w_i(\boldsymbol{\ell}) w_j(\boldsymbol{\ell}') (\mathbf{h}_i(\boldsymbol{\ell}) \mathbf{L}_i \mathbf{L}_j^\top \mathbf{h}_j(\boldsymbol{\ell}') + \xi(\boldsymbol{\ell}, \boldsymbol{\ell}'))$, leading to $\mathbf{C}(\mathcal{S}) = \{\oplus \mathbf{L}_i \mathbf{D}_{w_i}\} (\Sigma \otimes \mathbf{I}_n) \{\oplus \mathbf{D}_{w_i} \mathbf{L}_i^\top\}$, in which case \mathbf{w}_i^2 models the spatially-varying sill of out-

come *i*. IOX may also facilitate fitting multivariate extensions of the deformation method of Sampson & Guttorp (1992) by assuming multiple outcomes share the same latent input space, which is realistic with “omics” data.

Future methodological development may lead to novel models for spatial time series data based on IOX. We consider a single spatial outcome measured at T discrete time points and n sites. At each $t = 1, \dots, T$, we can let $\rho_t(\cdot, \cdot)$ evolve with t according to some dynamics, as well as impose structure on $\mathbf{Q} = \mathbf{\Sigma}^{-1}$ (its dimension is now $T \times T$), e.g., via Markovian assumptions leading to a sparse and banded \mathbf{Q} .

Acknowledgements

The author thanks D. Dunson and B. Jin for helpful comments and suggestions, and the Associate Editor and referees for constructive feedback that improved both the manuscript and the reproducibility code.

Disclosure statement

The author reports there are no competing interests to declare.

SUPPLEMENTARY MATERIAL

A Proofs

Proposition 2.1 (Marginal covariance).

$$C_{ii}(\boldsymbol{\ell}, \boldsymbol{\ell}') = \begin{cases} \sigma_{ii}\rho_i(\boldsymbol{\ell}, \boldsymbol{\ell}') & \text{if } \boldsymbol{\ell} \in \mathcal{S} \text{ or } \boldsymbol{\ell}' \in \mathcal{S} \text{ or } \boldsymbol{\ell} = \boldsymbol{\ell}', \\ \sigma_{ii}\rho_i(\boldsymbol{\ell}, \mathcal{S})\rho_i(\mathcal{S})^{-1}\rho_i(\mathcal{S}, \boldsymbol{\ell}') & \text{if } \boldsymbol{\ell}, \boldsymbol{\ell}' \in \mathcal{S}^c \text{ and } \boldsymbol{\ell} \neq \boldsymbol{\ell}'. \end{cases}$$

Proof. Letting $i = j$ we have

$$\begin{aligned} C_{ii}(\boldsymbol{\ell}, \boldsymbol{\ell}') &= \sigma_{ii} [\mathbf{h}_i(\boldsymbol{\ell})\rho_i(\mathcal{S})\mathbf{h}_i(\boldsymbol{\ell}')^\top + \mathbb{1}_{\{\boldsymbol{\ell}=\boldsymbol{\ell}'\}}r_i(\boldsymbol{\ell})] \\ &= \sigma_{ii} [\rho_i(\boldsymbol{\ell}, \mathcal{S})\rho_i(\mathcal{S})^{-1}\rho_i(\mathcal{S}, \boldsymbol{\ell}') + \mathbb{1}_{\{\boldsymbol{\ell}=\boldsymbol{\ell}'\}}(\rho_i(\boldsymbol{\ell}, \boldsymbol{\ell}) - \rho_i(\boldsymbol{\ell}, \mathcal{S})\rho_i(\mathcal{S})^{-1}\rho_i(\mathcal{S}, \boldsymbol{\ell}))]. \end{aligned}$$

We immediately notice that if $\boldsymbol{\ell} = \boldsymbol{\ell}'$ then $C_{ii}(\boldsymbol{\ell}, \boldsymbol{\ell}) = \sigma_{ii}\rho_i(\boldsymbol{\ell}, \boldsymbol{\ell}) = \sigma_{ii}$. If $\boldsymbol{\ell} \neq \boldsymbol{\ell}'$ and $\boldsymbol{\ell}, \boldsymbol{\ell}' \in \mathcal{S}^c$ then we obtain the stated result by just dropping the indicator term. Finally, suppose $\boldsymbol{\ell} \in \mathcal{S}$ (the case $\boldsymbol{\ell}' \in \mathcal{S}$ is analogous). This means there is $r \in \{1, \dots, n\}$ such that $\boldsymbol{\ell} = \boldsymbol{\ell}_r$, which implies the vector $\mathbf{h}_i(\boldsymbol{\ell}) = \mathbf{e}_\ell = (e_1, \dots, e_n)^\top$ has $e_r = 1$ and $e_h = 0$ for $h \neq r$. We see this e.g. by letting $\mathbf{x} = (x_1, \dots, x_n)^\top$, $E[\mathbf{x}] = 0$, and $\text{cov}(\mathbf{x}, \mathbf{x}) = \rho_i(\mathcal{S})$. Then, $\mathbf{h}_i(\boldsymbol{\ell})\mathbf{x} = E[x_r | \mathbf{x}] = x_r$. In other words, if $\boldsymbol{\ell} = \boldsymbol{\ell}_r \in \mathcal{S}$ then $\mathbf{h}_i(\boldsymbol{\ell})$ selects the r th row from the matrix to which it is premultiplied. Therefore, we select the r th row of $\rho_i(\mathcal{S}, \boldsymbol{\ell}')$, which is equal to $\rho_i(\boldsymbol{\ell}_r, \boldsymbol{\ell}') = \rho_i(\boldsymbol{\ell}, \boldsymbol{\ell}')$.

Proposition 2.2 (Cross-covariance and σ_{ij}). For all $\boldsymbol{\ell}, \boldsymbol{\ell}' \in \mathcal{D}$ and all $i, j = 1, \dots, q$, the cross-covariance is $C_{ij}(\boldsymbol{\ell}, \boldsymbol{\ell}') \leq \sigma_{ij}$. If $\rho_i(\cdot, \cdot) = \rho_j(\cdot, \cdot)$, then $C_{ij}(\boldsymbol{\ell}, \boldsymbol{\ell}) = \sigma_{ij}$.

Proof. We start by proving that $\|\mathbf{h}_i(\boldsymbol{\ell})\mathbf{L}_i\| \leq 1$. Because $\rho_i(\cdot, \cdot)$ is a correlation function, then $r_i(\boldsymbol{\ell}) = \rho_i(\boldsymbol{\ell}, \boldsymbol{\ell}) - \rho(\boldsymbol{\ell}, \mathcal{S})\rho_i(\mathcal{S})^{-1}\rho_i(\mathcal{S}, \boldsymbol{\ell}) = 1 - \mathbf{h}_i(\boldsymbol{\ell})\rho_i(\mathcal{S})\mathbf{h}_i(\boldsymbol{\ell})^\top \geq 0$ which implies $\mathbf{h}_i(\boldsymbol{\ell})\rho_i(\mathcal{S})\mathbf{h}_i(\boldsymbol{\ell})^\top = \mathbf{h}_i(\boldsymbol{\ell})\mathbf{L}_i\mathbf{L}_i^\top\mathbf{h}_i(\boldsymbol{\ell})^\top = \|\mathbf{h}_i(\boldsymbol{\ell})\mathbf{L}_i\|^2 \leq 1$.

Let $\mathbf{a}^\top = \mathbf{h}_i(\boldsymbol{\ell})\mathbf{L}_i$ and $\mathbf{b}^\top = \mathbf{h}_j(\boldsymbol{\ell}')\mathbf{L}_j$. We showed above that $\|\mathbf{a}\| \leq 1$ and $\|\mathbf{b}\| \leq 1$.

Then

$$\begin{aligned} C_{ij}(\boldsymbol{\ell}, \boldsymbol{\ell}') &= \sigma_{ij} \left[\mathbf{h}_i(\boldsymbol{\ell})\mathbf{L}_i\mathbf{L}_j^\top\mathbf{h}_j(\boldsymbol{\ell}')^\top + \sqrt{r_i(\boldsymbol{\ell})r_j(\boldsymbol{\ell}')} \right] \\ &= \sigma_{ij} \left[\mathbf{a}^\top\mathbf{b} + \sqrt{(1 - \mathbf{a}^\top\mathbf{a})(1 - \mathbf{b}^\top\mathbf{b})} \right] \\ &\leq \sigma_{ij} \left[\|\mathbf{a}\|\|\mathbf{b}\| + \sqrt{(1 - \|\mathbf{a}\|^2)(1 - \|\mathbf{b}\|^2)} \right] \leq \sigma_{ij}. \end{aligned}$$

In particular, consider the case $\boldsymbol{\ell} = \boldsymbol{\ell}'$. If $\rho_i(\cdot, \cdot) = \rho_j(\cdot, \cdot)$ then we obtain $C_{ij}(\boldsymbol{\ell}, \boldsymbol{\ell}') = \sigma_{ij}$, which implies that σ_{ij} is the zero-distance correlation between variables with the same marginal correlation.

Proposition 2.3 (IOX cross-covariance matrix function). Let $\boldsymbol{\ell}, \boldsymbol{\ell}' \in \mathcal{S}$.

$$\begin{aligned} \mathbf{C}(\boldsymbol{\ell}, \boldsymbol{\ell}') &= \boldsymbol{\Sigma} \odot [\mathbf{K}(\boldsymbol{\ell}, \boldsymbol{\ell}') + \mathbf{d}(\boldsymbol{\ell}, \boldsymbol{\ell}')\mathbf{d}(\boldsymbol{\ell}, \boldsymbol{\ell}')^\top] \\ &= \{\oplus\mathbf{h}_i(\boldsymbol{\ell})\mathbf{L}_i\}(\boldsymbol{\Sigma} \otimes \mathbf{I}_n)\{\oplus\mathbf{L}_i^\top\mathbf{h}_i(\boldsymbol{\ell}')^\top\} + \mathbf{D}(\boldsymbol{\ell}, \boldsymbol{\ell}')\boldsymbol{\Sigma}\mathbf{D}(\boldsymbol{\ell}, \boldsymbol{\ell}'), \end{aligned} \tag{8}$$

where $\mathbf{K}(\boldsymbol{\ell}, \boldsymbol{\ell}')$ is the $q \times q$ matrix whose i, j element is $\mathbf{h}_i(\boldsymbol{\ell})\mathbf{L}_i\mathbf{L}_j^\top\mathbf{h}_j(\boldsymbol{\ell}')^\top$, $\mathbf{d}(\boldsymbol{\ell}, \boldsymbol{\ell}')$ is a vector of dimension q whose i th element is $\mathbb{1}_{\{\boldsymbol{\ell}=\boldsymbol{\ell}'\}}\sqrt{r_i(\boldsymbol{\ell})}$, $\mathbf{D}(\boldsymbol{\ell}, \boldsymbol{\ell}') = \text{diag}\{\mathbf{d}(\boldsymbol{\ell}, \boldsymbol{\ell}')\}$, “ \oplus ” is the direct sum operator and we denote with $\{\oplus\mathbf{h}_i(\boldsymbol{\ell})\mathbf{L}_i\}$ the $q \times nq$ block-diagonal matrix with $\mathbf{h}_i(\boldsymbol{\ell})\mathbf{L}_i$ as its i th block, while “ \odot ” is the Hadamard element-by-element product.

Proof. Let $\boldsymbol{\ell} \neq \boldsymbol{\ell}'$. Then

$$\begin{aligned} \mathbf{C}(\boldsymbol{\ell}, \boldsymbol{\ell}') &= \left[C_{ij}(\boldsymbol{\ell}, \boldsymbol{\ell}') \right]_{i,j=1,\dots,q} \\ &= \left[\sigma_{ij}\mathbf{h}_i(\boldsymbol{\ell})\mathbf{L}_i\mathbf{L}_j^\top\mathbf{h}_j(\boldsymbol{\ell}')^\top \right]_{i,j=1,\dots,q} = \boldsymbol{\Sigma} \odot \left[\mathbf{h}_i(\boldsymbol{\ell})\mathbf{L}_i\mathbf{L}_j^\top\mathbf{h}_j(\boldsymbol{\ell}')^\top \right]_{i,j=1,\dots,q} \\ &= \begin{bmatrix} \sigma_{11}\mathbf{h}_1(\boldsymbol{\ell})\mathbf{L}_1\mathbf{L}_1^\top\mathbf{h}_1(\boldsymbol{\ell}')^\top & \cdots & \sigma_{1q}\mathbf{h}_1(\boldsymbol{\ell})\mathbf{L}_1\mathbf{L}_q^\top\mathbf{h}_q(\boldsymbol{\ell}')^\top \\ & \ddots & \\ \sigma_{q1}\mathbf{h}_q(\boldsymbol{\ell})\mathbf{L}_q\mathbf{L}_1^\top\mathbf{h}_1(\boldsymbol{\ell}')^\top & & \sigma_{qq}\mathbf{h}_q(\boldsymbol{\ell})\mathbf{L}_q\mathbf{L}_q^\top\mathbf{h}_q(\boldsymbol{\ell}')^\top \end{bmatrix} \end{aligned}$$

$$\begin{aligned}
&= \begin{bmatrix} \sigma_{11}\mathbf{h}_1(\boldsymbol{\ell})\mathbf{L}_1 & \cdots & \sigma_{1q}\mathbf{h}_1(\boldsymbol{\ell})\mathbf{L}_1 \\ & \ddots & \\ \sigma_{q1}\mathbf{h}_q(\boldsymbol{\ell})\mathbf{L}_q & & \sigma_{qq}\mathbf{h}_q(\boldsymbol{\ell})\mathbf{L}_q \end{bmatrix} \begin{bmatrix} \mathbf{L}_1^\top \mathbf{h}_1(\boldsymbol{\ell}')^\top & & \\ & \ddots & \\ & & \mathbf{L}_q^\top \mathbf{h}_q(\boldsymbol{\ell}')^\top \end{bmatrix} \\
&= \begin{bmatrix} \mathbf{h}_1(\boldsymbol{\ell})\mathbf{L}_1 & & \\ & \ddots & \\ & & \mathbf{h}_q(\boldsymbol{\ell})\mathbf{L}_q \end{bmatrix} \begin{bmatrix} \sigma_{11}\mathbf{I}_n & \cdots & \sigma_{1q}\mathbf{I}_n \\ \vdots & \ddots & \vdots \\ \sigma_{q1}\mathbf{I}_n & \cdots & \sigma_{qq}\mathbf{I}_n \end{bmatrix} \begin{bmatrix} \mathbf{L}_1^\top \mathbf{h}_1(\boldsymbol{\ell}')^\top & & \\ & \ddots & \\ & & \mathbf{L}_q^\top \mathbf{h}_q(\boldsymbol{\ell}')^\top \end{bmatrix} \\
&= \{\oplus \mathbf{h}_i(\boldsymbol{\ell})\mathbf{L}_i\}(\boldsymbol{\Sigma} \otimes \mathbf{I}_n)\{\oplus \mathbf{L}_i^\top \mathbf{h}_i(\boldsymbol{\ell}')^\top\}.
\end{aligned}$$

If $\boldsymbol{\ell} = \boldsymbol{\ell}'$ then we need to add $\sqrt{r_i(\boldsymbol{\ell})r_j(\boldsymbol{\ell})}$ to the (i, j) th element of $\mathbf{C}(\boldsymbol{\ell}, \boldsymbol{\ell}')$, which is the purpose of $\mathbf{d}(\boldsymbol{\ell}, \boldsymbol{\ell}')\mathbf{d}(\boldsymbol{\ell}, \boldsymbol{\ell}')^\top$ by construction. We conclude by noting that $\boldsymbol{\Sigma} \odot (\mathbf{d}(\boldsymbol{\ell}, \boldsymbol{\ell}')\mathbf{d}(\boldsymbol{\ell}, \boldsymbol{\ell}')^\top) = \mathbf{D}(\boldsymbol{\ell}, \boldsymbol{\ell}')\boldsymbol{\Sigma}\mathbf{D}(\boldsymbol{\ell}, \boldsymbol{\ell}')$.

Corollary 2.1. If $\boldsymbol{\ell} \in \mathcal{S}$ then $\mathbf{h}_i(\boldsymbol{\ell})\mathbf{L}_i = \mathbf{L}_i[\boldsymbol{\ell}, :]$, the row of \mathbf{L}_i corresponding to $\boldsymbol{\ell}$. Then,

$$\mathbf{C}(\mathcal{S}) = (\boldsymbol{\Sigma} \otimes \mathbf{1}_{n,n}) \odot \mathbf{K} = \{\oplus \mathbf{L}_i\}(\boldsymbol{\Sigma} \otimes \mathbf{I}_n)\{\oplus \mathbf{L}_i^\top\}, \quad (9)$$

where \mathbf{K} is the $nq \times nq$ matrix whose (i, j) th block is $\mathbf{L}_i\mathbf{L}_j^\top$; $\mathbf{1}_{n,n}$ is the $n \times n$ matrix of 1s.

Proof. If $\boldsymbol{\ell} = \boldsymbol{\ell}_r$ for some $r \in \{1, \dots, n\}$, then $\mathbf{h}_i(\boldsymbol{\ell}) = \mathbf{e}_\ell = (e_1, \dots, e_n)^\top$ has $e_r = 1$ and $e_h = 0$ for $h \neq r$. We see this e.g. by letting $\mathbf{x} = (x_1, \dots, x_n)^\top$, $E[\mathbf{x}] = \mathbf{0}$, and $\text{cov}(\mathbf{x}, \mathbf{x}) = \rho_i(\mathcal{S})$. Then, $\mathbf{h}_i(\boldsymbol{\ell})\mathbf{x} = E[x_r \mid \mathbf{x}] = x_r$. In other words, if $\boldsymbol{\ell} = \boldsymbol{\ell}_r \in \mathcal{S}$ then $\mathbf{h}_i(\boldsymbol{\ell})$ selects the r th row from the matrix to which it is premultiplied. Similarly, if $\boldsymbol{\ell} \in \mathcal{S}$ then $r_i(\boldsymbol{\ell}) = 0$ for all $i = 1, \dots, q$. The rest follows.

Proposition 2.4. $\mathbf{C}(\boldsymbol{\ell}, \boldsymbol{\ell}')$ is a valid cross-covariance matrix function.

Proof. The conditions stated in the introduction can be expressed as follows. Suppose \mathbf{Z} is a $m \times q$ random matrix whose i th row is $\mathbf{z}(\boldsymbol{\ell}_i)^\top$, $\boldsymbol{\ell}_i \in \mathcal{T} = \{\mathbf{t}_1, \dots, \mathbf{t}_m\}$ and j th column \mathbf{z}_j . Then, a cross-covariance matrix function must be such that the assumed covariance matrix

of $\mathbf{z} = \text{vec}(\mathbf{Z})$ (or, equivalently, of $\text{vec}(\mathbf{Z}^\top)$) is symmetric positive semidefinite for any \mathcal{T} and any m (Genton & Kleiber 2015). Because our assumption is that $\text{cov}(\mathbf{z}) = \mathbf{C}(\mathcal{T})$, we need to show that $\mathbf{C}(\mathcal{T})$ is symmetric positive semidefinite. If $\boldsymbol{\ell} \neq \boldsymbol{\ell}'$,

$$\begin{aligned} \mathbf{C}(\boldsymbol{\ell}, \boldsymbol{\ell}') &= \boldsymbol{\Sigma} \odot (\mathbf{K}(\boldsymbol{\ell}, \boldsymbol{\ell}') + \mathbf{D}(\boldsymbol{\ell}, \boldsymbol{\ell}')) \\ &= \boldsymbol{\Sigma} \odot \left[\mathbf{h}_i(\boldsymbol{\ell}) \mathbf{L}_i \mathbf{L}_j^\top \mathbf{h}_j(\boldsymbol{\ell}')^\top \right]_{i,j=1,\dots,q} \\ &= \boldsymbol{\Sigma} \odot \left[\mathbf{h}_i(\boldsymbol{\ell}') \mathbf{L}_i \mathbf{L}_j^\top \mathbf{h}_j(\boldsymbol{\ell})^\top \right]_{i,j=1,\dots,q}^\top \\ &= \boldsymbol{\Sigma} \odot \mathbf{K}(\boldsymbol{\ell}', \boldsymbol{\ell})^\top = \mathbf{C}(\boldsymbol{\ell}', \boldsymbol{\ell})^\top. \end{aligned}$$

The additional term $\mathbf{D}(\boldsymbol{\ell}, \boldsymbol{\ell}')$ is zero if $\boldsymbol{\ell} \neq \boldsymbol{\ell}'$; otherwise,

$$\mathbf{D}(\boldsymbol{\ell}, \boldsymbol{\ell}) = \begin{bmatrix} \sqrt{r_1(\boldsymbol{\ell})} \\ \vdots \\ \sqrt{r_q(\boldsymbol{\ell})} \end{bmatrix} \begin{bmatrix} \sqrt{r_1(\boldsymbol{\ell})} & \cdots & \sqrt{r_q(\boldsymbol{\ell})} \end{bmatrix},$$

which is symmetric by construction. As for positive semidefiniteness, define $\mathbf{H}_i(\mathcal{T}) = \rho_i(\mathcal{T}, \mathcal{S}) \rho_i(\mathcal{S})^{-1}$, i.e. the $m \times n$ matrix whose j th row is $\mathbf{h}_i(\mathbf{t}_j)$ and assume $\boldsymbol{\Sigma} = \mathbf{A} \mathbf{A}^\top$ where \mathbf{A} is a $q \times k$ matrix of rank $k \leq q$. Then,

$$\begin{aligned} \mathbf{C}(\mathcal{T}) &= \{\oplus \mathbf{H}_i(\mathcal{T}) \mathbf{L}_i\} (\boldsymbol{\Sigma} \otimes \mathbf{I}_n) \{\oplus \mathbf{L}_i^\top \mathbf{H}_i(\mathcal{T})^\top\} + (\boldsymbol{\Sigma} \otimes \mathbf{1}_{m,m}) \odot \mathbf{D}_T \\ &= \{\oplus \mathbf{H}_i(\mathcal{T}) \mathbf{L}_i\} (\mathbf{A} \otimes \mathbf{I}_n) (\mathbf{A}^\top \otimes \mathbf{I}_n) \{\oplus \mathbf{L}_i^\top \mathbf{H}_i(\mathcal{T})^\top\} + (\boldsymbol{\Sigma} \otimes \mathbf{1}_{m,m}) \odot \mathbf{D}_T \\ &= \mathbf{G} \mathbf{G}^\top + (\boldsymbol{\Sigma} \otimes \mathbf{1}_{m,m}) \odot \mathbf{D}_T, \end{aligned}$$

where $\mathbf{G} = \{\oplus \mathbf{H}_i(\mathcal{T}) \mathbf{L}_i\} (\mathbf{A} \otimes \mathbf{I}_n)$ and \mathbf{D}_T is a $mq \times mq$ block matrix whose (i, j) th block of dimension $m \times m$ is a diagonal matrix whose diagonal entries are $\sqrt{r_i(\boldsymbol{\ell}_h) r_j(\boldsymbol{\ell}_h)}$ for $h = 1, \dots, m$. The first term is non-negative definite because $\mathbf{x}^\top \mathbf{G} \mathbf{G}^\top \mathbf{x} = \tilde{\mathbf{x}}^\top \tilde{\mathbf{x}} \geq 0$. As for the second term, $(\boldsymbol{\Sigma} \otimes \mathbf{1}_{m,m})$ is non-negative definite because $\boldsymbol{\Sigma}$ is assumed to be. Finally, suppose \mathbf{P} is a permutation matrix that rearranges rows and columns of \mathbf{D}_T so

that $\mathbf{P}\mathbf{D}_T\mathbf{P}^\top$ is a block diagonal matrix with $\mathbf{D}(\boldsymbol{\ell}_i, \boldsymbol{\ell}_i)$ as its i th diagonal block, with $i = 1, \dots, m$. $\mathbf{D}(\boldsymbol{\ell}_i, \boldsymbol{\ell}_i)$ is non-negative definite rank 1. Therefore, $\mathbf{P}\mathbf{D}_T\mathbf{P}^\top$ is non-negative definite of rank m , and so is \mathbf{D}_T . Hadamard product and matrix sum retain non-negative definiteness.

Proposition 2.5. In the separable specification, i.e., $\rho_i(\cdot, \cdot) = \rho(\cdot, \cdot)$ for all i , IOX and LMC coincide at \mathcal{S} .

Proof. For IOX,

$$\begin{aligned} \mathbf{C}(\mathcal{S}) &= \{\oplus \mathbf{L}_i\}(\boldsymbol{\Sigma} \otimes \mathbf{I}_n)\{\oplus \mathbf{L}_i^\top\} \\ &= (\mathbf{I}_q \otimes \mathbf{L})(\boldsymbol{\Sigma} \otimes \mathbf{I}_n)(\mathbf{I}_q \otimes \mathbf{L}^\top) \\ &= \boldsymbol{\Sigma} \otimes \mathbf{L}\mathbf{L}^\top = \boldsymbol{\Sigma} \otimes \rho(\mathcal{S}). \end{aligned}$$

For LMC,

$$\begin{aligned} \mathbf{C}(\mathcal{S}) &= (\mathbf{A} \otimes \mathbf{I}_n)\{\oplus \rho_i(\mathcal{S})\}(\mathbf{A}^\top \otimes \mathbf{I}_n) \\ &= (\mathbf{A} \otimes \mathbf{I}_n)(\mathbf{I}_q \otimes \rho(\mathcal{S}))(\mathbf{A}^\top \otimes \mathbf{I}_n) \\ &= \mathbf{A}\mathbf{A}^\top \otimes \rho(\mathcal{S}) = \boldsymbol{\Sigma} \otimes \rho(\mathcal{S}). \end{aligned}$$

Proposition 2.6. Suppose $\boldsymbol{\ell}, \boldsymbol{\ell}' \in \mathcal{S}^c$, $\boldsymbol{\ell} \neq \boldsymbol{\ell}'$. Then, $\mathbf{C}(\boldsymbol{\ell}, \boldsymbol{\ell}') - \mathbf{C}(\boldsymbol{\ell}, \mathcal{S})\mathbf{C}(\mathcal{S})^{-1}\mathbf{C}(\mathcal{S}, \boldsymbol{\ell}') = \mathbf{0}$.

Proof. We have $\mathbf{C}(\boldsymbol{\ell}, \mathcal{S}) = \{\oplus \mathbf{h}_i(\boldsymbol{\ell})\mathbf{L}_i\}(\boldsymbol{\Sigma} \otimes \mathbf{I}_n)\{\oplus \mathbf{L}_i^\top\}$ and $\mathbf{C}(\mathcal{S})^{-1} = \{\oplus \mathbf{L}_i^{-\top}\}(\boldsymbol{\Sigma}^{-1} \otimes \mathbf{I}_n)\{\oplus \mathbf{L}_i^{-1}\}$. Together, these imply:

$$\mathbf{C}(\boldsymbol{\ell}, \mathcal{S})\mathbf{C}(\mathcal{S})^{-1}\mathbf{C}(\mathcal{S}, \boldsymbol{\ell}') = \{\oplus \mathbf{h}_i(\boldsymbol{\ell})\mathbf{L}_i\}(\boldsymbol{\Sigma} \otimes \mathbf{I}_n)\{\oplus \mathbf{L}_i^\top \mathbf{h}_i(\boldsymbol{\ell}')^\top\} = \mathbf{C}(\boldsymbol{\ell}, \boldsymbol{\ell}').$$

Proposition 3.1 (GP-IOX log-density).

$$\log p(\mathbf{w} \mid \boldsymbol{\theta}, \mathbf{Q}) = \text{const} + \frac{n}{2} \log \det(\mathbf{Q}) + \sum_{ij} \log \mathbf{L}_j^{-1}[i, i] - \frac{1}{2} \text{Tr}(\mathbf{V}\mathbf{Q}\mathbf{V}^\top), \quad (10)$$

where $\mathbf{L}_j^{-1}[i, i]$ is the i th diagonal element of \mathbf{L}_j^{-1} , and \mathbf{V} is the $n \times q$ matrix whose j th row is $\mathbf{v}_j = \mathbf{L}_j^{-1}\mathbf{w}_j$.

Proof. We start by noting that

$$\mathbf{C}^{-1} = \{\oplus \mathbf{L}_j^{-\top}\}(\boldsymbol{\Sigma}^{-1} \otimes \mathbf{I}_n)\{\oplus \mathbf{L}_j^{-1}\} = \{\oplus \mathbf{L}_j^{-\top}\}(\mathbf{Q}^{-1} \otimes \mathbf{I}_n)\{\oplus \mathbf{L}_j^{-1}\},$$

and because $\det(\mathbf{L}_j^{-1}) = \prod_i \mathbf{L}_j^{-1}[i, i]$, we get $-\frac{1}{2} \log \det(\mathbf{C}) = \frac{n}{2} \log \det(\mathbf{Q}) + \sum_{ij} \log \mathbf{L}_j^{-1}[i, i]$.

Then,

$$\begin{aligned} \log p(\mathbf{w} \mid \boldsymbol{\theta}, \boldsymbol{\beta}, \boldsymbol{\Sigma}) &= \text{const} - \frac{1}{2} \log \det(\mathbf{C}) - \frac{1}{2} \mathbf{w}^\top \mathbf{C}^{-1} \mathbf{w} \\ &= \text{const} + \frac{n}{2} \log \det(\mathbf{Q}) + \sum_{ij} \log \mathbf{L}_j^{-1}[i, i] - \frac{1}{2} \mathbf{w}^\top \{\oplus \mathbf{L}_j^{-\top}\}(\mathbf{Q} \otimes \mathbf{I}_n)\{\oplus \mathbf{L}_j^{-1}\} \mathbf{w} \\ &= \text{const} + \frac{n}{2} \log \det(\mathbf{Q}) + \sum_{ij} \log \mathbf{L}_j^{-1}[i, i] - \frac{1}{2} \text{vec}(\mathbf{V})^\top (\mathbf{Q} \otimes \mathbf{I}_n) \text{vec}(\mathbf{V}) \\ &= \text{const} + \frac{n}{2} \log \det(\mathbf{Q}) + \sum_{ij} \log \mathbf{L}_j^{-1}[i, i] - \frac{1}{2} \text{Tr}(\mathbf{V} \mathbf{Q} \mathbf{V}^\top). \end{aligned}$$

Proposition 3.2 (Conditional density). $p(\mathbf{w}_j \mid \mathbf{w}_{j^c}, \boldsymbol{\theta}, \mathbf{Q}) = N(\mathbf{w}_j; \mathbf{m}_j, \mathbf{M}_j)$, where $\mathbf{m}_j = -\mathbf{L}_j \sum_{r \in j^c} \frac{Q_{jr}}{Q_{jj}} \mathbf{v}_r$ and $\mathbf{M}_j^{-1} = Q_{jj} \rho_j(\mathcal{S})^{-1}$. Then, we evaluate $\log N(\mathbf{w}_j; \mathbf{m}_j, \mathbf{M}_j)$ as:

$$\begin{aligned} \log N(\mathbf{w}_j; \mathbf{m}_j, \mathbf{M}_j) &\propto -\frac{1}{2} \log |\mathbf{M}_j| - \frac{1}{2} (\mathbf{w}_j - \mathbf{m}_j)^\top \mathbf{M}_j^{-1} (\mathbf{w}_j - \mathbf{m}_j) \\ &= \frac{n}{2} \log Q_{jj} + \sum_{i=1}^n \log \mathbf{L}_j^{-1}[i, i] - \frac{1}{2Q_{jj}} \mathbf{Q}_j \cdot \mathbf{V}^\top \mathbf{V} \mathbf{Q}_j^\top, \end{aligned} \quad (11)$$

where Q_{jr} is the (j, r) th element and $\mathbf{Q}_j \cdot$ is the j th row of \mathbf{Q} .

Proof. Because the joint distribution of \mathbf{w} is Gaussian, we have $p(\mathbf{w}_j \mid \mathbf{w}_{j^c}, \boldsymbol{\theta}, \mathbf{Q}) = N(\mathbf{w}_j; \mathbf{m}_j, \mathbf{M}_j)$, where \mathbf{M}_j^{-1} is the (j, j) th block of the precision matrix $\mathbf{C}^{-1} = \{\oplus \mathbf{L}_j^{-\top}\}(\mathbf{Q} \otimes \mathbf{I}_n)\{\oplus \mathbf{L}_j^{-1}\}$. Therefore, we find $\mathbf{M}_j^{-1} = Q_{jj} \rho_j(\mathcal{S})^{-1}$ following the same steps as in Proposition 2.1. Again because the joint is Gaussian, the conditional mean is $\mathbf{m}_j = \mathbf{C}_{j,j^c} \mathbf{C}_{j^c}^{-1} \mathbf{w}_{j^c}$, which becomes

$$\begin{aligned} \mathbf{m}_j &= \mathbf{L}_j (\boldsymbol{\Sigma}_{j,j^c} \boldsymbol{\Sigma}_{j^c}^{-1} \otimes \mathbf{I}_n) \{\oplus_{j^c} \mathbf{L}_r^{-1}\} \mathbf{w}_{j^c} = -\mathbf{L}_j \left(\frac{\mathbf{Q}_{j,j^c}}{Q_{jj}} \otimes \mathbf{I}_n \right) \{\oplus_{j^c} \mathbf{L}_r^{-1}\} \mathbf{w}_{j^c} \\ &= -\mathbf{L}_j \sum_{r \in j^c} \frac{Q_{jr}}{Q_{jj}} \mathbf{L}_r^{-1} \mathbf{w}_r, \end{aligned}$$

where \mathbf{Q}_{j,j^c} is the $1 \times q - 1$ vector obtained from the j th row and j^c columns of \mathbf{Q} and we denote with “ \oplus_{j^c} ” the direct sum operator over j^c indices. As for evaluating the joint density,

$$\begin{aligned}
N(\mathbf{w}_j; \mathbf{m}_j, \mathbf{M}_j) &\propto |\mathbf{M}_j|^{-\frac{1}{2}} \exp\left\{-\frac{1}{2}(\mathbf{w}_j - \mathbf{m}_j)^\top \mathbf{M}_j^{-1}(\mathbf{w}_j - \mathbf{m}_j)\right\} \\
&= |\mathbf{M}_j|^{-\frac{1}{2}} \exp\left\{-\frac{Q_{jj}}{2}(\mathbf{w}_j - \mathbf{m}_j)^\top \mathbf{L}_j^{-\top} \mathbf{L}_j^{-1}(\mathbf{w}_j - \mathbf{m}_j)\right\} \\
(\star) \quad &= \sqrt{|Q_{jj}\rho_j(\mathcal{S})^{-1}|} \exp\left\{-\frac{1}{2Q_{jj}} \left(\sum_{r=1}^q Q_{jr} \mathbf{v}_r\right)^\top \left(\sum_{r=1}^q Q_{jr} \mathbf{v}_r\right)\right\} \\
&= \sqrt{|Q_{jj}\rho_j(\mathcal{S})^{-1}|} \exp\left\{-\frac{1}{2Q_{jj}} \mathbf{Q}_j \mathbf{V}^\top \mathbf{V} \mathbf{Q}_j^\top\right\}.
\end{aligned}$$

where for (\star) we use the following:

$$\begin{aligned}
\mathbf{L}_j^{-1}(\mathbf{w}_j - \mathbf{m}_j) &= \mathbf{L}_j^{-1}\mathbf{w}_j - \mathbf{L}_j^{-1}\mathbf{m}_j = \mathbf{L}_j^{-1}\mathbf{w}_j - \mathbf{L}_j^{-1}\mathbf{m}_j \\
&= \mathbf{L}_j^{-1}\mathbf{w}_j + \left(\frac{\mathbf{Q}_{j,j^c}}{Q_{jj}} \otimes \mathbf{I}_n\right) \{\oplus_{j^c} \mathbf{L}_r^{-1}\} \mathbf{w}_{j^c} = \mathbf{L}_j^{-1}\mathbf{w}_j + \sum_{r \in j^c} \frac{Q_{jr}}{Q_{jj}} \mathbf{L}_r^{-1} \mathbf{w}_r \\
&= \sum_{r=1}^q \frac{Q_{jr}}{Q_{jj}} \mathbf{L}_r^{-1} \mathbf{w}_r = \sum_{r=1}^q \frac{Q_{jr}}{Q_{jj}} \mathbf{v}_r.
\end{aligned}$$

Finally, by definition $\mathbf{L}_j \mathbf{L}_j = \rho_j(\mathcal{S})$ and we obtain the final result by taking logs.

Proposition 3.3. $\mathbf{H}(\mathbf{t}) = \{\oplus \mathbf{h}_i(\mathbf{t})\}$ and $\mathbf{R}(\mathbf{t}) = \mathbf{D}(\mathbf{t}, \mathbf{t}) \boldsymbol{\Sigma} \mathbf{D}(\mathbf{t}, \mathbf{t})$. For $\mathbf{t} \notin \mathcal{S}$, $p(\mathbf{w}_i(\mathbf{t}) \mid \mathbf{w}, \boldsymbol{\theta}, \boldsymbol{\Sigma})$ only depends on $\rho_i(\cdot, \cdot)$ at \mathcal{S} , σ_{ii} and \mathbf{w}_i .

Proof.

$$\begin{aligned}
\mathbf{H}(\mathbf{t}) &= \mathbf{C}(\mathbf{t}, \mathcal{S}) \mathbf{C}(\mathcal{S})^{-1} \\
&= \{\oplus \mathbf{h}_i(\mathbf{t}) \mathbf{L}_i\} (\boldsymbol{\Sigma} \otimes \mathbf{I}_n) \{\oplus \mathbf{L}_i^\top\} \{\oplus \mathbf{L}_i^{-\top}\} (\boldsymbol{\Sigma}^{-1} \otimes \mathbf{I}_n) \{\oplus \mathbf{L}_i^{-1}\} \\
&= \{\oplus \mathbf{h}_i(\mathbf{t}) \mathbf{L}_i\} \{\oplus \mathbf{L}_i^{-1}\} = \{\oplus \mathbf{h}_i(\mathbf{t})\},
\end{aligned}$$

$$\mathbf{R}(\mathbf{t}) = \mathbf{C}(\mathbf{t}) - \mathbf{H}(\mathbf{t}) \mathbf{C}(\mathcal{S}, \mathbf{t})$$

$$\begin{aligned}
&= \{\oplus \mathbf{h}_i(\mathbf{t}) \mathbf{L}_i\} (\boldsymbol{\Sigma} \otimes \mathbf{I}_n) \{\oplus \mathbf{L}_i^\top \mathbf{h}_i(\mathbf{t})^\top\} + \mathbf{D}(\mathbf{t}, \mathbf{t}) \boldsymbol{\Sigma} \mathbf{D}(\mathbf{t}, \mathbf{t}) - \\
&\quad - \{\oplus \mathbf{h}_i(\mathbf{t})\} \{\oplus \mathbf{L}_i\} (\boldsymbol{\Sigma} \otimes \mathbf{I}_n) \{\oplus \mathbf{L}_i^\top \mathbf{h}_i(\mathbf{t})^\top\} \\
&= \{\oplus \mathbf{h}_i(\mathbf{t}) \mathbf{L}_i\} (\boldsymbol{\Sigma} \otimes \mathbf{I}_n) \{\oplus \mathbf{L}_i^\top \mathbf{h}_i(\mathbf{t})^\top\} + \mathbf{D}(\mathbf{t}, \mathbf{t}) \boldsymbol{\Sigma} \mathbf{D}(\mathbf{t}, \mathbf{t}) - \\
&\quad - \{\oplus \mathbf{h}_i(\mathbf{t}) \mathbf{L}_i\} (\boldsymbol{\Sigma} \otimes \mathbf{I}_n) \{\oplus \mathbf{L}_i^\top \mathbf{h}_i(\mathbf{t})^\top\} \\
&= \mathbf{D}(\mathbf{t}, \mathbf{t}) \boldsymbol{\Sigma} \mathbf{D}(\mathbf{t}, \mathbf{t}).
\end{aligned}$$

The conclusion follows because the i th row of $\mathbf{H}(\mathbf{t})$ (which is $\mathbf{h}_i(\mathbf{t})$) and the (i, i) element of $\mathbf{R}(\mathbf{t})$ are constructed using $\rho_i(\cdot)$, \mathcal{S} , σ_{ii} , and the predictive mean is thus $\mathbf{h}_i(\mathbf{t}) \mathbf{w}_i$.

Proposition 3.4. Suppose $q = 2$ and $\mathcal{S} = \{\ell_1, \ell_2\}$. Then $p(w_i(\ell_r) \mid \mathbf{w}(\ell_s))$ depends on both $w_i(\ell_s)$ and $w_j(\ell_s)$, for each choice of $i, j, r, s \in \{1, 2\}$, $i \neq j$ and $r \neq s$.

Proof.

$$\mathbf{W} = \begin{bmatrix} w_1(\ell_1) & w_2(\ell_1) \\ w_1(\ell_2) & w_2(\ell_2) \end{bmatrix}, \quad \mathbf{w} = \text{vec}(\mathbf{W}) = (w_1(\ell_1), w_1(\ell_2), w_2(\ell_1), w_2(\ell_2))^\top.$$

$$\mathbf{w} \sim N \left(\boldsymbol{\mu} = \begin{bmatrix} \boldsymbol{\mu}_1 \\ \boldsymbol{\mu}_2 \end{bmatrix}, \mathbf{G} = \begin{bmatrix} \sigma_{11} \mathbf{C}_1 & \sigma_{12} \mathbf{L}_1 \mathbf{L}_2^\top \\ \sigma_{12} \mathbf{L}_2 \mathbf{L}_1^\top & \sigma_{22} \mathbf{C}_2 \end{bmatrix} \right),$$

with $\mathbf{C}_j = \rho_j(\{\ell_1, \ell_2\}, \{\ell_1, \ell_2\}; \boldsymbol{\theta}_j) = \mathbf{L}_j \mathbf{L}_j^\top$ for $j = 1, 2$. Define

$$\mathbf{S}_1 = \begin{bmatrix} 1 & 0 & 0 & 0 \\ 0 & 0 & 1 & 0 \end{bmatrix}, \quad \mathbf{S}_2 = \begin{bmatrix} 0 & 1 & 0 & 0 \\ 0 & 0 & 0 & 1 \end{bmatrix}.$$

Then, $\mathbf{w}(\ell_1) = \mathbf{S}_1 \mathbf{w}$, $\mathbf{w}(\ell_2) = \mathbf{S}_2 \mathbf{w}$, $\boldsymbol{\mu}_{\ell_i} = \mathbf{S}_i \boldsymbol{\mu}$, and $\mathbf{G}_{\ell_i, \ell_j} = \mathbf{S}_i \mathbf{G} \mathbf{S}_j^\top$ for $i, j \in \{1, 2\}$.

Then $\mathbf{w}(\ell_1) \mid \mathbf{w}(\ell_2) = \mathbf{v} \sim N(\mathbf{m}_{1|2}, \mathbf{V}_{1|2})$, where

$$\mathbf{m}_{1|2} = \boldsymbol{\mu}_{\ell_1} + \mathbf{G}_{\ell_1, \ell_2} \mathbf{G}_{\ell_2, \ell_2}^{-1} (\mathbf{v} - \boldsymbol{\mu}_{\ell_2}), \tag{12}$$

$$\mathbf{V}_{1|2} = \mathbf{G}_{\ell_1, \ell_1} - \mathbf{G}_{\ell_1, \ell_2} \mathbf{G}_{\ell_2, \ell_2}^{-1} \mathbf{G}_{\ell_2, \ell_1}. \tag{13}$$

Because $\mathbf{G}_{\ell_1, \ell_2} \mathbf{G}_{\ell_2, \ell_2}^{-1}$ is generally a dense 2×2 matrix, the second element of $\mathbf{m}_{1|2}$ will depend on the first element of \mathbf{v} , and vice-versa. Therefore, marginal predictions at $\mathbf{w}(\ell_1)$ depend on all data at $\mathbf{w}(\ell_2)$ (as well as all covariance parameters).

Proposition 3.5. $p(\mathbf{w}_m(\mathbf{t}) \mid \mathbf{w}_o(\mathbf{t}), \mathbf{w}) = N(\mathbf{w}_m(\mathbf{t}); \mathbf{h}_{m|o}, \mathbf{R}_{m|o}(\mathbf{t}))$, where $\mathbf{h}_{m|o} = \mathbf{H}_m(\mathbf{t})\mathbf{w} + \mathbf{H}_{m|o}(\mathbf{t})(\mathbf{w}_o(\mathbf{t}) - \mathbf{H}_o(\mathbf{t})\mathbf{w})$, $\mathbf{H}_o(\mathbf{t})$ is the submatrix of $\mathbf{H}(\mathbf{t})$ where we take the rows corresponding to o (similarly $\mathbf{H}_m(\mathbf{t})$ with rows m), and

$$\begin{aligned} \mathbf{H}_{m|o}(\mathbf{t}) &= \mathbf{D}_m(\mathbf{t}, \mathbf{t}) \Sigma_{m,o} \Sigma_o^{-1} \mathbf{D}_o^{-1}(\mathbf{t}, \mathbf{t}) = -\mathbf{D}_m(\mathbf{t}, \mathbf{t}) \mathbf{Q}_m^{-1} \mathbf{Q}_{m,o} \mathbf{D}_o^{-1}(\mathbf{t}, \mathbf{t}) \\ \mathbf{R}_{m|o}(\mathbf{t}) &= \mathbf{D}_m(\mathbf{t}, \mathbf{t}) (\Sigma_m - \Sigma_{m,o} \Sigma_o^{-1} \Sigma_{o,m}) \mathbf{D}_m(\mathbf{t}, \mathbf{t}) = \mathbf{D}_m(\mathbf{t}, \mathbf{t}) \mathbf{Q}_m^{-1} \mathbf{D}_m(\mathbf{t}, \mathbf{t}), \end{aligned}$$

where $\Sigma_{m,o}$ subsets Σ to its m rows and o columns, and similarly for \mathbf{Q} .

Proof. All the results are a consequence of the properties of multivariate Gaussians and the previous proposition.

B Section 1: *Introduction*

B.1 Details on Figure 2

The figure displays a 4-outcome multivariate GP with IOX cross-covariance with the following settings:

$$\Sigma = \begin{bmatrix} 1 & -0.9 & 0.7 & 0.8 \\ -0.9 & 1 & -0.5 & -0.7 \\ 0.7 & -0.5 & 1 & 0.8 \\ 0.8 & -0.7 & 0.8 & 1 \end{bmatrix} \quad \begin{aligned} \rho_1(\ell, \ell') &= \mathcal{M}_{\nu=1}(\ell, \ell'; \phi_1 = 15) \\ \rho_2(\ell, \ell') &= \exp\{-15 \cdot \|\ell - \ell'\|\} \cos\{14.9 \cdot \|\ell - \ell'\|\} \\ \rho_3(\ell, \ell') &= \mathcal{M}_{\nu_3=1.5}(\tilde{\ell}, \tilde{\ell}'; \phi_3 = 15) \quad \text{where } \tilde{\ell} = \ell + \mathbf{u}(\ell) \\ \rho_4(\ell, \ell') &= |1 + v(\ell)| |1 + v(\ell')| \mathcal{M}_{\nu_4=1.5}(\ell, \ell'; \phi_4 = 15), \end{aligned}$$

where $\mathbf{u}(\cdot) = (u_1(\cdot), u_2(\cdot))^\top$ is a bivariate GP with independent Matérn margins with parameters $\sigma^2 = 0.03$, $\phi = 1$, $\nu = 1$, and $v(\cdot)$ is a Matérn GP with parameters $\sigma^2 = 0.5$, $\phi =$

30, $\nu = 1.5$. We generate data at a regular grid of 40,000 locations after applying a Vecchia approximation of each univariate GP using $m = 40$ neighbors.

B.2 Key shortcomings of LMCs

The LMC is a tractable model of multivariate spatial dependence which leads to structured covariance matrices and gives rise to a multitude avenues for flexible and scalable models. Here, we provide more details about the limitations of LMCs which we have mentioned in the Introduction section of the main article. LMCs are inadequate in modeling outcomes with different smoothness because the smoothness of outcome j is always equal to the smoothness of the roughest of the k correlation functions (Genton & Kleiber 2015). The difficulty in interpretations and prior elicitation is exemplified by, e.g., a situation in which one builds a LMC on k exponential correlation functions: in this case, the spatial range of outcome j is a non-linear function of all the k spatial range parameters (Schmidt & Gelfand 2003, Section 3.4). For analogous reasons, scalable GP approximations using LMCs are not easy to build: the lack of a direct link between the k constituent spatial processes and each outcome means that it is not straightforward to implement, e.g., outcome-specific neighbor sets for building Vecchia approximations or NNGPs.

LMCs lack flexibility in modeling independent measurement errors because nugget effects in the constituent processes are linearly combined into correlated noise. One must then use LMCs as priors for latent effects, leading to slower computations even when using scalable alternatives to GPs (Finley et al. 2019). In a LMC, nugget effects are linearly combined into correlated measurement error for the outcomes. In fact, the LMC can be expressed as $\mathbf{y}(\boldsymbol{\ell}) = \mathbf{A}(\mathbf{v}(\boldsymbol{\ell}) + \boldsymbol{\nu}(\boldsymbol{\ell}))$ where $\mathbf{v}(\boldsymbol{\ell})$ is the k -variate spatial GP and $\boldsymbol{\nu}(\boldsymbol{\ell}) \stackrel{iid}{\sim} N(\mathbf{0}, \mathbf{D}_\nu)$. Then, $\mathbf{y}(\boldsymbol{\ell}) = \mathbf{A}\mathbf{v}(\boldsymbol{\ell}) + \mathbf{A}\boldsymbol{\nu}(\boldsymbol{\ell})$ implies that the measurement error has covariance $\mathbf{A}\mathbf{D}_\nu\mathbf{A}^\top$,

resulting in considerable inflexibility due to its dependence on \mathbf{A} . We mention two possible ways to address this issue: first, we can build a response model under certain identifiability constraints on the loadings matrix \mathbf{A} (Ren & Banerjee 2013) by letting the last of the k factors be standard normal white noise. The data are directly modeled as a multivariate GP with LMC cross-covariance: $\mathbf{y}(\cdot) \sim GP(\mathbf{x}(\cdot)^\top \boldsymbol{\beta}, \mathbf{C}_{LMC}(\cdot, \cdot))$. Then, the square of the (i, k) element of \mathbf{A} can be interpreted as the (independent) nugget effect for the i th outcome. This choice limits the number of spatial factors to $q - 1$. If, instead, one wants to represent q spatial outcomes as the linear combination of q spatial factors, plus measurement error, then one must resort to an additional set of latent variables, leading to a multivariate regression model with latent effects. In this case, $\mathbf{y}(\cdot) = \mathbf{x}(\cdot)^\top \boldsymbol{\beta} + \mathbf{w}(\cdot) + \boldsymbol{\varepsilon}(\cdot)$, where $\mathbf{w}(\cdot) \sim GP(\mathbf{0}, \mathbf{C}_{LMC}(\cdot, \cdot))$ and $\boldsymbol{\varepsilon}(\cdot)$ is independent Gaussian white noise with covariance D . The distinction between response and latent models is important when building scalable GPs; for instance, a NNGP approximation on the response model is more restrictive than the corresponding approximation on the spatial latent effects. On the other hand, computations with latent models tend to be more inefficient (Finley et al. 2019). IOX introduces nugget effects more directly in response models and thus offers new ways for modeling multivariate spatially-correlated noisy data. Another scenario where a model incorporating nugget effects is preferable arises with multivariate spatial count data. In a log-Gaussian multivariate spatial GLM, accounting for overdispersion typically requires introducing an additional set of random effects, which complicates computation. By contrast, models based on IOX can accommodate overdispersion more directly: the covariance structure on the latent Gaussian field can include a nugget effect without the need for extra random effects.

A subtle feature of LMCs is that they link the number of constituent spatial processes

k to the rank of $\mathbf{A}\mathbf{A}^\top = \mathbf{C}(\boldsymbol{\ell}, \boldsymbol{\ell})$. The q observed outcomes may each be characterized by specific spatial features (e.g., range, smoothness, anisotropy, nonstationarity). However, there may also exist a low rank community structure describing cross-outcome dependence. A possible real-world example is a natural habitat where multiple species coexist and interact within the same spatial niches: although they may form interaction communities, each species may also spread spatially in unique ways. A related issue is that because LMCs define both $C_{ii}(\cdot, \cdot)$ and $C_{ij}(\cdot, \cdot)$, $i \neq j$, based on the same set of k functions, a reduction in k reduces flexibility and expressiveness of both cross- and marginal covariances.

The infill asymptotic properties of LMCs remain poorly understood. LMCs likely inherit inconsistencies of univariate Matérn models (Zhang 2007, Section 6; see also Velandia et al. 2017). In the univariate case, however, the functional form of the microergodic parameter is known and can be estimated consistently (Stein 1990, Zhang 2004). This provides reassurance: even when individual covariance parameters are difficult or inefficient to estimate, the microergodic parameter remains identifiable. For LMCs, no such functional form is currently available. As a result, in applied settings, one may encounter high variance in parameter estimates or inefficient posterior sampling, without a clear way to determine whether these issues stem from the sampling algorithm or from a fundamental lack of asymptotic identifiability of the model parameters.

IOX likely inherits infill behavior from the marginal correlation functions used to define it; an in-depth study of the asymptotic properties of IOX is beyond the scope of this article. The infill asymptotic scenario occurs in practical settings when the Matérn spatial decay is too small relative to the dimension of the spatial domain. By setting ϕ_j large enough in simulations, we ensured its practical estimability. Specifically, we show that IOX performs well in estimating marginal parameters even in the misspecified setting where we generate

data from a multivariate Matérn.

The general inability of a LMC to directly estimate outcome-specific parameters does not depend on whether or not those parameters are identifiable in an infill asymptotic setting. For example, consider the case of a multivariate model with squared exponential marginal correlations (i.e., Matérn with $\nu \rightarrow \infty$). This model is asymptotically identifiable in an infill setting (we did not consider this model in simulations because it is typically considered too smooth for geostatistical applications), yet the LMC remains unable to estimate outcome-specific parameters.

B.3 Comparison with multivariate Matérn

The multivariate Matérn model (Gneiting et al. 2010) defines each $C_{ij}(\cdot, \cdot)$ to be a Matérn function parametrized via $\sigma_{ij}, \phi_{ij}, \nu_{ij}$, with the possible addition of nugget effects. The fact that $C_{ij}(\cdot, \cdot)$ are valid univariate covariance functions for each i, j does not guarantee that the resulting cross-covariance matrix function will also be valid. The validity of the latter depends on the values of the entire set of parameters $\sigma_{ij}, \phi_{ij}, \nu_{ij}$ for $i, j = 1, \dots, q$ in non-trivial ways. Finding the least restrictive constraints on the parameters is an active research area, see, e.g., (Apanasovich et al. 2012, Emery et al. 2022). An additional problem is that if each $C_{ij}(\cdot, \cdot)$ has m free parameters, then the total number of parameters to be estimated from the data is $mq(q+1)/2$ and the constraints on them become increasingly cumbersome to satisfy. The parsimonious Matérn model of Gneiting et al. (2010) resolves this issue by proposing to restrict the parameter space to guarantee the validity of the resulting cross-covariance matrix function. One defines the cross-covariances as

$$C_{ij}(\boldsymbol{\ell}, \boldsymbol{\ell}') = \sigma_{ij} S(\nu_i, \nu_j, d) M_{\frac{1}{2}(\nu_i + \nu_j)}(\boldsymbol{\ell}, \boldsymbol{\ell}'; \phi),$$

$$\text{where } S(\nu_i, \nu_j, d) = \frac{\Gamma(\nu_i + d/2)^{\frac{1}{2}} \Gamma(\nu_j + d/2)^{\frac{1}{2}}}{\Gamma(\nu_i)^{\frac{1}{2}} \Gamma(\nu_j)^{\frac{1}{2}}} \frac{\Gamma(\frac{1}{2}(\nu_i + \nu_j))}{\Gamma(\frac{1}{2}(\nu_i + \nu_j) + d/2)}, \quad (14)$$

and $M_\nu(\boldsymbol{\ell}, \boldsymbol{\ell}'; \phi)$ is the Matérn correlation function with smoothness ν and range $1/\phi$ and $\boldsymbol{\Sigma} = (\sigma_{ij})_{ij}$ is a covariance matrix. In other words, the parsimonious Matérn forces the cross-covariances to have smoothness equal to the average smoothness of the variables they refer to, and all covariances (marginal and cross) to share a single range parameter. Furthermore, the scaling factor $0 < S(\nu_i, \nu_j, d) \leq 1$ operates to ensure validity of the cross-covariance matrix function. Like in IOX, σ_{ij} is the upper bound of $C_{ij}(\boldsymbol{\ell}, \boldsymbol{\ell})$ which is achieved if $\nu_i = \nu_j$. Also similar to IOX is the fact that the smoothness of C_{ij} cannot be chosen freely. However, while IOX allows different ranges, the multivariate Matérn requires additional constraints to be imposed on other parameters to achieve the same result. The validity of IOX is derived directly from the validity of the component correlation functions, whereas one needs to perform further checks in multivariate Matérn models. This makes IOX advantageous when implementing multivariate extensions of non-stationary correlations.

Finally, IOX is advantageous in leading to a structured sample covariance matrix which we take advantage of in developing the models appearing in the main article. The multivariate Matérn does not lead to similar structure.

C Section 2: *Inside-out cross-covariance*

C.1 Constructive interpretation of IOX

We offer a constructive interpretation of IOX. Let \mathcal{T} be sample locations. We consider two scenarios. The first is $\mathcal{S} = \mathcal{T}$, the second is $\mathcal{T} \subset \mathcal{S}^c$. For the scenario $\mathcal{S} = \mathcal{T}$, from $\rho_j(\cdot, \cdot)$, compute \mathbf{L}_j for $j = 1, \dots, q$. For all $\boldsymbol{\ell}_i \in \mathcal{T}$ let $\mathbf{v}(\boldsymbol{\ell}_i) \stackrel{iid}{\sim} N(\mathbf{0}, \boldsymbol{\Sigma})$. Denote $\mathbf{V} = [\mathbf{v}(\boldsymbol{\ell}_1) \cdots \mathbf{v}(\boldsymbol{\ell}_n)]^\top$ —therefore, \mathbf{V} is a matrix-normal random matrix $\mathbf{V} \sim MN(\mathbf{0}, \mathbf{I}_n, \boldsymbol{\Sigma})$.

Then, $\mathbf{w} = \{\oplus \mathbf{L}_j\} \text{vec}(\mathbf{V})$ is $\mathbf{w} \sim N(\mathbf{0}, \{\oplus \mathbf{L}_j\}(\boldsymbol{\Sigma} \otimes \mathbf{I}_n)\{\oplus \mathbf{L}_j^\top\})$ as desired. Figure 1 in the main article shows an example in which we generate 3 spatially correlated outcomes with different smoothness via IOX. If only \mathbf{L}_i^{-1} is available for $i = 1, \dots, q$, then from \mathbf{v}_j (the j th column of \mathbf{V}), one obtains $\mathbf{w}_j = \text{solve}(\mathbf{L}_j^{-1}, \mathbf{v}_j)$ without needing to compute \mathbf{L}_i directly.

For the second scenario, let $\mathcal{T} = \{\mathbf{t}_1, \dots, \mathbf{t}_N\}$ be sample locations and $\mathcal{S} = \{\boldsymbol{\ell}_1, \dots, \boldsymbol{\ell}_n\}$. We assume $\mathcal{T} \subset \mathcal{S}^c$. From $\rho_j(\cdot, \cdot)$, compute $\mathbf{L}_j = \text{chol}(\rho_j(\mathcal{S}))$ for $j = 1, \dots, q$. For all $\boldsymbol{\ell}_i \in \mathcal{S}$ let $\mathbf{v}(\boldsymbol{\ell}_i) \stackrel{iid}{\sim} N(\mathbf{0}, \boldsymbol{\Sigma})$. Denote $\mathbf{V} = [\mathbf{v}(\boldsymbol{\ell}_1) \cdots \mathbf{v}(\boldsymbol{\ell}_n)]^\top$ —therefore, \mathbf{V} is a matrix-normal random matrix $\mathbf{V} \sim MN(\mathbf{0}, \mathbf{I}_n, \boldsymbol{\Sigma})$. Then, $\mathbf{w}_\mathcal{S} = \{\oplus \mathbf{L}_j\} \text{vec}(\mathbf{V})$ is $\mathbf{w} \sim N(\mathbf{0}, \{\oplus \mathbf{L}_j\}(\boldsymbol{\Sigma} \otimes \mathbf{I}_n)\{\oplus \mathbf{L}_j^\top\})$ as desired. Finally, for each $\mathbf{t} \in \mathcal{T}$ sample from $N(\mathbf{w}(\mathbf{t}); \mathbf{m}_w(\mathbf{t}), \mathbf{R}(\mathbf{t}))$, where $\mathbf{m}_w(\mathbf{t}) = \mathbf{H}(\mathbf{t})\mathbf{w}_\mathcal{S}$, $\mathbf{H}(\mathbf{t}) = \{\oplus \mathbf{h}_j(\mathbf{t})\}$ and $\mathbf{R}(\mathbf{t}) = \mathbf{D}(\mathbf{t}, \mathbf{t})\boldsymbol{\Sigma}\mathbf{D}(\mathbf{t}, \mathbf{t})$. We take \mathcal{S} as a 100×100 regular grid in $\mathcal{D} = [0, 1]^2$ and sample a noise-free trivariate GP-IOX at a regular grid of dimension 200×200 using the same parameter settings as in Figure 1 in the main article. Figure 9 shows the resulting maps.

We outline an equivalent method for prior sampling. Call $\mathcal{G}_\mathcal{S}$ the DAG at \mathcal{S} and let the DAG for $\mathcal{S} \cup \mathcal{T}$, \mathcal{G} , be such that each node from \mathcal{T} has \mathcal{S} as its set of parents. For Vecchia-GP models, the set of parents for $\mathbf{t} \in \mathcal{T}$ is restricted to the nearest neighbors within \mathcal{S} . Based on the DAG, compute \mathbf{L}_j^{-1} from $j = 1, \dots, q$. The elements of \mathbf{L}_j^{-1} can be directly computed in the following way. Let $\mathbf{h}_l = \rho_i(\boldsymbol{\ell}_l, \boldsymbol{\ell}_{[l]})\rho_i(\boldsymbol{\ell}_{[l]})^{-1}$, $\mathbf{r}_l = \rho_i(\boldsymbol{\ell}_l, \boldsymbol{\ell}_l) - \mathbf{h}_l\rho_i(\boldsymbol{\ell}_{[l]}, \boldsymbol{\ell}_l)$, where $[l]$ denotes the set of parents of node l in the graph \mathcal{G} . Then, the diagonal elements of \mathbf{L}_j^{-1} are $1/\sqrt{\mathbf{r}_\boldsymbol{\ell}}$ for $\boldsymbol{\ell} \in \mathcal{S} \cup \mathcal{T}$. The non-zero elements of row a are $-\mathbf{h}_a/\sqrt{\mathbf{r}_a}$. Moving on, for all $\boldsymbol{\ell} \in \mathcal{S} \cup \mathcal{T}$, let $\mathbf{v}(\boldsymbol{\ell}) \stackrel{iid}{\sim} N(\mathbf{0}, \boldsymbol{\Sigma})$. Denote $\mathbf{V} = [\mathbf{v}(\boldsymbol{\ell}_1) \cdots \mathbf{v}(\boldsymbol{\ell}_n), \mathbf{v}(\mathbf{t}_1), \dots, \mathbf{v}(\mathbf{t}_N)]^\top$ —therefore, \mathbf{V} is a matrix-normal random matrix $\mathbf{V} \sim MN(\mathbf{0}, \mathbf{I}_{n+N}, \boldsymbol{\Sigma})$. Then, let $\mathbf{w} = \{\oplus \mathbf{L}_j\} \text{vec}(\mathbf{V})$ and build the $(n + N) \times q$ matrix \mathbf{W} from \mathbf{w} in column-major ordering. The last N rows of \mathbf{W} have the desired marginal distribution.

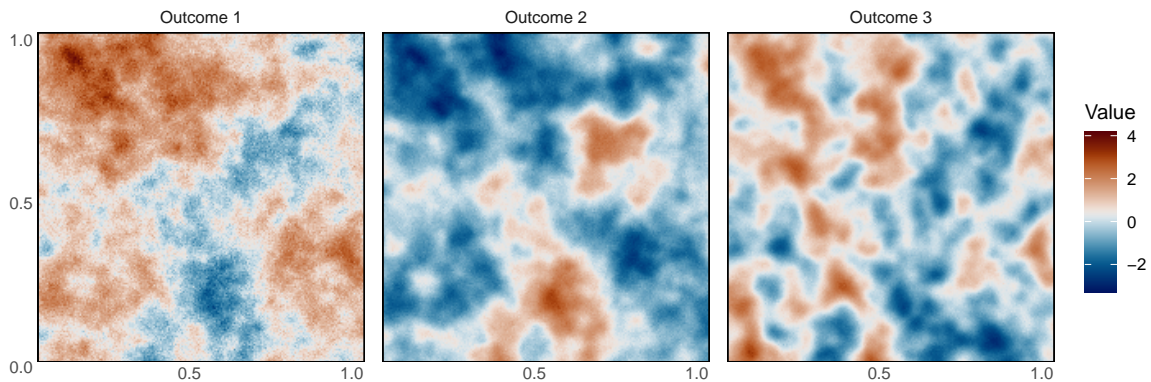


Figure 9: Three spatially correlated outcomes generated via GP-IOX at $n = 40,000$ gridded locations from a reference set of size $n_S = 2,500$. We let $\sigma_{ii} = 1$ for $i \in \{1, 2, 3\}$ and $\sigma_{12} = -0.9, \sigma_{13} = 0.7, \sigma_{23} = -0.5$ and choose $\rho_i(\cdot, \cdot)$ as Matérn (Vecchia-approximated with $m = 40$ neighbors) with range $1/5, 1/15, 1/30$ and smoothness $0.5, 1.2, 1.9$, respectively.

We can compare how IOX is defined constructively relative to a LMC. In LMCs, one introduces spatial dependence first, and then multivariate dependence, whereas the order of these operations is inverted in IOX. In Table 4 we outline prior sampling for IOX and LMCs in a way that clarifies this point visually. Figure 10 visualizes the resulting sample covariances.

Step	IOX	Separable model	LMC
1	\mathcal{S} sample locations		
2	$U \sim MN(\mathbf{0}, \mathbf{I}_n, \mathbf{I}_q)$		
3	$\mathbf{A}\mathbf{A}^T = \Sigma$		
4	$\mathbf{R}_j = \rho_j(\mathcal{S})$ for $j = 1, \dots, q$	$\mathbf{R} = \rho(\mathcal{S})$	$\mathbf{R}_j = \rho_j(\mathcal{S})$ for $j = 1, \dots, k$
5	$\mathbf{L}_j = \text{chol}(\mathbf{R}_j)$	$\mathbf{L} = \text{chol}(\mathbf{R})$	$\mathbf{L}_j = \text{chol}(\mathbf{R}_j)$
6	$\mathbf{v} = (\mathbf{A} \otimes \mathbf{I}_n) \text{vec}(\mathbf{U})$	$\mathbf{W} = \mathbf{L}\mathbf{U}\mathbf{A}^T$	$\mathbf{v} = \{\oplus \mathbf{L}_j\} \text{vec}(\mathbf{U})$
7	$\mathbf{w} = \{\oplus \mathbf{L}_j\} \mathbf{v}$	$\mathbf{w} = \text{vec}(\mathbf{W})$	$\mathbf{w} = (\mathbf{A} \otimes \mathbf{I}_n) \mathbf{v}$
8	$\mathbf{w} \sim N(\mathbf{0}, \mathbf{C})$	$\mathbf{w} \sim N(\mathbf{0}, \mathbf{C})$	$\mathbf{w} \sim N(\mathbf{0}, \mathbf{C})$
$\mathbf{C} =$	$\{\oplus \mathbf{L}_j\} (\Sigma \otimes \mathbf{I}_n) \{\oplus \mathbf{L}_j^T\}$	$\Sigma \otimes \mathbf{R}$	$(\mathbf{A} \otimes \mathbf{I}_n) \{\oplus \mathbf{R}_j\} (\mathbf{A} \otimes \mathbf{I}_n)^T$

Table 4: Comparison of prior sampling of $\mathbf{w}(\cdot) \sim GP(\mathbf{0}, \mathbf{C}(\cdot, \cdot))$ at \mathcal{S} using IOX and coregionalization models. We color code the spatial components of the sample cross-covariance matrix in **pink**, the multivariate components in **emerald**.

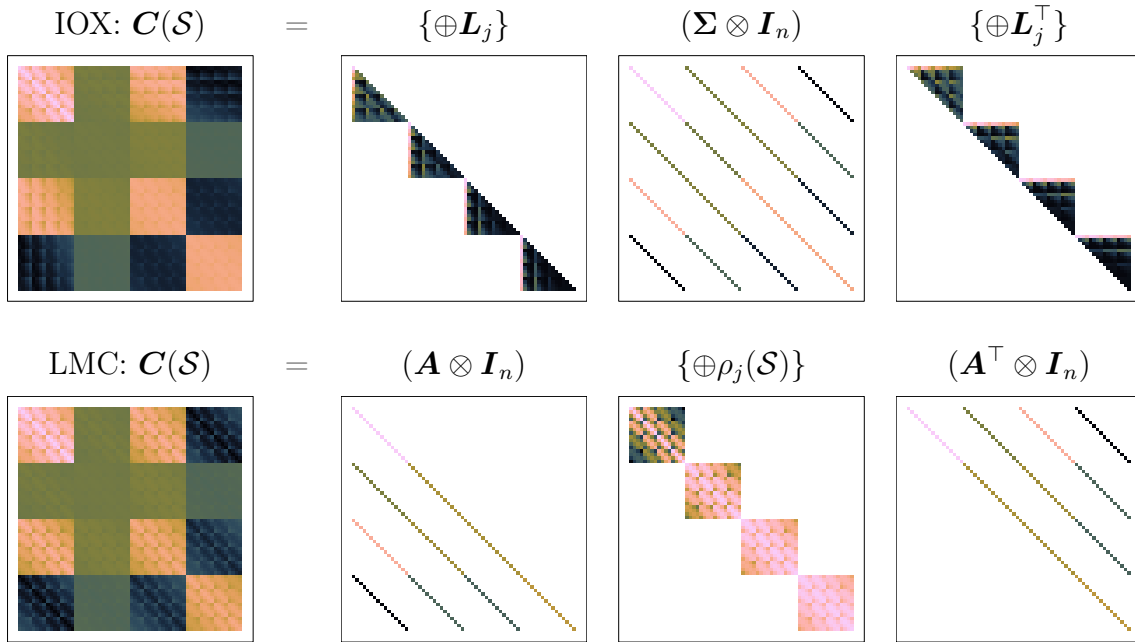


Figure 10: Visualization of IOX and LMC sample covariance matrices and the sparsity patterns of their components.

C.2 Additional considerations on $C_{ij}(\cdot, \cdot), i \neq j$

Our IOX cross-covariance matrix function is built on the idea that, in practice, we aim to primarily infer about $C_{ii}(\cdot, \cdot)$ while *accounting* for cross-variable spatial dependence, without the latter being the primary inferential target. In IOX the cross-covariance $C_{ij}(\cdot, \cdot)$ is not as directly interpretable as $C_{ii}(\cdot, \cdot)$. Here, we provide details on (1) how to interpret $C_{ij}(\cdot, \cdot)$ and (2) how to model $C_{ij}(\cdot, \cdot)$ more flexibly when explicit parametric models are needed.

For a given \mathcal{S} and a set of $\rho_i(\cdot, \cdot)$ and associated parameters, let \mathcal{T} be a set of m test locations, and $\mathbf{h} = (h_x, h_y)$. Then, compute

$$\tilde{C}_{ij}(\mathbf{h}) = \frac{1}{mn_a} \sum_{a=1}^{n_a} \sum_{\ell \in \mathcal{T}} C_{ij}(\ell, \ell + \mathbf{h}_a), \quad \text{where } \mathbf{h}_a = \begin{bmatrix} h_x \cos(2\pi a/n_a) \\ h_y \sin(2\pi a/n_a) \end{bmatrix}. \quad (15)$$

In particular, we may be interested in computing $\tilde{C}_{ij}(\mathbf{0})$, which reduces (15) to

$$\tilde{C}_{ij}(\mathbf{0}) = \frac{1}{mn_a} \sum_{a=1}^{n_a} \sum_{\ell \in \mathcal{T}} C_{ij}(\ell, \ell). \quad (16)$$

IOX includes a scaling factor which as we showed in the main article results in $C_{ij}(\ell, \ell') < \sigma_{ij}$ for any i, j such that $\rho_i(\cdot, \cdot) \neq \rho_j(\cdot, \cdot)$. This is unsurprising; suppose \mathbf{y}_1 and \mathbf{y}_2 are two noise-free, jointly IOX variables at \mathcal{S} . The limit case $\sigma_{12} \rightarrow 1$ implies near-collinearity of the spatially uncorrelated matrix-normal matrix \mathbf{V} used to generate \mathbf{Y} (see Section C.1), not of \mathbf{Y} itself.

Our method restricts the cross-covariances $C_{ij}(\cdot, \cdot)$ through a product of the marginal Cholesky factors. Consequently, $C_{ij}(\cdot, \cdot)$ is parametrized directly via σ_{ij} but implicitly on $\rho_i(\cdot, \cdot)$ and $\rho_j(\cdot, \cdot)$ and their parameters. For example, if $\rho_j(\cdot, \cdot)$ is Matérn for all j , $C_{ij}(\cdot, \cdot)$ in IOX is not Matérn and is also not explicitly parametrized via range and smoothness parameters—it depends indirectly on $1/\phi_i, 1/\phi_j, \nu_i, \nu_j$. In a bivariate Matérn, on the other hand, $C_{ij}(\cdot, \cdot)$ is Matérn with smoothness ν_{ij} and range $1/\phi_{ij}$. We note that these parameters must be chosen carefully to ensure validity of the resulting cross-covariance matrix function (Emery et al. 2022), and interpreting them is also not straightforward (Kleiber 2017). Refer to the discussion at Section B.3 comparing IOX to multivariate Matérns.

In situations in which it is desirable to model $C_{ij}(\cdot, \cdot)$ flexibly for some i, j , perhaps as a Matérn, we can straightforwardly generalize IOX. Without loss of generality, let $\xi = \{1, 2\}$ be the pair of outcomes we wish to model more flexibly and $\boldsymbol{\rho}_\xi(\cdot, \cdot)$ the marginal cross-correlation matrix function for the ξ variables. $\boldsymbol{\rho}_\xi(\cdot, \cdot)$ must be a valid cross-correlation matrix function with $\rho_{11}(\cdot, \cdot)$, $\rho_{12}(\cdot, \cdot)$ and $\rho_{22}(\cdot, \cdot)$ margins. Let \mathbf{L}_ξ the $2n \times 2n$ lower Cholesky factor of $\boldsymbol{\rho}_\xi(\mathcal{S})$, and let $\mathbf{h}_\xi(\ell) = \boldsymbol{\rho}_\xi(\ell, \mathcal{S})\boldsymbol{\rho}_\xi(\mathcal{S})^{-1}$, $\mathbf{r}_\xi(\ell) = \boldsymbol{\rho}_\xi(\ell, \ell) - \mathbf{h}_\xi(\ell)\boldsymbol{\rho}_\xi(\mathcal{S}, \ell)$.

Finally, let

$$\mathbf{D}_\xi(\boldsymbol{\ell}, \boldsymbol{\ell}') = \mathbb{1}_{\{\boldsymbol{\ell}=\boldsymbol{\ell}'\}} \begin{bmatrix} \text{chol}(\mathbf{r}_\xi(\boldsymbol{\ell})) & & & \\ & \sqrt{r_3(\boldsymbol{\ell})} & & \\ & & \ddots & \\ & & & \sqrt{r_q(\boldsymbol{\ell})} \end{bmatrix}.$$

Then, we can define the IOX cross-covariance matrix function as

$$\begin{aligned} \mathbf{C}(\boldsymbol{\ell}, \boldsymbol{\ell}') &= (\mathbf{h}_\xi(\boldsymbol{\ell})\mathbf{L}_\xi \oplus \{\oplus_{j>2} \mathbf{h}_j(\boldsymbol{\ell})\mathbf{L}_j\}) (\boldsymbol{\Sigma} \otimes \mathbf{I}_n) (\mathbf{L}_\xi^\top \mathbf{h}_\xi(\boldsymbol{\ell})^\top \oplus \{\oplus_{j>2} \mathbf{L}_j^\top \mathbf{h}_j(\boldsymbol{\ell})^\top\}) + \\ &\quad + \mathbf{D}_\xi(\boldsymbol{\ell}, \boldsymbol{\ell}') \boldsymbol{\Sigma} \mathbf{D}_\xi^\top(\boldsymbol{\ell}, \boldsymbol{\ell}') \\ &= \begin{bmatrix} \mathbf{h}_\xi(\boldsymbol{\ell})\mathbf{L}_\xi & & & \\ & \mathbf{h}_3(\boldsymbol{\ell})\mathbf{L}_3 & & \\ & & \ddots & \\ & & & \mathbf{h}_q(\boldsymbol{\ell})\mathbf{L}_q \end{bmatrix} (\boldsymbol{\Sigma} \otimes \mathbf{I}_n) \begin{bmatrix} \mathbf{L}_\xi^\top \mathbf{h}_\xi(\boldsymbol{\ell})^\top & & & \\ & \mathbf{L}_3^\top \mathbf{h}_3(\boldsymbol{\ell})^\top & & \\ & & \ddots & \\ & & & \mathbf{L}_q^\top \mathbf{h}_q(\boldsymbol{\ell})^\top \end{bmatrix} + \\ &\quad + \mathbf{D}_\xi(\boldsymbol{\ell}, \boldsymbol{\ell}') \boldsymbol{\Sigma} \mathbf{D}_\xi^\top(\boldsymbol{\ell}, \boldsymbol{\ell}'), \end{aligned}$$

where we essentially treat ξ as a grouped variable. The computationally convenient structure of IOX is lost at ξ but retained for all other variables. Following Proposition 2.1, the marginal cross-covariance of ξ will be a function of $\boldsymbol{\rho}_\xi(\cdot, \cdot)$ as desired. We can extend this further to allow explicit models of any groups of variables, at additional computational costs.

C.3 Choice of \mathcal{S}

Our recommendation in the main article is to take \mathcal{S} as the set of observed locations. This recommendation follows from the consideration that in doing so, IOX leads to straightforward interpretations of marginal covariance as in Proposition 2.1. The set \mathcal{S} is also where IOX allows cross-spatial-dependence, as in Proposition 3.4. However, one can in principle choose \mathcal{S} as any set of locations. In Figure 11 we investigate the effect the size of \mathcal{S} on the

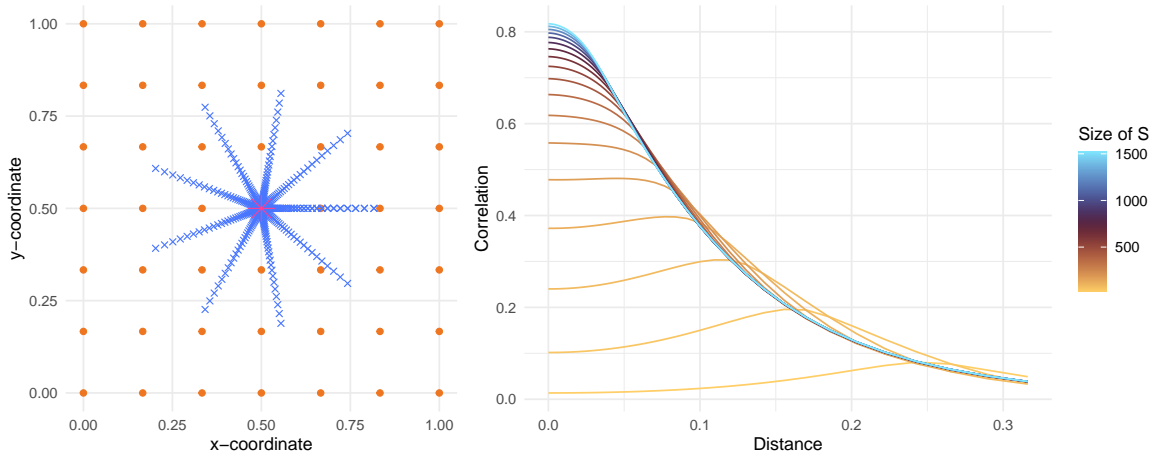


Figure 11: Left: orange points correspond to \mathcal{S} locations. Here, \mathcal{S} is computed as a regular grid on 7^2 coordinates, minus the center point with coordinate $(1/2, 1/2)$. We compute $C_{ij}(\boldsymbol{\ell}, \boldsymbol{\ell}')$ where $\boldsymbol{\ell} = (1/2, 1/2)$ and $\boldsymbol{\ell}'$ is each blue location with “x” shape. We choose the marginal correlations as Matérn with $\phi_i = 10$, $\phi_j = 20$, and smoothness $\nu_i = \nu_j = 1$. We average $C_{ij}(\boldsymbol{\ell}, \boldsymbol{\ell}')$ across pairs of locations at the same distance to ultimately obtain the plot on the right, where each line corresponds to a different \mathcal{S} .

resulting $C_{ij}(\cdot, \cdot)$, where $i \neq j$. We consider a scenario where we evaluate $C_{ij}(\cdot, \cdot)$ at pairs locations $\boldsymbol{\ell}, \boldsymbol{\ell}'$ neither of which are in \mathcal{S} . This matches a situation in which, say, the data are observed irregularly in the domain, and we choose \mathcal{S} as a grid, akin to the typical knot setup of a “predictive process” (Banerjee et al. 2008). In this setting, Figure 11 shows that choosing \mathcal{S} too small leads to a shrinkage the cross-correlation function at all distances.

Therefore, although a small \mathcal{S} facilitates computations, it also leads to a reduction in the allowed cross-spatial dependence.

C.4 Covariance-based definition of IOX

We have defined IOX on the basis of q univariate correlation functions in the main article, but we can equivalently define IOX on a given list of q covariance functions. Let $\boldsymbol{\Sigma} = (\sigma_{ij})_{i,j=1}^q$ be a positive semidefinite matrix, $K_i(\cdot, \cdot) = s_i^2 \rho_i(\cdot, \cdot)$ for $i = 1, \dots, q$, where $\rho_i(\cdot, \cdot)$

is a univariate correlation function and let \mathcal{S} be the reference set. Then, we define IOX as

$$C_{ij}(\boldsymbol{\ell}, \boldsymbol{\ell}') = \sigma_{ij} s_i s_j [\mathbf{h}_i(\boldsymbol{\ell}) \mathbf{L}_i \mathbf{L}_j^\top \mathbf{h}_j(\boldsymbol{\ell}') + \varepsilon(\boldsymbol{\ell}, \boldsymbol{\ell}')],$$

where $s_j > 0$ for all j , $\mathbf{h}_i(\boldsymbol{\ell}) = \rho_i(\boldsymbol{\ell}, \mathcal{S}) \rho_i(\mathcal{S})^{-1}$, \mathbf{L}_i is the lower Cholesky factor of $\rho_i(\mathcal{S})$, $\varepsilon(\boldsymbol{\ell}, \boldsymbol{\ell}') = \mathbb{1}_{\{\boldsymbol{\ell}=\boldsymbol{\ell}'\}} \sqrt{r_i(\boldsymbol{\ell}) r_j(\boldsymbol{\ell}')}$, and $r_i(\boldsymbol{\ell}) = \rho_i(\boldsymbol{\ell}, \boldsymbol{\ell}) - \mathbf{h}_i(\boldsymbol{\ell}) \rho_i(\mathcal{S}, \boldsymbol{\ell})$. The validity of the resulting IOX model is verified straightforwardly following the main article. The only change here is that we use $\boldsymbol{\Sigma}^* = \mathbf{D}_s \boldsymbol{\Sigma} \mathbf{D}_s$, where $\mathbf{D}_s = \text{diag}\{s_i\}_{i=1}^q$, rather than $\boldsymbol{\Sigma}$. Clearly, $\boldsymbol{\Sigma}^*$ is positive semidefinite if $\boldsymbol{\Sigma}$ is. All other components of the model remain the same. In the above model, \mathbf{D}_s and $\boldsymbol{\Sigma}$ are not identifiable, but $\boldsymbol{\Sigma}^*$ is. This suggests strategies for parameter expansion, which may improve the efficiency of posterior sampling algorithms; see, e.g., Papaspiliopoulos et al. (2007), Peruzzi et al. (2025).

D Section 3: IOX Gaussian process models

D.1 Latent factor models for the large q case

IOX can operate dimension reduction by assuming $\boldsymbol{\Sigma}$ is low rank, i.e., $\boldsymbol{\Sigma} = \mathbf{A} \mathbf{A}^\top$ where \mathbf{A} is a $q \times k$ matrix of full column rank. Changing k has no impact on the marginal properties of IOX because Proposition 2.1 does not depend on k . Let $\tilde{\mathbf{y}} = \{\oplus \mathbf{L}_j^{-1}\}(\mathbf{y} - \mathbf{X}_q \boldsymbol{\beta})$ and $\tilde{\boldsymbol{\varepsilon}} = \{\oplus \mathbf{L}_j^{-1}\} \boldsymbol{\varepsilon}$. We can rewrite the latent model as

$$\tilde{\mathbf{y}} = \mathbf{v} + \tilde{\boldsymbol{\varepsilon}}, \quad \mathbf{v} \sim N(\mathbf{0}, \boldsymbol{\Sigma} \otimes \mathbf{I}_n), \quad \tilde{\boldsymbol{\varepsilon}} \sim N(\mathbf{0}, \mathbf{B}), \quad (17)$$

where \mathbf{B} is a block-diagonal matrix whose j th block is $\mathbf{L}_i^{-1} \mathbf{L}_i^{-\top}$. Then, letting $\mathbf{u}(\boldsymbol{\ell}) \stackrel{iid}{\sim} N(\mathbf{0}, \mathbf{I}_k)$ we have $\mathbf{v}(\boldsymbol{\ell}) = \mathbf{A} \mathbf{u}(\boldsymbol{\ell})$. In matrix form, $\tilde{\mathbf{Y}} = \mathbf{U} \mathbf{A}^\top + \tilde{\mathbf{E}}$, where $\mathbf{U} \sim MN(\mathbf{0}, \mathbf{I}_n, \mathbf{I}_k)$ and $\tilde{\mathbf{E}} \sim MN(\mathbf{0}, \mathbf{B}, \mathbf{I}_q)$. A low-rank $\boldsymbol{\Sigma}$ leads to computational savings in sampling \mathbf{w} . We

obtain

$$\begin{aligned}
\mathbf{M}_{w|y}^{-1} &= \{\oplus \mathbf{L}_i^{-\top}\}(\boldsymbol{\Sigma}^{-1} \otimes \mathbf{I}_n)\{\oplus \mathbf{L}_i^{-1}\} + (\boldsymbol{\Delta}^{-1} \otimes \mathbf{I}_n) \\
&= \{\oplus \mathbf{L}_i^{-\top}\}(\mathbf{A}^{+\top} \otimes \mathbf{I}_n)(\mathbf{A}^+ \otimes \mathbf{I}_n)\{\oplus \mathbf{L}_i^{-1}\} + (\boldsymbol{\Delta}^{-1} \otimes \mathbf{I}_n) \\
&= \mathbf{K}\mathbf{K}^\top + (\boldsymbol{\Delta}^{-1} \otimes \mathbf{I}_n)
\end{aligned}$$

where $\mathbf{K} = \{\oplus \mathbf{L}_i^{-\top}\}(\mathbf{A}^{+\top} \otimes \mathbf{I}_n)$ is a $nq \times nk$ matrix, and \mathbf{A}^+ is the $k \times q$ Moore-Penrose pseudoinverse of \mathbf{A} . Although the prior on \mathbf{w} is singular if $k < q$, the posterior is well-defined, since $\mathbf{M}_{w|y}$ is full rank. We can then take advantage of the Woodbury matrix identity in sampling \mathbf{w} a posteriori to make the cost for sampling \mathbf{w} depend on k rather than q . Finally, to update \mathbf{A} we first deterministically compute $\mathbf{u} = \mathbf{A}^+\{\oplus \mathbf{L}_i^{-1}\}\mathbf{w}$, then, since $\tilde{\mathbf{y}}_i = \mathbf{U}\mathbf{A}[i, :]^\top + \tilde{\boldsymbol{\varepsilon}}_i$, we update each row of \mathbf{A} in parallel. Under a Gaussian prior on $\mathbf{A}[i, :]^\top$ with prior covariance \mathbf{M}_A , the full conditional distribution is Gaussian with precision matrix $\mathbf{U}^\top \mathbf{L}_i^\top \mathbf{L}_i \mathbf{U} + \mathbf{M}_A^{-1}$. Here, computing $\mathbf{L}_i \mathbf{U}$ involves solving the linear system $\mathbf{L}_i^{-1} \boldsymbol{\alpha} = \mathbf{U}$, which is cheap because \mathbf{L}_i^{-1} is triangular.

Due to the dimension of $\mathbf{M}_{w|y}$, single block updates of \mathbf{w} may be computationally prohibitive in large n settings, even if we assume a sparse DAG, k is relatively small, and we use sparse Cholesky (Chen et al. 2008) or preconditioned conjugate gradient methods (Nishimura & Suchard 2023). Instead of block sampling, we can take advantage of an assumed sparse DAG GP and sample from the full conditional distributions at DAG nodes.

E Section 4: *Computations with GP-IOX models*

E.1 Posterior sampling: response model

We outline the remainder of the Gibbs sampler for the response model outlined in the main article. For $\boldsymbol{\beta}$, we have $p(\boldsymbol{\beta} \mid \mathbf{y}, \boldsymbol{\theta}, \boldsymbol{\Sigma}) = N(\mathbf{m}_{\boldsymbol{\beta}|\mathbf{y}}, \mathbf{M}_{\boldsymbol{\beta}|\mathbf{y}})$, where

$$\mathbf{M}_{\boldsymbol{\beta}|\mathbf{y}}^{-1} = \mathbf{M}_{\boldsymbol{\beta}}^{-1} + \mathbf{X}_q^\top \mathbf{C}^{-1} \mathbf{X}_q \quad \text{and} \quad \mathbf{M}_{\boldsymbol{\beta}|\mathbf{y}}^{-1} \mathbf{m}_{\boldsymbol{\beta}|\mathbf{y}} = \mathbf{V}_{\boldsymbol{\beta}}^{-1} \mathbf{m}_{\boldsymbol{\beta}} + \mathbf{X}_q^\top \mathbf{C}^{-1} \mathbf{y}.$$

For updating $\boldsymbol{\Sigma}$, first compute $\mathbf{U} = \mathbf{Y} - \mathbf{X}\mathbf{B}$, where \mathbf{B} is the $p \times q$ matrix of regression coefficients. Then, compute the nq -dimensional vector $\mathbf{v} = \{\oplus \mathbf{L}_i^{-1}\} \text{vec}(\mathbf{U})$, where dependence on $\boldsymbol{\theta}$ is through \mathbf{L}_i , $i = 1, \dots, q$. Then build the $n \times q$ matrix \mathbf{V} such that $\text{vec}(\mathbf{V}) = \mathbf{v}$. Notice that \mathbf{V} is the centered and spatially “whitened” version of \mathbf{Y} , and according to our model, $\mathbf{V} \sim MN(\mathbf{0}, \mathbf{I}_n, \boldsymbol{\Sigma})$. Then, with the prior $p(\boldsymbol{\Sigma}) \propto \det(\boldsymbol{\Sigma})^{-\frac{\nu_{\boldsymbol{\Sigma}}+q+1}{2}} \exp\{-\frac{\text{tr}(\boldsymbol{\Psi}\boldsymbol{\Sigma}^{-1})}{2}\}$, i.e., $\boldsymbol{\Sigma} \sim \mathcal{W}^{-1}(\nu_{\boldsymbol{\Sigma}}, \boldsymbol{\Psi}^{-1})$, the conditional posterior is $p(\boldsymbol{\Sigma} \mid \mathbf{y}, \boldsymbol{\theta}, \boldsymbol{\beta}) = \mathcal{W}^{-1}(\nu_{\boldsymbol{\Sigma}|\mathbf{y}}, \boldsymbol{\Psi}_{\boldsymbol{\Sigma}|\mathbf{y}}^{-1})$, where $\nu_{\boldsymbol{\Sigma}|\mathbf{y}} = \nu_{\boldsymbol{\Sigma}} + n$ and $\boldsymbol{\Psi}_{\boldsymbol{\Sigma}|\mathbf{y}} = \boldsymbol{\Psi} + \mathbf{V}^\top \mathbf{V}$.

E.2 Posterior sampling: latent model

We outline the remainder of the Gibbs sampler for the latent model outlined in the main article. For $\boldsymbol{\beta}$, we have $p(\boldsymbol{\beta} \mid \mathbf{y}, \mathbf{w}, \boldsymbol{\Delta}) = N(\mathbf{m}_{\boldsymbol{\beta}|\mathbf{y}}, \mathbf{M}_{\boldsymbol{\beta}|\mathbf{y}})$, where

$$\mathbf{M}_{\boldsymbol{\beta}|\mathbf{y}}^{-1} = \mathbf{M}_{\boldsymbol{\beta}}^{-1} + \mathbf{X}_q^\top (\boldsymbol{\Delta}^{-1} \otimes \mathbf{I}_n) \mathbf{X}_q \quad \text{and} \quad \mathbf{M}_{\boldsymbol{\beta}|\mathbf{y}}^{-1} \mathbf{m}_{\boldsymbol{\beta}|\mathbf{y}} = \mathbf{M}_{\boldsymbol{\beta}}^{-1} \mathbf{m}_{\boldsymbol{\beta}} + \mathbf{X}_q^\top (\boldsymbol{\Delta}^{-1} \otimes \mathbf{I}_n) (\mathbf{y} - \mathbf{w}).$$

For $\boldsymbol{\Sigma}$, the Bayesian DAG implies $p(\boldsymbol{\Sigma} \mid \mathbf{y}, \boldsymbol{\beta}, \mathbf{w}, \boldsymbol{\Delta}, \boldsymbol{\theta}) = p(\boldsymbol{\Sigma} \mid \mathbf{w}, \boldsymbol{\theta})$. We again let $\boldsymbol{\Sigma} \sim \mathcal{W}^{-1}(\nu_{\boldsymbol{\Sigma}}, \boldsymbol{\Psi}^{-1})$. Compute the nq -dimensional vector $\mathbf{v} = \{\oplus \mathbf{L}_i^{-1}\} \text{vec}(\mathbf{W})$, where dependence on $\boldsymbol{\theta}$ is through \mathbf{L}_i , $i = 1, \dots, q$. Then build the $n \times q$ matrix \mathbf{V} such that $\text{vec}(\mathbf{V}) = \mathbf{v}$. Then, $p(\boldsymbol{\Sigma} \mid \mathbf{w}) = \mathcal{W}^{-1}(\nu_{\boldsymbol{\Sigma}|\mathbf{w}}, \boldsymbol{\Psi}_{\boldsymbol{\Sigma}|\mathbf{w}}^{-1})$, where $\nu_{\boldsymbol{\Sigma}|\mathbf{w}} = \nu_{\boldsymbol{\Sigma}} + n$ and $\boldsymbol{\Psi}_{\boldsymbol{\Sigma}|\mathbf{w}}^{-1} = \boldsymbol{\Psi} + \mathbf{V}^\top \mathbf{V}$. Finally, we update $\boldsymbol{\Delta} = \text{diag}\{\delta_{ii}\}_{i=1, \dots, q}$. For each j , we sample $\delta_{jj} \mid \mathbf{y}_j, \boldsymbol{\beta}_j, \mathbf{w}_j$

from an Inverse Gamma distribution with parameters $a_{d|y} = a_d + n/2$ and $b_{d|y} = b_d + \frac{1}{2}\tilde{\mathbf{y}}_j^\top \tilde{\mathbf{y}}$, where $\tilde{\mathbf{y}}_j = \mathbf{y}_j - \mathbf{X}\boldsymbol{\beta}_j - \mathbf{w}_j$.

E.3 Sequential single-site sampler for sparse latent models

Suppose we build IOX with a Vecchia-approximated $\tilde{\rho}_j(\cdot, \cdot)$ for each $i = 1, \dots, q$. As a consequence, $\tilde{\rho}_j(\mathcal{S})^{-1} = \tilde{\mathbf{L}}_j^{-1} \tilde{\mathbf{L}}_j^{-1}$ where $\tilde{\mathbf{L}}_j^{-1}$ is sparse. Moving forward, we will denote $\mathbf{L}_i = \tilde{\mathbf{L}}_i$ to reduce the burden of notation and similarly for $\tilde{\rho}_j(\cdot, \cdot)$. A consequence of our sparsity assumption is that we want to work with \mathbf{L}_j^{-1} and $\rho_j(\mathcal{S})^{-1}$, and *not* with \mathbf{L}_j and $\rho_i(\mathcal{S})$, because the former pair are sparse, whereas the latter are high dimensional and dense even when the DAG is sparse.

Without loss of generality, we assume a single sparse DAG for each $j = 1, \dots, q$, resulting in \mathbf{L}_j^{-1} having the same sparsity pattern for all j . Assume a nearest-neighbor DAG for simplicity, so the first m nodes in the DAG have $0, 1, \dots, m-1$ parents, respectively, and all remaining ones have m parents. In this DAG, there is one node for each location of \mathcal{S} . At \mathcal{S} , the latent model is

$$\begin{aligned} \mathbf{w} &\sim N(\mathbf{0}, \mathbf{C}) & \mathbf{C} &= \{\oplus \mathbf{L}_i\}(\boldsymbol{\Sigma} \otimes \mathbf{I}_n)\{\oplus \mathbf{L}_i^\top\} \\ \mathbf{y} &= \mathbf{w} + \boldsymbol{\varepsilon} & \boldsymbol{\varepsilon} &\sim N(\mathbf{0}, \boldsymbol{\Delta} \otimes \mathbf{I}_n). \end{aligned}$$

We have discussed block-updating \mathbf{w} in the main article. Here, we target sequential single-site updates. Let $[i]$ denote the set of parent nodes of i . For simplicity, consider a location $\boldsymbol{\ell}_i$ corresponding to node i with m parents. In this section we let $\mathbf{y}_i = \mathbf{y}(\boldsymbol{\ell}_i) - (\mathbf{I}_q \otimes \mathbf{x}^\top(\boldsymbol{\ell}_i))\boldsymbol{\beta}$ and $\mathbf{w}_i = \mathbf{w}(\boldsymbol{\ell}_i)$, $\boldsymbol{\varepsilon}_i = \boldsymbol{\varepsilon}(\boldsymbol{\ell}_i)$ to simplify notation. The single-site hierarchical model is

$$\begin{aligned} \mathbf{w}_i &= \mathbf{H}_i \mathbf{w}_{[i]} + \boldsymbol{\eta}_i & \boldsymbol{\eta}_i &\sim N(\mathbf{0}, \mathbf{R}_i) \\ \mathbf{y}_i &= \mathbf{w}_i + \boldsymbol{\varepsilon}_i & \boldsymbol{\varepsilon}_i &\sim N(\mathbf{0}, \boldsymbol{\Delta}) \end{aligned}$$

where $\ell_{[i]} = \{\ell_j \in \mathcal{S} : j \rightarrow i\}$, $\mathbf{w}_{[i]}$ is a $qm \times 1$ vector storing the values of the latent effects at $\ell_{[i]}$, and $\mathbf{H}_i = \mathbf{C}(i, [i])\mathbf{C}([i])^{-1}$ and $\mathbf{R}_i = \mathbf{C}(i, i) - \mathbf{H}_i\mathbf{C}(i, [i])^\top$, where we let $\mathbf{C}(i, [i]) = \mathbf{C}(\ell_i, \ell_{[i]})$. Here, we refer to \mathbf{C} as the sample cross-covariance matrix as well as the IOX cross-covariance matrix function since $\mathbf{C}(i, [i])$ is the cross-covariance computed at ℓ_i against $\ell_{[i]}$ and, equivalently, the $q \times mq$ matrix reading the rows and columns of \mathbf{C} corresponding to i and $[i]$, respectively.

Single-site updates generally proceed by sequentially updating \mathbf{w}_i conditional on \mathbf{w}_{i^c} , i.e., the value of \mathbf{w} at $\mathcal{S} \setminus \{i\}$. Let the $nq \times nq$ precision matrix be $\mathbf{P} = \mathbf{C}^{-1}$ and let $i^c = \mathcal{S} \setminus \{i\}$. The properties of block matrix inverses imply that we can define

$$\begin{aligned} \mathbf{B}_i &:= \mathbf{C}(i, i) - \mathbf{C}(i, i^c)\mathbf{C}(i^c)^{-1}\mathbf{C}(i, i^c)^\top = \mathbf{P}(i, i)^{-1} \\ \mathbf{b}_i &:= \mathbf{C}(i, i^c)\mathbf{C}(i^c)^{-1} = -\mathbf{P}(i, i)^{-1}\mathbf{P}(i, i^c), \end{aligned} \tag{18}$$

where $\mathbf{P}(i, i)$ is a $q \times q$ and $\mathbf{P}(i, i^c)$ a $q \times (n-1)q$ submatrix of \mathbf{P} , which is sparse. Then, let \mathbf{w}_{i^c} be the vector of \mathbf{w} at $\mathcal{S} \setminus \{i\}$. The full conditional update for \mathbf{w}_i is $p(\mathbf{w}_i \mid \mathbf{w}_{i^c}, \mathbf{y}_i) = N(\mathbf{g}_i, \mathbf{G}_i)$, where, after seeing that $\mathbf{B}_i^{-1}\mathbf{b}_i = -\mathbf{P}(i, i^c)$, we have

$$\mathbf{G}_i^{-1} = \mathbf{P}(i, i) + \mathbf{\Delta}^{-1}, \quad \mathbf{G}_i^{-1}\mathbf{g}_i = -\mathbf{P}(i, i^c)\mathbf{w}_{i^c} + \mathbf{\Delta}^{-1}\mathbf{y}_i. \tag{19}$$

This result follows from a conjugate update of the Gaussian ‘‘prior’’ $N(\mathbf{w}_i; \mathbf{b}_i\mathbf{w}_{i^c}, \mathbf{B}_i)$ on the Gaussian likelihood $N(\mathbf{y}_i; \mathbf{w}_i, \mathbf{\Delta})$.

Without sparsity assumptions on the DAG, single-site updates are as costly if not more costly than block updates, due to the size of i^c which leads to large costs in computing and sampling from each $p(\mathbf{w}_i \mid \mathbf{w}_{i^c})$. But because we assume a sparse DAG on \mathbf{w} , we can write $p(\mathbf{w}_i \mid \mathbf{w}_{i^c}) = p(\mathbf{w}_i \mid \mathbf{w}_{b_i})$, where b_i is the Markov blanket of i in the DAG. The Markov blanket of i is the set of nodes (locations) j such that j is either (1) a parent of i , that is $j \rightarrow i$ in the DAG, (2) a child of i : $i \rightarrow j$, or (3) a co-parent of i : there is r such that $i \rightarrow r$ and $j \rightarrow r$. Based on the precision matrix $\rho_r(\mathcal{S})^{-1}$, we find b_i as the list of non-zero indices

of its i th column (or row), minus i itself. Then, (18) simplifies with $\mathbf{b}_i = -\mathbf{P}(i, i)^{-1}\mathbf{P}(i, b_i)$ and similarly in (19) where we replace $\mathbf{P}(i, i^c)$ with $\mathbf{P}(i, b_i)$.

Further, we can avoid calculating \mathbf{P} and instead directly use \mathbf{L}_j^{-1} for each $j = 1, \dots, q$ for all computations. Denote as $\mathbf{F}_j[:, i]$ the i th column of $\mathbf{F}_j = \mathbf{L}_j^{-1}$. Then,

$$\begin{aligned} \mathbf{P}(i, i) &= \{\oplus \mathbf{F}_j[:, i]^\top\}(\boldsymbol{\Sigma}^{-1} \otimes \mathbf{I}_n)\{\oplus \mathbf{F}_j[:, i]\} = \boldsymbol{\Sigma}^{-1} \odot \left[\mathbf{F}_r[:, i]^\top \mathbf{F}_s[:, i] \right]_{r,s=1,\dots,q} \\ \mathbf{P}(i, b_i) &= \{\oplus \mathbf{F}_j[:, i]^\top\}(\boldsymbol{\Sigma}^{-1} \otimes \mathbf{I}_n)\{\oplus \mathbf{F}_j[:, b_i]\} = (\boldsymbol{\Sigma}^{-1} \odot \mathbf{1}_{1,|b_i|}) \left[\mathbf{F}_r[:, i]^\top \mathbf{F}_s[:, b_i] \right]_{r,s=1,\dots,q}, \end{aligned} \quad (20)$$

where $|b_i|$ is the dimension of b_i and we use a similar argument to Proposition 2.3 in the first row to express $\mathbf{P}(i, i)$ as a Hadamard product. Computing (20) for each $i = 1, \dots, n$ as well as \mathbf{G}_i (and its Cholesky factor) in (19) can be performed in parallel.

If q is large and we factorize $\boldsymbol{\Sigma} = \mathbf{A}\mathbf{A}^\top$ where \mathbf{A} has $k \ll q$ columns, then we have shown in the main article how we can achieve speedups in the block sampler via the Woodbury matrix identity. We can do something similar here. First, denote $c_i = \{i\} \cup \{j : i \rightarrow j\}$, i.e., the set of children of i along with i itself; the dimension of c_i is $|c_i|$. Then, we can write

$$\mathbf{P}(i, i) = \{\oplus \mathbf{F}_j[c_i, i]^\top\}(\boldsymbol{\Sigma}^{-1} \otimes \mathbf{I}_{|c_i|})\{\oplus \mathbf{F}_j[c_i, i]\}$$

which is useful in reducing the inner matrix dimension. Then, $\boldsymbol{\Sigma}^{-1}$ does not exist, but the unique pseudoinverse $\boldsymbol{\Sigma}^+ = \mathbf{A}^{+\top}\mathbf{A}^+$ does, and is such that \mathbf{A}^+ is of dimension $k \times q$. Then, in (19) we find

$$\begin{aligned} \mathbf{G}_i^{-1} &= (\mathbf{P}(i, i) + \boldsymbol{\Delta}^{-1})^{-1} = (\{\oplus \mathbf{F}_j[c_i, i]^\top\}(\mathbf{A}^{+\top} \otimes \mathbf{I}_{|c_i|})(\mathbf{A}^+ \otimes \mathbf{I}_{|c_i|})\{\oplus \mathbf{F}_j[c_i, i]\} + \boldsymbol{\Delta}^{-1})^{-1} \\ &= (\mathbf{J}\mathbf{J}^\top + \boldsymbol{\Delta}^{-1})^{-1} = \boldsymbol{\Delta} - \boldsymbol{\Delta}\mathbf{J}(\mathbf{I}_{|c_i|k} + \mathbf{J}^\top\boldsymbol{\Delta}\mathbf{J})^{-1}\mathbf{J}^\top\boldsymbol{\Delta}, \end{aligned} \quad (21)$$

where we let $\mathbf{J} = \{\oplus \mathbf{F}_j[c_i, i]^\top\}(\mathbf{A}^{+\top} \otimes \mathbf{I}_{|c_i|})$, which is of dimension $|c_i|q \times |c_i|k$ and we use the Woodbury matrix identity to find the last equality. The required inverse is of dimension $|c_i|k$, meaning that for (21) to be advantageous compared to (20), we need $|c_i|k < q$. In

nearest-neighbor DAGs, one controls the number of parents m whereas the number of children varies across locations and may be large. For this reason, the radial neighbors DAG (Zhu et al. 2024) may be a convenient choice in this case; in a radial neighbors DAG, all neighbors of ℓ_i within radius r are either parents or children of i in the DAG. Consequently, r indirectly bounds $|c_i| \leq |\{\ell \in \mathcal{S} : |\ell - \ell_i| \leq r\}|$.

What we have just shown is that the structure induced by IOX leads to computations of the conditional mean and covariance of $p(\mathbf{w}_i | \mathbf{w}_{b_i}, \mathbf{y}_i)$ by either reading elements of the precision matrix \mathbf{P} , or via simple dot products between columns of the sparse matrices $\mathbf{\Gamma}_j = \mathbf{L}_j^{-1}$ and without ever directly computing \mathbf{L}_i or $\rho_i(\mathcal{S})$.

E.4 Compute cost of proposed scalable algorithms

We detail the computational complexity of the scalable algorithms outlined in the main article. Our assumption here is that n , the size of \mathcal{S} , is very large and $n \gg q$, leading to computational cost being dominated by operations along the spatial sites. We also assume a sparse DAG GP using m nearest neighbors. We compute \mathbf{L}_i at $O(nm^3)$ flops for each $i = 1, \dots, q$, for a total of $O(qnm^3)$. Determinant and inverse of $\mathbf{\Sigma}$ are cheap to compute in requiring $O(q^3)$ flops, independent of n .

In the block sampler for the latent model $\mathbf{M}_{w|y}$ is a $nq \times nq$ sparse matrix. One can use iterative matrix solvers such as conjugate gradient (CG); at each iteration, CG performs a matrix-vector multiplication (cost $O(n_{\text{nz}})$), for a total number of iterations that is guaranteed to be less than nq and can be reduced via preconditioning. The cost for solving $\mathbf{M}_{w|y}$ is in the order of $O(n_{\text{nz}}c)$ where n_{nz} is the number of nonzeros of \mathbf{C}^{-1} , and c is the condition number of $\mathbf{M}_{w|y}$.

F Applications and software

F.1 Simulation setup: trivariate data

In all 120 datasets, we let Σ be a correlation matrix with off-diagonal entries $\sigma_{12} = -0.9, \sigma_{13} = 0.7, \sigma_{23} = -0.5$. The decay, smoothness, and nugget effect parameters of the three outcomes are set as $\phi_1 = \phi_2 = \phi_3 = 30$, $\nu_1 = 0.5, \nu_2 = 0.8, \nu_3 = 1.2$, and $\tau_1^2 = \tau_2^2 = \tau_3^2 = 10^{-3}$. No other parameters are necessary for IOX datasets. For the multivariate Matérn, we let the cross-variable decay be fixed at $\phi_{ij} = 30$ and the smoothness as $\nu_{ij} = \frac{\nu_i + \nu_j}{2}$ for all i, j and we fix the cross-variable nugget effects at $\tau_{ij}^2 = 10^{-3}$ for all i, j , resulting in a parsimonious Matérn specification as in Gneiting et al. (2010). We evaluate the performance in estimating the marginal parameters as well as the cross-correlations at zero distance ρ_{ij} , which are computed in the multivariate Matérn cases as $\rho_{ij} = \sigma_{ij} \frac{\sqrt{\Gamma(\nu_i+1)}}{\sqrt{\Gamma(\nu_i)}} \frac{\sqrt{\Gamma(\nu_j+1)}}{\sqrt{\Gamma(\nu_j)}} \frac{\Gamma(\nu_i/2+\nu_j/2)}{\Gamma(\nu_i/2+\nu_j/2+1)}$, whereas in the IOX cases we average the values of $C_{ij}(\mathbf{0})$ at each observed location to compute the resulting scaling factor (the Supplement details this procedure for interpreting C_{ij}). In LMCs the cross-correlation at zero is $D_S^{-1}\Sigma D_S^{-1}$, where $\Sigma = \mathbf{A}\mathbf{A}^\top + \mathbf{I}_q$, $D_S = \text{diag}\{\sqrt{\Sigma_{jj}}\}$, and \mathbf{A} is the loadings matrix.

F.2 Simulation setup: data with 24 outcomes

Of the 40 datasets, we generate 20 by sampling from a GP-IOX such that the j th variable has Matérn marginal correlation with range $\phi_j = 30$, nugget effect parameter $\tau_j^2 = 10^{-3}$; we sample ν_j independently from a discrete uniform prior on $\{0.5, 0.8, 1.1, 1.4, 1.7, 2.0\}$ and $\Sigma \sim \mathcal{W}_{q+1}^{-1}(\frac{1}{2}\mathbf{I}_q)$. The figure in the main article shows one of the IOX synthetic datasets. The other 20 datasets are generated as GPs with LMC cross-covariance with rank $k = 8$ such that each of the 8 constituent processes is Matérn with smoothness $\nu_j = 1$,

no nugget effect, and spatial range ϕ_j sampled uniformly for each $j = 1, \dots, 8$ from a discrete distribution on a sequence of length 10 starting from 5 and ending at 20 with equal spacing. We generate the 24×8 loading matrix \mathbf{A} by independently sampling each of its elements as $a_{ij} \sim N(0, 1)$. Finally, we add independent Gaussian measurement error with unit variance to each of the outcomes.

F.3 Additional details on simulated data applications

We report boxplots that expand on the results of Tables 1 and 2 in the main article.

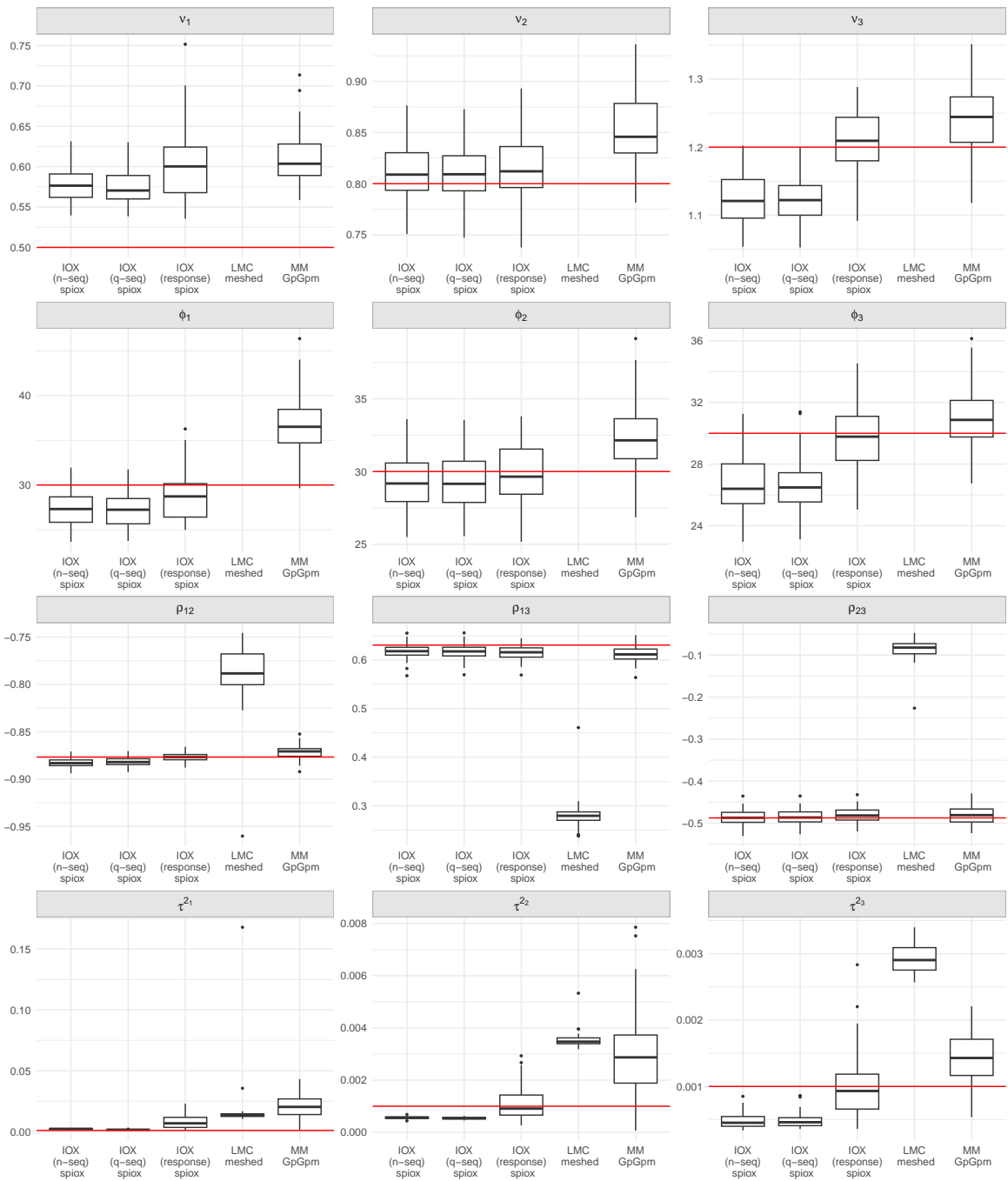


Figure 12: Box plots summarizing each tested model’s point estimates of the corresponding covariance parameter across all 60 IOX-generated datasets. True values are in red. Table 1 in the main article reports averages based on these boxplots.

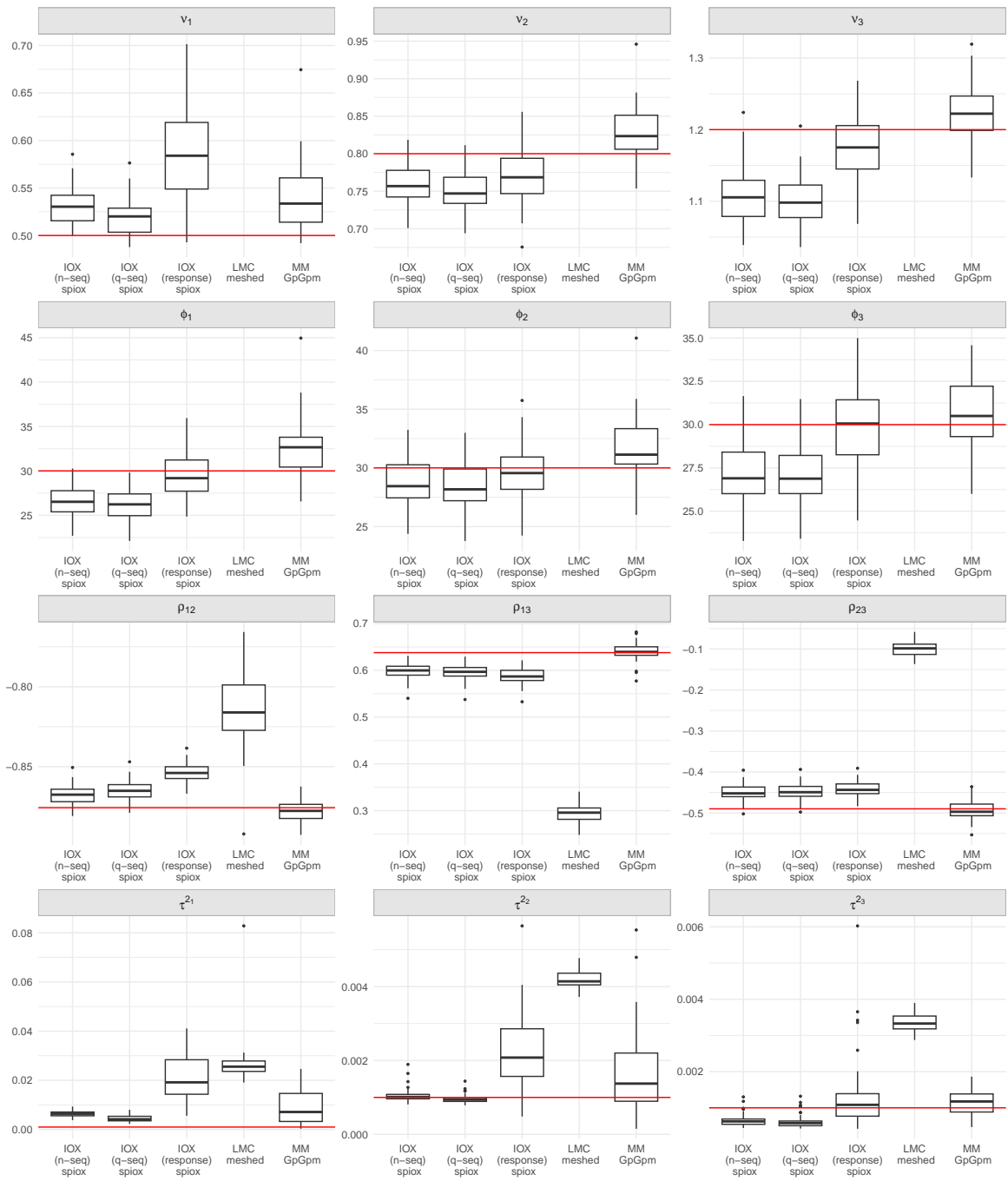


Figure 13: Box plots summarizing each tested model’s point estimates of the corresponding covariance parameter across all 60 multivariate Matérn-generated datasets. True values are in red. Table 1 in the main article reports averages based on these boxplots.

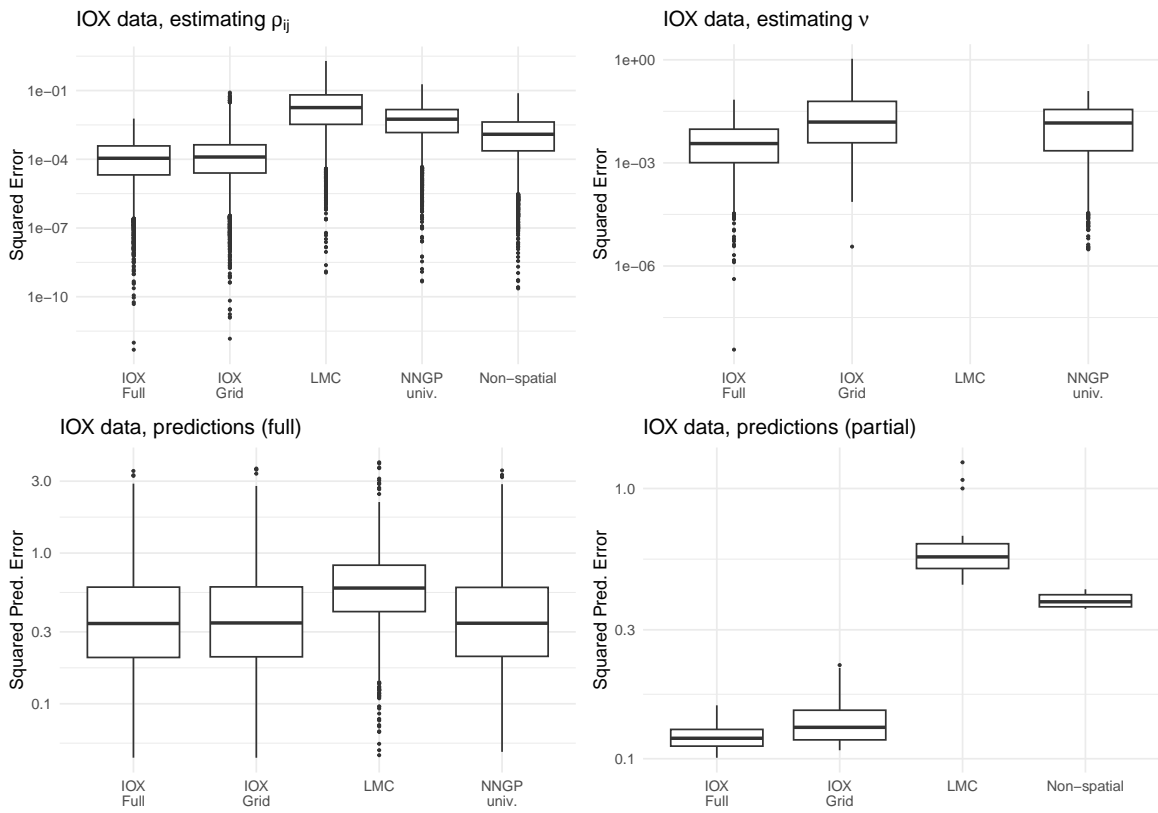


Figure 14: Box plots summarizing each tested model’s squared error in estimating the corresponding covariance parameters across all IOX-generated datasets. True values are in red. Table 2 in the main article reports averages based on these boxplots.

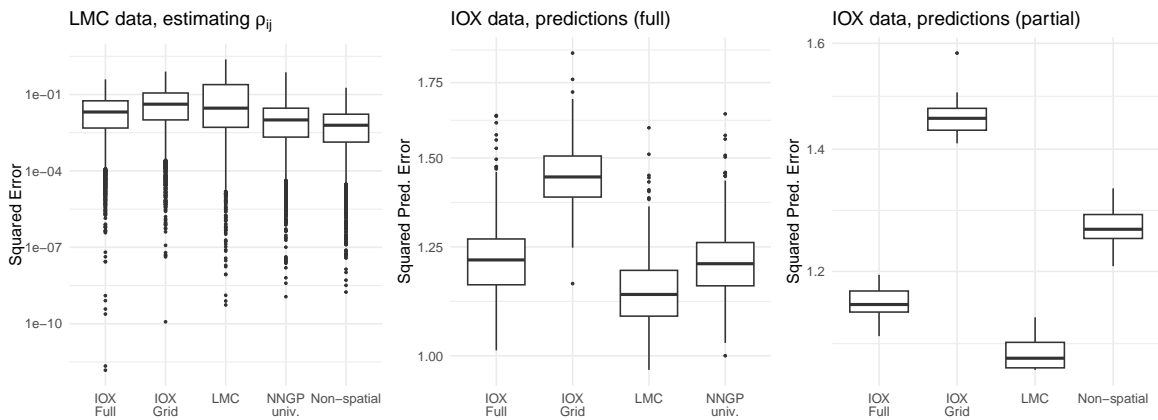


Figure 15: Box plots summarizing each tested model’s squared error in estimating the corresponding covariance parameters across all LMC-generated datasets. True values are in red. Table 2 in the main article reports averages based on these boxplots.

F.4 spiox R package and code to reproduce analyses

The supplementary material includes code to generate figures and run analyses. The R package (github.com/mkln/spiox) is general purpose and fits the response model as well as the latent model via the three algorithms we outlined (block, q sequential, n sequential). The R package is implemented in C++ using the Armadillo library (Sanderson & Curtin 2016) via RcppArmadillo (Eddelbuettel & Sanderson 2014). Parallel operations are performed via OpenMP (Dagum & Menon 1998). For fast linear algebra, we recommend to link R with efficient BLAS/LAPACK libraries (Anderson et al. 1999) such as OpenBLAS (Zhang 2020). All our analyses are run on a workstation equipped with a 16-core AMD Ryzen 9 7950X3D CPU, 192GB memory, using Intel Math Kernel Library version 2024.2 (Intel Corporation 2024) for fast linear algebra and SuperLU (Li 2005) as a sparse solver.

References

- Albert, J. H. & Chib, S. (1993), ‘Bayesian analysis of binary and polychotomous response data’, *Journal of the American Statistical Association* **88**(422), 669–679. [doi:10.2307/2290350](https://doi.org/10.2307/2290350).
- Alie, R., Stephens, D. A. & Schmidt, A. M. (2024), ‘Computational considerations for the linear model of coregionalization’. [arXiv:2402.08877](https://arxiv.org/abs/2402.08877).
- Álvarez, M. A. & Lawrence, N. D. (2011), ‘Computationally efficient convolved multiple output Gaussian processes’, *Journal of Machine Learning Research* **12**(41), 1459–1500.
- Anderson, E., Bai, Z., Bischof, C., Blackford, S., Demmel, J., Dongarra, J., Du Croz, J., Greenbaum, A., Hammarling, S., McKenney, A. & Sorensen, D. (1999), *LAPACK Users’ Guide*, third edn, Society for Industrial and Applied Mathematics, Philadelphia, PA.
- Apanasovich, T. V. & Genton, M. G. (2010), ‘Cross-covariance functions for multivariate random fields based on latent dimensions’, *Biometrika* **97**, 15–30. [doi:10.1093/biomet/asp078](https://doi.org/10.1093/biomet/asp078).
- Apanasovich, T. V., Genton, M. G. & Sun, Y. (2012), ‘A valid Matérn class of cross-covariance functions for multivariate random fields with any number of components’, *Journal of the American Statistical Association* **107**(497), 180–193. [doi:10.1080/01621459.2011.643197](https://doi.org/10.1080/01621459.2011.643197).
- Banerjee, S., Finley, A. O., Waldmann, P. & Ericsson, T. (2010), ‘Hierarchical spatial process models for multiple traits in large genetic trials’, *Journal of American Statistical Association* **105**(490), 506–521. [doi:10.1198/jasa.2009.ap09068](https://doi.org/10.1198/jasa.2009.ap09068).
- Banerjee, S., Gelfand, A. E., Finley, A. O. & Sang, H. (2008), ‘Gaussian predictive process models for large spatial data sets’, *Journal of the Royal Statistical Society, Series B* **70**, 825–848. [doi:10.1111/j.1467-9868.2008.00663.x](https://doi.org/10.1111/j.1467-9868.2008.00663.x).
- Berrocal, V., Gelfand, A. E. & Holland, D. M. (2010), ‘A bivariate space–time downscaler under space and time misalignment’, *The Annals of Applied Statistics* **4**(4), 1942–1975.
- Bradley, J. R., Holan, S. H. & Wikle, C. K. (2015), ‘Multivariate spatio-temporal models for high-dimensional areal data with application to Longitudinal Employer-Household Dynamics’, *The Annals of Applied Statistics* **9**(4), 1761–1791. [doi:10.1214/15-A0AS862](https://doi.org/10.1214/15-A0AS862).
- Bradley, J. R., Holan, S. H. & Wikle, C. K. (2018), ‘Computationally Efficient Multivariate Spatio-Temporal Models for High-Dimensional Count-Valued Data (with Discussion)’, *Bayesian Analysis* **13**(1), 253–310. [doi:10.1214/17-BA1069](https://doi.org/10.1214/17-BA1069).
- Chen, Y., Davis, T. A., Hager, W. W. & Rajamanickam, S. (2008), ‘Algorithm 887: CHOLMOD, supernodal sparse Cholesky factorization and update/downdate’, *ACM Trans. Math. Softw.* **35**(3). [doi:10.1145/1391989.1391995](https://doi.org/10.1145/1391989.1391995).
- Dagum, L. & Menon, R. (1998), ‘OpenMP: an industry standard api for shared-memory programming’, *Computational Science & Engineering, IEEE* **5**(1), 46–55.

- Datta, A., Banerjee, S., Finley, A. O. & Gelfand, A. E. (2016), ‘Hierarchical nearest-neighbor Gaussian process models for large geostatistical datasets’, *Journal of the American Statistical Association* **111**, 800–812. doi:10.1080/01621459.2015.1044091.
- De Iaco, S., Palma, M. & Posa, D. (2019), ‘Choosing suitable linear coregionalization models for spatio-temporal data’, *Stochastic Environmental Research and Risk Assessment* **33**, 1419–1434. doi:10.1007/s00477-019-01701-2.
- de Visser, K. E. & Joyce, J. A. (2023), ‘The evolving tumor microenvironment: From cancer initiation to metastatic outgrowth’, *Cancer Cell* **41**(3), 374–403. doi:10.1016/j.ccell.2023.02.016.
- Dey, D., Datta, A. & Banerjee, S. (2022), ‘Graphical Gaussian process models for highly multivariate spatial data’, *Biometrika* **109**(4), 993–1014. doi:10.1093/biomet/asab061.
- Eddelbuettel, D. & Sanderson, C. (2014), ‘RcppArmadillo: Accelerating R with high-performance C++ linear algebra’, *Computational Statistics and Data Analysis* **71**, 1054–1063. doi:10.1016/j.csda.2013.02.005.
- Emery, X., Porcu, E. & White, P. (2022), ‘New validity conditions for the multivariate Matérn coregionalization model, with an application to exploration geochemistry’, *Mathematical Geosciences* **54**(6), 1043–1068.
- Fahmy, Y. & Guinness, J. (2022), ‘Vecchia approximations and optimization for multivariate Matérn models’, *Journal of Data Science* **20**(4), 475–492. doi:10.6339/22-JDS1074.
- Finazzi, F. & Fassò, A. (2014), ‘D-STEM: A software for the analysis and mapping of environmental space-time variables’, *Journal of Statistical Software* **62**(6), 1–29. doi:10.18637/jss.v062.i06.
- Finley, A. O., Banerjee, S. & Gelfand, A. E. (2015), ‘spBayes for large univariate and multivariate point-referenced spatio-temporal data models’, *Journal of Statistical Software* **63**(13), 1–28. doi:10.18637/jss.v063.i13.
- Finley, A. O., Banerjee, S., Ek, A. R. & McRoberts, R. E. (2008), ‘Bayesian multivariate process modeling for prediction of forest attributes’, *Journal of Agricultural, Biological, and Environmental Statistics* **13**, 60. doi:10.1198/108571108X273160.
- Finley, A. O., Datta, A. & Banerjee, S. (2022), ‘spnngp r package for nearest neighbor Gaussian process models’, **103**(5). doi:10.18637/jss.v103.i05.
- Finley, A. O., Datta, A., Cook, B. D., Morton, D. C., Andersen, H. E. & Banerjee, S. (2019), ‘Efficient algorithms for Bayesian nearest neighbor Gaussian processes’, *Journal of Computational and Graphical Statistics* **28**, 401–414. doi:10.1080/10618600.2018.1537924.
- Finley, A. O., Sang, H., Banerjee, S. & Gelfand, A. E. (2009), ‘Improving the performance of predictive process modeling for large datasets’, *Computational Statistics and Data Analysis* **53**, 2873–2884. doi:10.1016/j.csda.2008.09.008.
- Fricke, T. E., Oakley, J. E. & Urban, N. M. (2013), ‘Multivariate Gaussian process emulators with nonseparable covariance structures’, *Technometrics* **55**(1), 47–56.

- Gaspari, G. & Cohn, S. E. (1999), ‘Construction of correlation functions in two and three dimensions’, *Quarterly Journal of the Royal Meteorological Society* **125**(554), 723–757. doi:10.1002/qj.49712555417.
- Gelfand, A. E., Kim, H. J., Sirmans, C. F. & Banerjee, S. (2003), ‘Spatial modeling with spatially varying coefficient processes’, *Journal of the American Statistical Association* **98**(462), 387–396. doi:10.1198/016214503000170.
- Gelfand, A., Schmidt, A., Banerjee, S. & Sirmans, C. F. (2004), ‘Nonstationary multivariate process modeling through spatially varying coregionalization’, *Test* **13**(2), 263–312. doi:10.1007/BF02595775.
- Genton, M. G. & Kleiber, W. (2015), ‘Cross-covariance functions for multivariate geostatistics’, *Statistical Science* **30**, 147–163. doi:10.1214/14-STS487.
- Giraldo, N. A., Sanchez-Salas, R., Peske, J. D., Vano, Y., Becht, E., Petitprez, F., Validire, P., Ingels, A., Cathelineau, X., Fridman, W. H. & Sautès-Fridman, C. (2019), ‘The clinical role of the TME in solid cancer’, *British Journal of Cancer* **120**(1), 45–53. doi:10.1038/s41416-018-0327-z.
- Girolami, M. & Calderhead, B. (2011), ‘Riemann manifold Langevin and Hamiltonian Monte Carlo methods’, *Journal of the Royal Statistical Society: Series B* **73**(2), 123–214. doi:10.1111/j.1467-9868.2010.00765.x.
- Gneiting, T., Kleiber, W. & Schlather, M. (2010), ‘Matérn cross-covariance functions for multivariate random fields’, *Journal of the American Statistical Association* **105**(491), 1167–1177. doi:10.1198/jasa.2010.tm09420.
- Hanahan, D. & Weinberg, R. A. (2011), ‘Hallmarks of Cancer: The Next Generation’, *Cell* **144**(5), 646–674. doi:10.1016/j.cell.2011.02.013.
- Heaton, M. J., Datta, A., Finley, A. O., Furrer, R., Guinness, J., Guhaniyogi, R., Gerber, F., Gramacy, R. B., Hammerling, D., Katzfuss, M., Lindgren, F., Nychka, D. W., Sun, F. & Zammit-Mangion, A. (2019), ‘A case study competition among methods for analyzing large spatial data’, *Journal of Agricultural, Biological and Environmental Statistics* **24**(3), 398–425. doi:10.1007/s13253-018-00348-w.
- Intel Corporation (2024), *Intel Math Kernel Library*. Version 2024-2, Software available at <https://software.intel.com/content/www/us/en/develop/tools/math-kernel-library.html>.
- Katzfuss, M. (2017), ‘A multi-resolution approximation for massive spatial datasets’, *Journal of the American Statistical Association* **112**, 201–214. doi:10.1080/01621459.2015.1123632.
- Katzfuss, M. & Gong, W. (2019), ‘A class of multi-resolution approximations for large spatial datasets’, *Statistica Sinica* **30**, 2203–2226. doi:10.5705/ss.202018.0285.
- Katzfuss, M. & Guinness, J. (2021), ‘A general framework for Vecchia approximations of Gaussian processes’, *Statistical Science* **36**(1), 124–141. doi:10.1214/19-STS755.

- Kleiber, W. (2017), ‘Coherence for multivariate random fields’, *Statistica Sinica* **27**(4), 1675–1697. doi:10.5705/ss.202015.0309.
- Krainski, E. T., Gómez-Rubio, V., Bakka, H., Lenzi, A., Castro-Camilo, D., Simpson, D., Lindgren, F. & Rue, H. (2019), *Advanced Spatial Modeling with Stochastic Partial Differential Equations Using R and INLA*, Chapman & Hall/CRC Press.
- Krock, M. L., Kleiber, W., Hammerling, D. & Becker, S. (2023), ‘Modeling Massive Highly Multivariate Nonstationary Spatial Data with the Basis Graphical Lasso’, *Journal of Computational and Graphical Statistics* **32**(4), 1472–1487. doi:10.1080/10618600.2023.2174126.
- Li, X. S. (2005), ‘An overview of SuperLU: Algorithms, implementation, and user interface’, *ACM Transactions on Mathematical Software* **31**(3), 302–325.
- Liu, H., Ding, J., Xie, X., Jiang, X., Zhao, Y. & Wang, X. (2022), ‘Scalable multi-task Gaussian processes with neural embedding of coregionalization’, *Knowledge-Based Systems* **247**, 108775. doi:10.1016/j.knosys.2022.108775.
- Majumdar, A. & Gelfand, A. E. (2007), ‘Multivariate spatial modeling for geostatistical data using convolved covariance functions’, *Mathematical Geology* **39**(2), 225–245. doi:10.1007/s11004-006-9072-6.
- Matheron, G. (1982), ‘Pour une analyse krigeante des données régionalisées’, *Technical report N.732, Centre de Géostatistique*.
- Moreno-Muñoz, P., Artés, A. & Álvarez, M. (2018), Heterogeneous multi-output Gaussian process prediction, in S. Bengio, H. Wallach, H. Larochelle, K. Grauman, N. Cesa-Bianchi & R. Garnett, eds, ‘Advances in Neural Information Processing Systems’, Vol. 31, Curran Associates, Inc.
- Nishimura, A. & Suchard, M. A. (2023), ‘Prior-preconditioned conjugate gradient method for accelerated Gibbs sampling in “large n, large p” Bayesian sparse regression’, *Journal of the American Statistical Association* **118**(544), 2468–2481. doi:10.1080/01621459.2022.2057859.
- Papaspiliopoulos, O., O., R. G. & Sköld, M. (2007), ‘A general framework for the parametrization of hierarchical models’, *Statistical Science* **22**(1), 59–73. doi:10.1214/088342307000000014.
- Pebesma, E. J. (2004), ‘Multivariable geostatistics in S: the gstat package’, *Computers & Geosciences* **30**(7), 683–691.
- Peruzzi, M., Banerjee, S., Dunson, D. B. & Finley, A. O. (2025), ‘Gridding and parameter expansion for scalable latent Gaussian models of spatial multivariate data’, *Bayesian Analysis* pp. 1–27.
- Peruzzi, M., Banerjee, S. & Finley, A. O. (2022), ‘Highly scalable Bayesian geostatistical modeling via meshed Gaussian processes on partitioned domains’, *Journal of the American Statistical Association* **117**(538), 969–982. doi:10.1080/01621459.2020.1833889.

- Peruzzi, M. & Dunson, D. B. (2022), ‘Spatial multivariate trees for big data Bayesian regression’, *Journal of Machine Learning Research* **23**(17), 1–40. <http://jmlr.org/papers/v23/20-1361.html>.
- Peruzzi, M. & Dunson, D. B. (2024), ‘Spatial meshing for general Bayesian multivariate models’, *Journal of Machine Learning Research* **25**(87), 1–49. <http://jmlr.org/papers/v25/22-0083.html>.
- Polson, N. G., Scott, J. G. & Windle, J. (2013), ‘Bayesian inference for logistic models using Polya-Gamma latent variables’, *Journal of the American Statistical Association* **108**, 1339–1349. doi:10.1080/01621459.2013.829001.
- Quiroz, Z. C., Prates, M. O., Dey, D. K. & Rue, H. (2023), ‘Fast Bayesian inference of block nearest neighbor Gaussian process for large data’, *Statistics and Computing* **33**(2), 54. doi:10.1007/s11222-023-10227-1.
- Reich, B. J., Fuentes, M., Herring, A. H. & Evenson, K. R. (2010), ‘Bayesian variable selection for multivariate spatially varying coefficient regression’, *Biometrics* **66**(3), 772–782. doi:10.1111/j.1541-0420.2009.01333.x.
- Ren, Q. & Banerjee, S. (2013), ‘Hierarchical factor models for large spatially misaligned data: A low-rank predictive process approach’, *Biometrics* **69**(1), 19–30. doi:10.1111/j.1541-0420.2012.01832.x.
- Sampson, P. D. & Guttorp, P. (1992), ‘Nonparametric estimation of nonstationary spatial covariance structure’, *Journal of the American Statistical Association* **87**(417), 108–119. doi:10.1080/01621459.1992.10475181.
- Sanderson, C. & Curtin, R. (2016), ‘Armadillo: a template-based C++ library for linear algebra’, *Journal of Open Source Software* **1**, 26.
- Schmidt, A. M. & Gelfand, A. E. (2003), ‘A Bayesian coregionalization approach for multivariate pollutant data’, *Journal of Geophysical Research* **108**, D24. doi:10.1029/2002JD002905.
- Schürch, C. M., Bhate, S. S., Barlow, G. L., Phillips, D. J., Noti, L., Zlobec, I., Chu, P., Black, S., Demeter, J., Mellwain, D. R., Kinoshita, S., Samusik, N., Goltsev, Y. & Nolan, G. P. (2020), ‘Coordinated cellular neighborhoods orchestrate antitumoral immunity at the colorectal cancer invasive front’, *Cell* **182**(5), 1341–1359.e19. doi:10.1016/j.cell.2020.07.005.
- Schäfer, F., Katzfuss, M. & Owhadi, H. (2024), ‘Sparse Cholesky factorization by Kullback–Leibler minimization’, *SIAM Journal on Scientific Computing* . doi:10.1137/20M1336254.
- Shirota, S., Finley, A. O., Cook, B. D. & Banerjee, S. (2019), ‘Conjugate nearest neighbor Gaussian process models for efficient statistical interpolation of large spatial data’. [arXiv:1907.10109](https://arxiv.org/abs/1907.10109).

- Stein, M. (1990), ‘Uniform asymptotic optimality of linear predictions of a random field using an incorrect second-order structure’, *The Annals of Statistics* **18**(2), 850–872. doi:10.1214/aos/1176347629.
- Stein, M. L., Chi, Z. & Welty, L. J. (2004), ‘Approximating likelihoods for large spatial data sets’, *Journal of the Royal Statistical Society, Series B* **66**, 275–296. doi:10.1046/j.1369-7412.2003.05512.x.
- Taylor-Rodriguez, D., Finley, A. O., Datta, A., Babcock, C., Andersen, H. E., Cook, B. D., Morton, D. C. & Banerjee, S. (2019), ‘Spatial factor models for high-dimensional and large spatial data: An application in forest variable mapping’, *Statistica Sinica* **29**(3), 1155–1180. doi:10.5705/ss.202018.0005.
- Teh, Y. W., Seeger, M. & Jordan, M. I. (2005), Semiparametric latent factor models, in R. G. Cowell & Z. Ghahramani, eds, ‘Proceedings of the Tenth International Workshop on Artificial Intelligence and Statistics’, Society for Artificial Intelligence and Statistics, pp. 333–340. <http://proceedings.mlr.press/r5/teh05a/teh05a.pdf>.
- Tikhonov, G., Opedal, O. H., Abrego, N., Lehtikoinen, A., de Jonge, M. M. J., Oksanen, J. & Ovaskainen, O. (2020), ‘Joint species distribution modelling with the R-package hmsc’, *Methods in Ecology and Evolution* **11**(3), 442–447. doi:10.1111/2041-210X.13345.
- Townes, F. W. & Engelhardt, B. E. (2023), ‘Nonnegative spatial factorization applied to spatial genomics’, *Nature Methods* **20**, 229–238. doi:10.1038/s41592-022-01687-w.
- Tsujikawa, T., Mitsuda, J., Ogi, H., Miyagawa-Hayashino, A., Konishi, E., Itoh, K. & Hirano, S. (2020), ‘Prognostic significance of spatial immune profiles in human solid cancers’, *Cancer Science* **111**(10), 3426–3434. doi:10.1111/cas.14591.
- Vecchia, A. V. (1988), ‘Estimation and model identification for continuous spatial processes’, *Journal of the Royal Statistical Society, Series B* **50**, 297–312. doi:10.1111/j.2517-6161.1988.tb01729.x.
- Velandia, D., Bachoc, F., Bevilacqua, M., Gendre, X. & Loubes, J.-M. (2017), ‘Maximum likelihood estimation for a bivariate Gaussian process under fixed domain asymptotics’, *Electronic Journal of Statistics* **11**(2), 2978 – 3007. doi:10.1214/17-EJS1298.
- Wackernagel, H. (2003), *Multivariate Geostatistics: An Introduction with Applications*, Springer, Berlin. doi:10.1007/978-3-662-05294-5.
- Yarger, D., Stoev, S. & Hsing, T. (2024), ‘Multivariate Matérn models – a spectral approach’. [arXiv:2309.02584](https://arxiv.org/abs/2309.02584).
- Yuan, Y. (2016), ‘Spatial Heterogeneity in the Tumor Microenvironment’, *Cold Spring Harbor Perspectives in Medicine* **6**(8), a026583. doi:10.1101/cshperspect.a026583.
- Zhang, H. (2004), ‘Inconsistent estimation and asymptotically equal interpolations in model-based geostatistics’, *Journal of the American Statistical Association* **99**(465), 250–261. doi:10.1198/016214504000000241.

- Zhang, H. (2007), ‘Maximum-likelihood estimation for multivariate spatial linear coregionalization models’, *Environmetrics* **18**(2), 125–139. doi:[10.1002/env.807](https://doi.org/10.1002/env.807).
- Zhang, L. & Banerjee, S. (2022), ‘Spatial factor modeling: A Bayesian matrix-normal approach for misaligned data’, *Biometrics* **78**(2), 560–573. doi:[10.1111/biom.13452](https://doi.org/10.1111/biom.13452).
- Zhang, L., Banerjee, S. & Finley, A. O. (2021), ‘High-dimensional multivariate geostatistics: A Bayesian matrix-normal approach’, *Environmetrics* **32**(4), e2675. doi:[10.1002/env.2675](https://doi.org/10.1002/env.2675).
- Zhang, X. (2020), *An Optimized BLAS Library Based on GotoBLAS2*.
URL: <https://github.com/xianyi/OpenBLAS/>
- Zhu, Y., Peruzzi, M., Li, C. & Dunson, D. B. (2024), ‘Radial neighbours for provably accurate scalable approximations of Gaussian processes’, *Biometrika* **111**(4), 1151–1167. doi:[10.1093/biomet/asae029](https://doi.org/10.1093/biomet/asae029).